

AD-A181 532

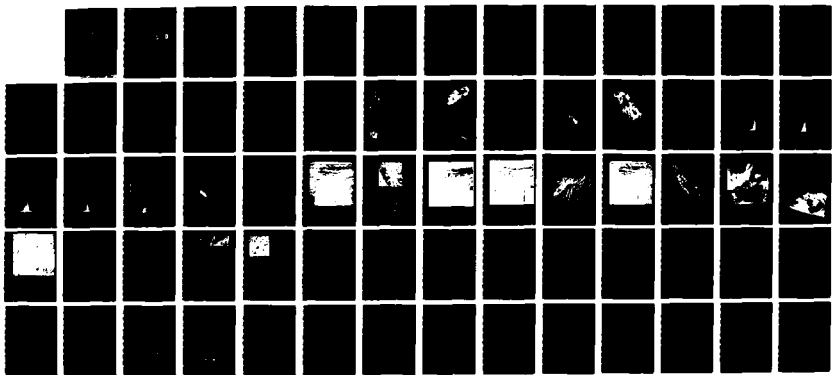
REGIONAL NETWORK SEISMICITY OF ASIA AND  
FREQUENCY-DEPENDENT Q(U) COLUMBIA UNIV NEW YORK  
D W SIMPSON ET AL 15 FEB 87 AFGL-TR-87-0049  
F19628-85-K-0022

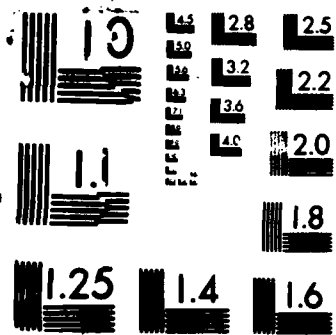
1/1

UNCLASSIFIED

F/G 8/11

NL





AFGL-TR-87-0049

**AD-A181 532**

Regional Network: Seismicity of Asia:  
and Frequency-Dependent Q

David W. Simpson  
Paul G. Richards  
Arthur Lerner-Lam

Trustees of Columbia University  
in the City of New York  
Box 20, Low Memorial Library  
New York, NY 10027

**DTIC**  
**ELECTE**  
JUN 19 1987  
**S** **D**  
D

15 February 1987

Final Report  
1 February 1985-30 September 1986


APPROVED FOR PUBLIC RELEASE; DISTRIBUTION UNLIMITED

AIR FORCE GEOPHYSICS LABORATORY  
AIR FORCE SYSTEMS COMMAND  
UNITED STATES AIR FORCE  
HANSCOM AIR FORCE BASE, MASSACHUSETTS 01731

87 6 10 023

"This technical report has been reviewed and is approved for publication"

  
JAMES F. LEWKOWICZ  
Contract Manager

  
HENRY A. OSSING  
Branch Chief

FOR THE COMMANDER

  
DONALD H. ECKHARDT  
Division Director

This report has been reviewed by the ESD Public Affairs Office (PA) and is releasable to the National Technical Information Service (NTIS).

Qualified requestors may obtain additional copies from the Defense Technical Information Center. All others should apply to the National Technical Information Service.

If your address has changed, or if you wish to be removed from the mailing list, or if the addressee is no longer employed by your organization, please notify AFGL/DAA, Hanscom AFB, MA 01731. This will assist us in maintaining a current mailing list.

Do not return copies of this report unless contractual obligations or notices on a specific document requires that it be returned.

**REPORT DOCUMENTATION PAGE**

|  |   |  |                                |
|--|---|--|--------------------------------|
| 1a REPORT SECURITY CLASSIFICATION<br>Unclassified  |   | 1b RESTRICTIVE MARKINGS.   |                                |
| 2a SECURITY CLASSIFICATION AUTHORITY   |   | 3 DISTRIBUTION/AVAILABILITY OF REPORT<br>Approved for Public Release<br>Distribution Unlimited |                                |
| 2b DECLASSIFICATION/DOWNGRADING SCHEDULE   |   |  |                                |
| 4. PERFORMING ORGANIZATION REPORT NUMBER(S)  |   | 5. MONITORING ORGANIZATION REPORT NUMBER(S)<br>AFGL-TR-87-0049                                 |                                |
| 6a NAME OF PERFORMING ORGANIZATION<br>The Trustees of Columbia Univ. in the City of NY   | 6b. OFFICE SYMBOL<br>(if applicable)        | 7a NAME OF MONITORING ORGANIZATION<br>Air Force Geophysics Laboratory                          |                                |
| 6c ADDRESS (City, State, and ZIP Code)<br>Box 20, Low Memorial Library<br>New York, NY 10027   |   | 7b ADDRESS (City, State, and ZIP Code)<br>Hanscom Air Force Base<br>Massachusetts 01731-5000   |                                |
| 8a. NAME OF FUNDING/SPONSORING ORGANIZATION<br>Air Force Systems Command   | 8b OFFICE SYMBOL<br>(if applicable)         | 9. PROCUREMENT INSTRUMENT IDENTIFICATION NUMBER<br>F 19628-85-K-0022                           |                                |
| 8c ADDRESS (City, State, and ZIP Code)<br>Hanscom AFB, MA 01731-5000   |   | 10. SOURCE OF FUNDING NUMBERS  |                                |
|  |   | PROGRAM ELEMENT NO.<br>61101E  | PROJECT NO.<br>5A10            |
|  |   | TASK NO.<br>DA   | WORK UNIT ACCESSION NO.<br>AH  |
| 11 TITLE (Include Security Classification)<br>Regional Network: Seismicity of Asia: and Frequency-Dependent Q  |   |  |                                |
| 12 PERSONAL AUTHOR(S)<br>Simpson, David W.; Richards, Paul G.; Lerner-Lam, Arthur  |   |  |                                |
| 13a. TYPE OF REPORT<br>Final   | 13b. TIME COVERED<br>FROM 2/1/85 TO 9/30/86 | 14. DATE OF REPORT (Year, Month, Day)<br>1987 February 15                                      | 15. PAGE COUNT<br>72           |
| 16 SUPPLEMENTARY NOTATION  |   |  |                                |
| 17. COSATI CODES   |   | 18 SUBJECT TERMS (Continue on reverse if necessary and identify by block number)               |                                |
| FIELD  | GROUP                                       | SUB-GROUP  |                                |
|  |   | synthetic seismograms, regional seismicity, regional networks                                  |                                |
| 19. ABSTRACT (Continue on reverse if necessary and identify by block number)<br>This report has three components:<br><br>1. A method is developed for the computation of body-wave synthetics which is suitable to a medium having smooth variation with depth and anelasticity having arbitrary variation with frequency. The method is applied to an anelastic earth model where Q is assumed to follow a power-law frequency dependence. The outcome is a pulse shape with properties quite different from what might be expected if the familiar constant-Q pulse shapes are surveyed.<br><br>2. The seismicity of Soviet Central Asia is studied using Soviet catalogs, and the relationship between topography and seismicity is analyzed using digital terrain data. The seismicity is concentrated along the major topographic gradients dividing the distinct physiographic/tectonic provinces of the region, with relatively low activity in both high plateaus and low basins and higher activity along the flanks of mountainous areas. Further, there is a distinct relationship between seismic activity and active ...OVER... |   |  |                                |
| 20 DISTRIBUTION/AVAILABILITY OF ABSTRACT<br><input type="checkbox"/> UNCLASSIFIED/UNLIMITED <input type="checkbox"/> SAME AS RPT. <input type="checkbox"/> DTIC USERS  |   | 21 ABSTRACT SECURITY CLASSIFICATION<br>Unclassified  |                                |
| 22a NAME OF RESPONSIBLE INDIVIDUAL<br>James Lewkowicz  |   | 22b. TELEPHONE (Include Area Code)<br>(617) 377-3028   | 22c. OFFICE SYMBOL<br>AFGL/LWH |

...CONT...

salt diapirism.

3. The capabilities of the New York State Seismic Array for studying teleseismic waveforms and sub-array structure are evaluated. The array is positioned uniquely with respect to major seismogenic zones to record core phases from earthquakes with magnitudes greater than 6.0. Only minor modification of the triggering algorithm is required to lower the magnitude threshold to 5.5. Estimates of inter-station coherence are also obtained, but interpretation of the results in terms of the distribution of crustal and upper-mantle scatterers is difficult due to uncertainties in instrument response. Nevertheless, it appears as if vertically-incident signals are reasonably coherent to distances greater than 50 to 60 km, somewhat larger than observed at NORSAR and LASA in the early seventies.



|                    |                                     |
|--------------------|-------------------------------------|
| Accession For      |                                     |
| NTIS CRA&I         | <input checked="" type="checkbox"/> |
| DTIC TAB           | <input type="checkbox"/>            |
| Unannounced        | <input type="checkbox"/>            |
| Justification      |                                     |
| By                 |                                     |
| Distribution /     |                                     |
| Availability Codes |                                     |
| Dist               | Avail and/or Special                |
| A-1                |                                     |

# CALCULATION OF BODY-WAVE PULSE SHAPES, WITH ALLOWANCE FOR FREQUENCY-DEPENDENT Q

Paul G. Richards

## INTRODUCTION

The computation of body-wave synthetics, in elastic Earth models that vary purely with depth, is now routinely done by several different methods. In practice, the resulting synthetics either look the same, or differ for reasons that are quite well understood and which indicate which methods are fallible in certain situations (Helmberger and Burdick, 1979; Aki and Richards, 1980; Kennett, 1983; Richards, 1985; Chapman and Orcutt, 1985).

But, for computation of pulse shapes in anelastic models, there is a less satisfactory experience, in part because only a limited number of plausible types of attenuation have been explored to the extent of incorporation into packages for the computation of synthetic seismograms. The most common type of attenuation incorporated into synthetics is that characterized by constant  $Q$  (i.e. a  $Q$  that is frequency-independent, but which is allowed to vary with depth), which is handled by methods suggested by Carpenter (1967). But seismic data indicate that in many practical situations the assumption of a constant  $Q$  is demonstrably false. Unfortunately, once the false assumption is dropped, it is not yet clear what should replace it.

Our recent work in this area has been based on a method of computing synthetics that is effective in elastic media for situations where geometrical ray theory is accurate. These include the interpretation of body-wave waveform data for earthquakes and explosions at distances from about  $30^\circ$  to  $85^\circ$ . We first describe this method, which would hardly be needed (since there are so many other effective methods for evaluating the predictions of ray theory in elastic media that smoothly vary with depth), were it not for the generalization it allows in the case of anelastic media - generalizations that other methods usually cannot supply. Then we show an application of the method to an anelastic Earth model where  $Q$  is assumed to follow a power law frequency dependence. The outcome is a pulse shape with properties quite different from what might be expected if the familiar constant- $Q$  pulse shapes are surveyed.

Our conclusion is, that a fundamental problem in the interpretation of body-wave broadband pulse shapes - namely, the appropriate choice of attenuation model to explain both spectral content and pulse width, and how these quantities are affected by propagation - is unresolved. But, the conventional model that uses constant Q is flawed.

## RAY CALCULATIONS WITHOUT RAY TRACING

An elementary use of the relationship between travel time ( $T$ ), distance ( $X$ ) and intercept time ( $\tau$ ) concerns fitting a ray between a fixed source and receiver, and finding the geometrical spreading, without actually doing any ray tracing.

Thus, in the frequency domain, the wavefield for a generalized ray in a structure that varies solely with depth can be written

$$W(X_0, \omega) = \int f(p, \omega) \exp[i\omega\{T(p, \omega) - pX(p, \omega) + pX_0\}] dp \quad (1)$$

where  $T(p, \omega) - pX(p, \omega)$  is the vertical integral of vertical slowness along the ray path,

$$T - pX = \tau = \int_{\text{ray}} \sqrt{[1/v^2 - p^2]} dz, \quad (2)$$

in which  $v(z)$  is the velocity (complex, if there is attenuation, and also frequency-dependent if there is dispersion); and  $f(p, \omega)$  includes the radiation pattern as well as relevant reflection/transmission coefficients for the generalized ray of interest. There are minor differences of detail between plane stratified and spherically stratified media. Richards (1973) obtained examples of (1) even for rays that have turning points, rather than reflection from a specific interface.

In order to obtain the ray-theory approximation for an array of receivers, consider the following six steps:

(i) One fixes  $\omega$  and computes  $f$  and  $\tau(p)$  for a set of equally spaced real  $p$ -values, in a range of the real ray-parameter axis that is close to where one expects complex saddle points to lie for the range of distances (i.e.  $X_0$ -values) at which one wishes to know  $W$ . Let the increment in  $p$  here be  $\Delta p$ .

(ii) At fixed  $X_0$ , one searches through the array of  $\text{Real}[T - pX + pX_0]$  to see at which of the sampled points in  $p$  it has a minimum (or, a maximum for certain kinds of ray). Label this discrete point as  $p_{js}$ . The complex

saddle must presumably lie near this point of the real  $p$ -axis. If there is no attenuation, the saddle will lie on the real  $p$ -axis if there is a real ray between source and receiver.

(iii) Find the values (complex, if there is attenuation) of the three constants  $T_0$ ,  $p_0$ , and  $DXDP$  that best fit the sampled phase factor according to

$$T - pX + pX_0 = T_0 - (p - p_0)^2 \times DXDP / 2 \quad (3)$$

in the vicinity of  $p_{js}$ . Note that if one just uses  $p_{js}$  itself, and the points just before and just after it, closed form expressions that in practice are often very accurate can easily be given for  $p_0$ ,  $T_0$ , and  $DXDP$ . Aki and Richards (1980) introduce the function  $J(p) = T - pX + pX_0$  (see their page 423). In terms of this sampled function,

$$J_{js-1} = J(p_{js-1}) = T_0 - (p_{js} - p_0)^2 \times DXDP / 2 + \Delta p \cdot p_0 \cdot DXDP - (\Delta p)^2 \cdot DXDP / 2$$

$$J_{js} = J(p_{js}) = T_0 - (p_{js} - p_0)^2 \times DXDP / 2$$

$$J_{js+1} = J(p_{js+1}) = T_0 - (p_{js} - p_0)^2 \times DXDP / 2 - \Delta p \cdot p_0 \cdot DXDP - (\Delta p)^2 \cdot DXDP / 2.$$

Therefore, the closed form expressions for the desired constants are

$$DXDP = - [J_{js+1} - 2J_{js} + J_{js-1}] / (\Delta p)^2 ,$$

$$p_0 = - [J_{js+1} - J_{js-1}] / (2 \cdot \Delta p \cdot DXDP)$$

and finally

$$T_0 = J_{js} + (p_{js} - p_0)^2 \times DXDP / 2. \quad (4)$$

The point of this exercise, of course, is that  $p_0$  is an estimate of the position of the complex saddle;  $T_0$  is an estimate of the complex travel time; and  $DXDP$  (signifying  $dX/dp$  at the saddle) is the relevant constant, complex in general, needed to evaluate geometrical spreading.

(iv) Interpolate from  $f(p_{js}, \omega)$  and  $f(p_{js+1}, \omega)$  to evaluate  $f(p_0, \omega)$ .

(v) Claim that the saddle point approximation to  $W$  is

$$W(X_0, \omega) = f(p_0, \omega) \exp(i\omega T_0) \times \sqrt{[2\pi + (i\omega \cdot DXDP)]}. \quad (5)$$

Choose the next value of  $X_0$ , and loop back to the second step to do various distances. Choose the next value of frequency  $\omega$ , and loop back to the first step. This loop is necessary only if  $Q$  is frequency-dependent, and/or if there is allowance for body-wave dispersion. Also, for some types of anelasticity, it may be possible to abbreviate this step and estimate more directly the global frequency-dependence of the saddle-point approximation.

(vi) Finally, one can go to the time domain:

$$W(X_0, t) = (1/2\pi) \int W(X_0, \omega) \exp[-i\omega t] d\omega. \quad (6)$$

Note that the whole effort is accomplished using real values of ray-parameter, at the time-consuming stage of tabulating  $f$  and  $\tau$  at discrete  $p$  values. Often, the dependence on frequency in (5) is sufficiently simple that (6) can be evaluated explicitly.

The method allows easily for investigation of different attenuation-dispersion pairs. This is handled just by insertion of some appropriate rule for evaluating  $v(z, \omega)$ , and then recognizing that  $\tau = \tau(p, \omega)$ . For example, in a constant  $Q$  medium in which the method of Carpenter (1967) is used to handle dispersion, the real body-wave velocity  $v_e(z)$  of an elastic model is replaced by

$$v(z, \omega) = v_e(z) \{ 1 + [1/Q(\omega)] [(1/\pi) \ln(\omega/\omega_0) - i/2] \} \quad (7)$$

The method is simple and rapid to execute, and has been found quite accurate for 1-D (that is, purely depth-dependent) problems (Richards, 1985). A comparison of synthetics produced by this method and Cagniard first motion method is given here in Figure 1.

A series of papers by Borchardt (most recently, Borchardt *et al.*, 1986) has drawn attention to the need for more careful handling of attenuation. Specifically he has advocated working with plane waves that may propagate in a direction that differs from the direction of most rapid attenuation. (The "direction of propagation" is the direction of most rapid phase increase.) He has shown that such waves have properties that much conventional analysis (i.e., that based on plane waves propagating in the direction of maximum attenuation) cannot reproduce. Fortunately, the method based on (1) through (5), which finds stationary values of the integrand at complex values of horizontal slowness, gets around Borchardt's

valid objections to conventional analysis, yet does so for attenuating media in a way that requires little change from computational experience with elastic media. The subject is further discussed in Richards (1984). Incidentally, we note here that the whole procedure has recently been generalized so that it carries over to 3-D problems in layered structures, with planar interfaces that can have any strike and dip. In effect one can develop a generalized ray theory for a medium built up from a stack of arbitrary wedges, and the geometrical ray approximation can be computed by a method that is an extension of (1) to (7) (Richards - 1987 proposal to the National Science Foundation).

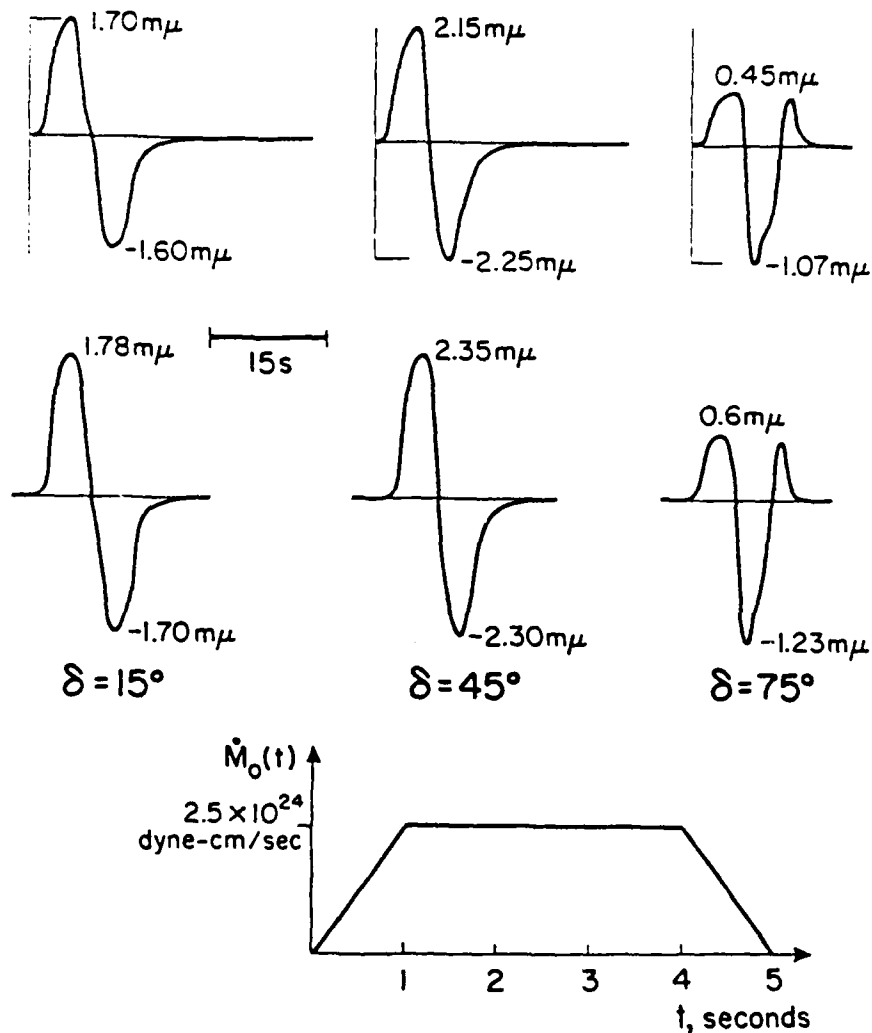


Fig. 1. Each pulse gives the  $P$ -wave group ( $P+pP+sp$ ) at distance  $80^\circ$ , and  $30^\circ$  off the strike direction, from a point source 15 km deep. Rake is  $90^\circ$ , and results are given for three different dips. These are displacements in the upward vertical direction (after a free surface correction).  $t^*$  is taken as 1 second, and the time dependence of the source is given at the bottom of the figure.

The upper row uses a Cagniard first motion approximation [Langston and Helmberger, 1975]. The lower row (which has the same time scale but is displayed with a slightly different amplitude scale) uses the complex saddle point spectral method reviewed in the text, with model PEM-C and a  $Q$  structure that gives  $t^* = 1$  at  $80^\circ$ .

Numbers displayed are displacement in  $m\mu$ . The two methods, each of which is basically geometrical ray theory adapted to an attenuating medium, agree to within about 10%.

## EXAMINATION OF BODY-WAVE PULSE SHAPES IN DIFFERENT TYPES OF MEDIA

We have used the method based on (1) through (7) to compare pulse shapes in three different Earth models. We have used a fixed source-receiver distance, one for which geometrical ray theory is usually deemed adequate even for broad-band body wave pulses, so that attention can be focussed on the single issue of what effects result from different choices about the frequency-dependence of  $Q$ .

Thus, in Figure 2 is shown the P-wave pulse shape from an impulsive source in Earth model SL8, for which  $Q$  is constant and quite low in value. Note the characteristic features of this pulse: high frequencies have been selectively removed, and the pulse shape is broadened with an asymmetric rise and fall. The attenuation-dispersion pair is based on equation (7).

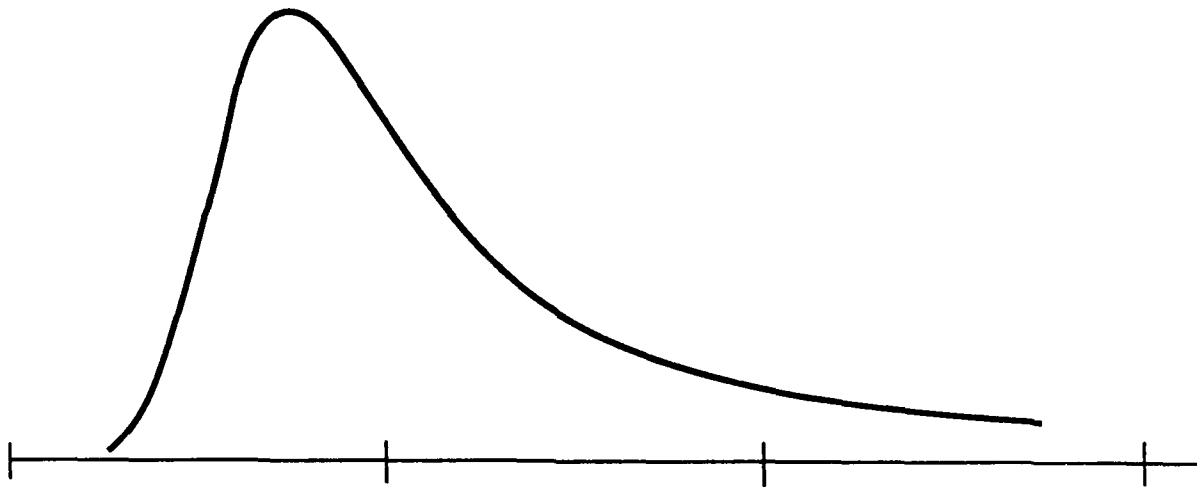


Figure 2. The P-wave pulse at  $48^\circ$  in Earth model SL8, for an impulsive shallow source. Constant  $Q$ , Carpenter law. Tick marks are at 1 s intervals.

In Figure 3 is shown the same pulse, but for Earth model AFL (i.e. from Archambeau, Flinn and Lambert, 1966).  $Q$  is again constant, but is significantly higher than the value for SL8.

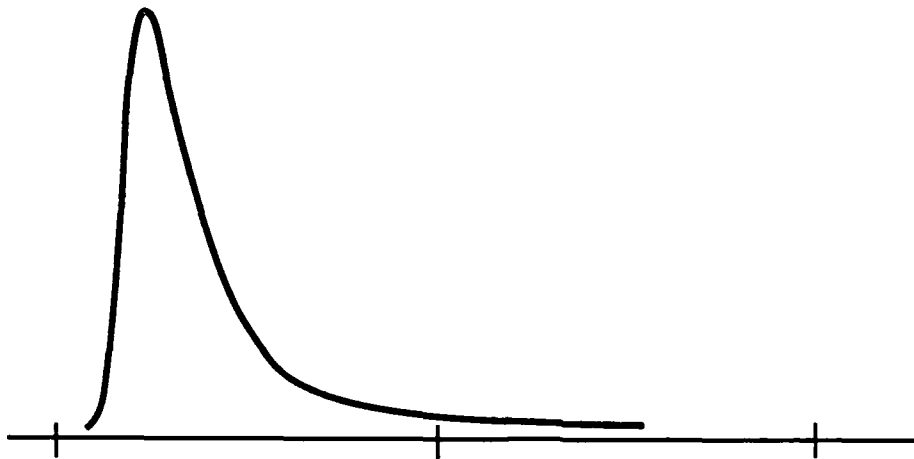


Figure 3. The P-wave pulse shape at  $48^\circ$  in Earth model AFL, from a shallow impulsive source. Tick marks, 1s.

Since both AFL and SL8 are data-driven anelastic Earth models, the first based on relatively high frequency signals (about 2 Hz) and the second based on relatively low frequencies (about 0.005 Hz), it is clearly unsatisfactory that each model is presented in terms of a frequency-independent  $Q$  structure. That is,  $Q$  is constant and has low value in SL8;  $Q$  is constant but with a high value in AFL. Various high-frequency phenomena displayed in seismic data are not present in SL8, and low frequency phenomena in seismic data are not present in AFL.

It is therefore appropriate to consider some kind of interpolation for  $Q$  across the frequency range whose extremes are represented by the frequency values typical of the data bases underlying these two Earth models. We have done this by assuming a  $Q$  that has a power-law dependence on frequency,

$$Q(\omega) = Q_0 (\omega / \omega_0)^{1-s} \quad (8)$$

for some choice of constant  $s$ .  $Q_0$  is a constant, the value of  $Q(\omega)$  at frequency  $\omega_0$ .

We find from causality rules and the evaluation of Hilbert transforms

that the appropriate replacement for equation (7) is now

$$v(z, \omega) = v_e(z) \{ 1 + [ 1/2 Q(\omega) ] [ ((Q(\omega)/Q_0) - 1) \tan(s\pi/2) - i ] \}. \quad (9)$$

Consideration of the difference in frequency ranges over which SL8 and AFL were generated, and the values of the two separate but constant Q values in each model, leads one to a value of about 0.7 for the constant s that appears in equation (8). Thus, Q has about a 0.3 power-law dependence on frequency, to fit the two kinds of data base underlying these models.

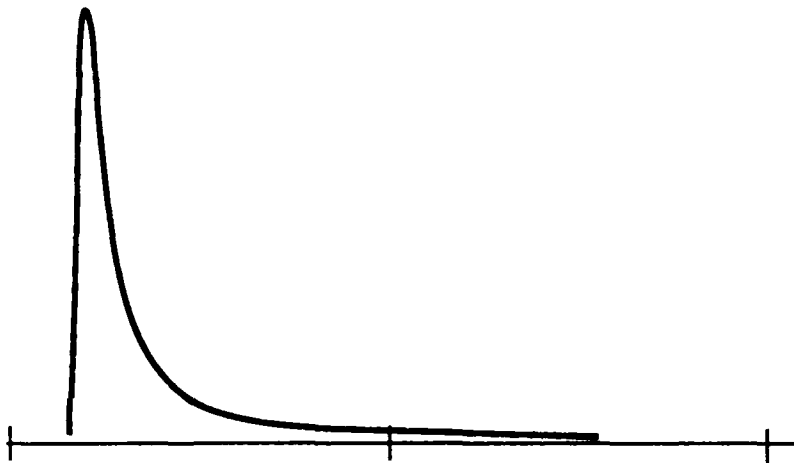


Figure 4. The P-wave at 48° in an Earth model with power-law Q, having approximately the Q of SL8 at frequencies for which the attenuation in SL8 was determined, and the Q of AFL at frequencies for which the attenuation of AFL was determined. Impulsive shallow source. Tick marks, at 1s intervals.

The outcome of computing a pulse shape based on this  $Q(\omega)$  might reasonably be expected to be a pulse somewhat intermediate between those of Figures 2 and 3, since we have merely found a way to interpolate for Q across a broad band of frequencies that is representative of SL8 at one end, and AFL at the other. But the actual outcome is different. It is shown in Figure 4, and one sees a pulse shape that has an even shorter rise time than does that of Figure 3 for AFL. The reason turns out not to be hard to find. It is, that at frequencies even higher than those which characterize the data base for AFL, equation (8) gives a higher value of Q than the constant Q value of AFL itself. Since it is the highest frequencies

that determine the rise time, this latter feature will, in the frequency-dependent Q model, be reflective of the assumptions built into (8) concerning the very-high frequency dependence of Q. In this case, Q is unbounded as frequency rises, which presumably is why the rise time is so short in Figure 4.

We therefore reach two conclusions. First, that a constant Q attenuation model is unsatisfactory. (This has long been known: such a model does not explain observations across the observed range of frequencies.) Second, that its replacement is not obvious. Artificial features, associated with attenuation laws applied outside the range of frequencies for which there is a good data base, can in the time domain be drawn into the appearance of a pulse shape computed within the frequency band at which data is acquired. Another example of this general problem was given by Richards (1985) in connection with an attenuation law appropriate for a spectrum of relaxation mechanisms.

A good research plan to resolve this issue is to see if high-quality broad-band pulse shape data can be acquired, for example from RSTN body-wave data of deep earthquakes observed teleseismically. It may then be possible to obtain the attenuation-dispersion pair directly from the data. We note a first attempt in this direction (Choy and Cormier, 1986). It is difficult to achieve results, because of the need to remove source effects, and effects of heterogeneity of structure at depth (e.g. the downgoing slab, which is always present as a cause of the earthquake activity itself). However, we are confident that an observational program will indeed result in suggestions for the attenuation-dispersion pair that is appropriate in computation of synthetics, and that will narrow the range of current trade-offs between source and propagation phenomena.

#### References.

- Aki, K., and P.G. Richards, *Quantitative Seismology - Theory and Methods*, vol. I, W.H. Freeman and Co., San Francisco, 1980.
- Archambeau, C.B., E.A. Flinn, and D.G. Lambert, Fine structure of the upper mantle, *J. Geophys. Res.*, 74, 5825-5866, 1966.
- Borcherdt, R.D., G. Glassmoyer, and L. Wennerberg, Influence of welded boundaries in anelastic media on energy flow, and characteristics of *P*, *S-I*, and *S-II* waves: observational

- evidence for inhomogeneous body waves in low-loss solids, *J. Geophys. Res.*, 91, 11503-11518, 1986.
- Carpenter, E.W., Teleseismic signals calculated for underground, underwater, and atmospheric explosions, *Geophysics*, 32, 17-32, 1967.
- Chapman, C.H., and J.A. Orcutt, The computation of body wave synthetic seismograms in laterally homogeneous media, *Rev. Geophys.*, 23, 105-163, 1985.
- Choy, G.L., and V.F. Cormier, Direct measurement of the Mantle attenuation operator for Broadband *P* and *S* waveforms, *J. Geophys. Res.*, 91, 7326-7342, 1986.
- HelMBERGER, D.V., and L.J. Burdick, Synthetic seismograms, *Ann. Rev. Earth Planet. Sci.*, 34, 417-442, 1979.
- Kennett, B.L.N., *Seismic Wave Propagation in Stratified Media*, Cambridge University Press, 1983.
- Langston, C.A., and D.V. HelMBERGER, A procedure for modeling shallow dislocation sources, *Geoph. J. Roy. astr. Soc.*, 42, 117-130, 1975.
- Richards, P.G., Calculation of body waves, for caustics and tunnelling in core phases, *Geoph. J. Roy. astr. Soc.*, 35, 243-264, 1973.
- Richards, P.G., On wavefronts and interfaces in anelastic media, *Bulletin of the Seismological Society of America*, 74, 2157-2165, 1984.
- Richards, P.G., *Seismic wave propagation effects -- development of theory and numerical modelling*, Chapter in DARPA commemorative volume "The VELA Program: A Twenty-Five Year Review of Basic Research", ed. A.U. Kerr, pp. 183-251, 1985.

## SEISMICITY OF CENTRAL ASIA

D.W. Simpson

### Soviet Earthquake Catalogs

The Institute of Physics of the Earth, Moscow issues an annual catalog of earthquakes in the USSR (*Zemletriaseniia v SSSR*, hereafter ZSSSR). These annual volumes contain articles and catalogs for different subregions of the USSR, based on seismic regionalization. The largest of these catalogs is for Central Asia, the active region along the USSR's southern border.

The Central Asia region includes the territory of the republics of Tadjikistan, Kazakhstan, Uzbekistan, Kirghizia and Turkmenia (Figure 1). The main physiographic divisions included are the Northern and Southern Tien Shan and Pamir Mountains, Tadjik Depression, Kyzul Kum desert and Hindu Kush (Figure 2b). The area covered by the ZSSSR catalog extends beyond the borders of the USSR into Iran, Afghanistan and China to the south. Coverage of these border regions becomes less complete, however, because of the lack of stations in southern azimuths.

### Comparison of ISC and ZSSSR catalogs

The increased coverage with regional and local stations results in a Soviet catalog that has a lower detection threshold and higher resolution than that of teleseismic catalogs such as the International Seismological Center (ISC). Figure 3 shows the annual and cumulative numbers of earthquakes reported by ISC and ZSSSR for the period 1964 - 1979 and maps derived from the two catalogs are shown in Figures 4 and 5.

The availability of a detailed catalog for Central Asia, compiled entirely from local data sources provides an interesting opportunity to examine the completeness and accuracy of the ISC catalog. Unfortunately, the ZSSSR and ISC catalogs are not completely independent, since some of the Soviet data are provided to and used by ISC. Only a subset of stations are reported to ISC however, so that the ZSSSR catalog can be assumed to be more accurate and, because of the increased density of stations, it is certainly more complete.

We have used an algorithm based on nearness in space and time to identify entries for common events in the two catalogs. Of the 3720 events reported by ISC for 1964-1978, 3602 are found in ZSSSR. Most of the events reported by ISC but not found in ZSSSR are either of low magnitude and located near the southern limits of the Soviet catalog or are poorly determined locations (i.e. reported by less than 5 stations). The only well located events above magnitude 5.0 reported only by ISC within the area well covered by ZSSSR are events identified as peaceful nuclear explosions.

For those events that are common to both catalogs, we have determined the differences in location parameters ( $dx$  - longitude,  $dy$  - latitude,  $dr$  - epicenter ( $=\sqrt{dx^2+dy^2}$ ),  $dz$  - depth,  $dt$  - origin time and  $dm$  - magnitude).

Epicentral location - Map views of the differences in location ( $dx$ ,  $dy$ ), as a function of number of stations used by ISC, are shown in Figure 6. The origin is the ZSSSR location for each event with points placed at the end of the vector connecting the ZSSSR and ISC locations. The difference in epicentral location ( $dr$ ) is shown in Figure 7. For locations determined with less than 10 stations, differences of over 200 km are observed. The difference in location decreases as the number of stations used by ISC increases (usually a direct function of the magnitude). The differences in location are smaller in the EW direction and there is an absolute bias to the north, both most likely resulting from the paucity of ISC reports from stations to the north. For events for which more than 50 stations

are available in the ISC solution, the standard deviation in the difference between the ISC and ZSSSR location drops to about  $\pm 12$  km, with the ISC locations biased about 10 km to the ESE of those given by ZSSSR.

**Depth and origin time** - Figures 8 and 9 show the differences in depth (dz) and origin time (dt) as a function of the number of stations used in the ISC location. While dr (Figure 7) shows the gradual decrease with number of stations, both dz and dt show broad and biased ( $>0$ ) distributions even beyond 100 stations. The bias towards late origin times and greater depths apparent in Figures 8 and 9 results from the well-known trade-off between these two parameters in the earthquake location process. Many of the catalogs entries report no depths or standard depths of 0 km (ZSSSR) or 33 km (ISC). Figures 10 and 11 remove these "unknown" depths and attempt to classify the remaining data in terms of events which we can be confident are actually deep or shallow and those in which one of the catalogs is in error. In Figure 10 we assume that those events for which both ISC and ZSSSR report depths greater than 60 km are actually deep. In this case the distribution of dt is symmetrical about zero. We assume that events that are assigned shallow depths by both catalogs (but not 0 km in ZSSSR or 33 in ISC) are actually shallow. Figures 11 and 12 show that for these shallow events there is a clear tendency for the ISC origin times to be later (average of 3 s), which is compensated for (Figure 12) by the ISC depths being deeper.

**Magnitude** - The Soviet classification of earthquake size is energy class, k, where k is the log of energy release in joules. Rautian (1960) gives the following relationship, based on an analysis of determinations of both magnitude and energy class for regional and local earthquakes:

$$m = (k-4)/1.8$$

$$\text{or } k = 1.8m + 4$$

Figure 13 shows the relationship between k as reported in the ZSSSR catalog and  $m_b$  for those events with magnitude reported by ISC. The relationship found:

$$k = 1.93m + 3.29$$

is similar to that reported by Rautian.

## **SEISMICITY AND TOPOGRAPHY**

Many of the topographic features of Central Asia can be discerned in the patterns of seismicity from the Soviet Catalog in Figure 2 and 5. Among the more prominent features:

a) There is intense activity along the southern front of the northern and southern Tien Shan. This zone, the Gissar Kokshal seismic zone, is the site of the largest earthquakes in Central Asia (Leith and Simpson, 1986a) and marks the southern edge of what can be clearly identified as part of the "original" Asian plate.

b) Relatively low levels of seismicity are found within the high mountainous areas. The Gissar and Kokshal Ranges of the Tien Shan are flanked on the south and north by high seismicity, but the higher elevations are much less active. Relatively low levels of activity in regions of high elevation are also found in the Talas Fergana Ranges and the highest section of the Pamir.

c) Relatively low levels of seismicity are found within the major intermountain basins and depressions. Most prominent of these is the Issyk Kul Basin, where high activity along the ranges bordering the basin clearly outlines the relatively low seismicity of the basin itself. The Fergana Valley is similar but less obvious. The Tadjk Depression and Tarim Basin have high activity on their northern edges, near the Gissar Kokshal zone, but are less active in their interiors.

The seismicity is thus concentrated along the major topographic gradients dividing the distinct physiographic/tectonic provinces of the region, with relatively low activity in both high plateaus and low basins and higher activity along the flanks of the mountainous areas.

## Digital Terrain Data

To study the relationship between topography and seismicity in more detail, we have obtained digital terrain data for Central Asia from the Defense Mapping Agency (DMA) topographic database. Topographic elevations are provided at 3" intervals (1200 points per degree or approximately 100 m spacing).

We have carried out preliminary analysis of segments of these data making extensive use of the International Imaging Systems (I<sup>2</sup>S) image processor at Lamont Doherty. The original data are provided in blocks of 1° x 1° (1200 x 1200 points). While that resolution has been useful in some detailed studies (e.g. the Kulyab salt dome study described below or as part of our work on induced seismicity at Nurek reservoir), the volume of data is too large for synoptic studies of large areas and it is necessary to severely decimate the data. The image processing system provides a convenient environment for reading the data, creating and examining full resolution images, decimating into smaller panels and creating mosaics of larger map areas. The image processor can also be used to apply different enhancement techniques to the topographic images, combine the topography with other (eg. epicenter) data and show the results in glowing color. In this report we limit ourselves to low resolution greyscale versions of these images.

## Tadjik Depression and Southern Tien Shan

An example of an image created from the terrain data is shown in Figure 14. This area includes the Southern Tien Shan (Gissar and Zeravshan Ranges), Tadjik Depression and western Pamir. This is the most active part of Soviet Central Asia and has been extensively studied by Soviet groups at the Tadjik Institute of Seismoresistant Construction and Seismology (TISSS) in Dushanbe and the Complex Seismological Expedition (KSE) in Garm, an outpost of the Institute of the Physics of the Earth, Moscow. It is also the site of our earlier work on induced seismicity at Nurek Reservoir (Simpson and Negmatullaev 81, Keith et al 82, Leith et al 81) and regional tectonics (Kristy and Simpson 1980, Leith and Alvarez 1985, Leith and Simpson 1986a,b). Figure 15 identifies in more detail some of the geographic features in a subsection of Figure 14 near Nurek reservoir.

Figure 16 represents topography with intensity directly proportional to elevation. In Figure 17 a filter has been used to locally enhance the contrast within different topographic provinces. Thus the relationship between intensity and elevation is no longer linear or spatially constant, but many of the subtle topographic features are more clearly distinguished. In Figure 18 a simple shaded relief map has been produced by taking the first spatial derivative of the elevation in the NW-SE direction, giving the impression of illumination from the NW. This filter accentuates NE-SW striking features (eg. ridges in the Tadjik Depression). A similar image, with illumination from the NE (Figure 19) accentuates features perpendicular to those in Figure 18.

One of the first order features obvious in Figures 16-19 is the contrast between the topographic style in the northern half of the image and that in the south. The northern segment, with higher and smoother average topography, a general EW fabric and deeply incised rivers is composed primarily of Paleozoic granites of the Southern Tien Shan. The southern part, with pronounced, sharp ridges oriented more NE-SW, shows the results of recent folding and thrusting of the young foreland fold and thrust belt of the Tadjik Depression (Leith and Alvarez, 1985). The seismicity of this area (Figure 20) and its relationship to the major physiographic provinces is described in detail by Leith and Simpson (1986a). Three clear types of seismicity are found in the shallow earthquakes of the region (in addition to the intermediate depth activity of the Hindu Kush). The infrequent, large earthquakes (up to  $M=8^+$ ) are confined to the Gissar Kokshal zone, along the front of the Southern Tien Shan, but that zone has a relatively low level of microearthquake activity. The greatest concentration of seismicity, in terms of numbers, is within the sediments of the Tadjik Depression, but there are few events here with magnitude greater than 5.5. Beneath the sediments, the third type of seismicity is that within the basement itself. The activity in the Depression is especially high in its northeastern end near

Garm, in the area of greatest convergence between the Pamir and Tien Shan. In this area, the sediments have been thrust up and out of the Depression itself, onto the Gissar Kokshal zone, producing a complex three dimensional distribution of seismicity in which all three types of activity overlap (Leith and Simpson, 1986a).

### **Salt Domes and Seismicity near Kulyab, Tadjikistan**

A strong concentration of shallow seismicity (up to magnitude 5) stands out in the relatively low activity of the southern Tadjik Depression near the town of Kulyab (Figure 20). There are also large salt domes exposed at the surface in this same region. We have used Landsat and topographic data in conjunction with the seismicity catalog to investigate the correlation between the seismicity and the salt domes (Leith and Simpson, 1986b).

Figure 21 shows a black and white version of the Landsat image for the Kulyab area. Areas of high infrared return (vegetation) have been set black in this image so that the dark regions in valleys are irrigated farm land. The two light colored circular features are salt domes. Figure 22 shows a perspective view (from the SW) derived by creating a 3D image from the digital terrain data and adding texture from the Landsat image. The major dome to the south (Mumin dome) is devoid of vegetation and stands 870 meters above the surrounding plain. The high topography beyond the Mumin dome is associated with the Sari-Chashma salt diapir, a buried structure identified in geophysical surveys. Figure 23 shows the original and shaded relief versions of the topographic data with seismicity superimposed. Most of the cluster of seismicity in the southeastern corner of the image followed a  $m=5.2$  earthquake on April 2, 1973.

It is our conclusion (Leith and Simpson, 1986b) that the seismicity is clearly related to the salt doming. The highest level of current activity is not located at one of the domes which has pierced the surface, but is near the buried Sari-Chashma diapir, a buried structure which appears to be actively rising. Because of the lack of depth control in the Soviet hypocentral locations, it is not clear whether the earthquakes result from increased stress within the sediments above the dome structure or are related to fracturing near or within the salt layer at depth. To our knowledge, this is the only reported case of seismicity associated with active salt doming. More detail is to be found in Leith and Simpson (1986b, included as appendix to this report).

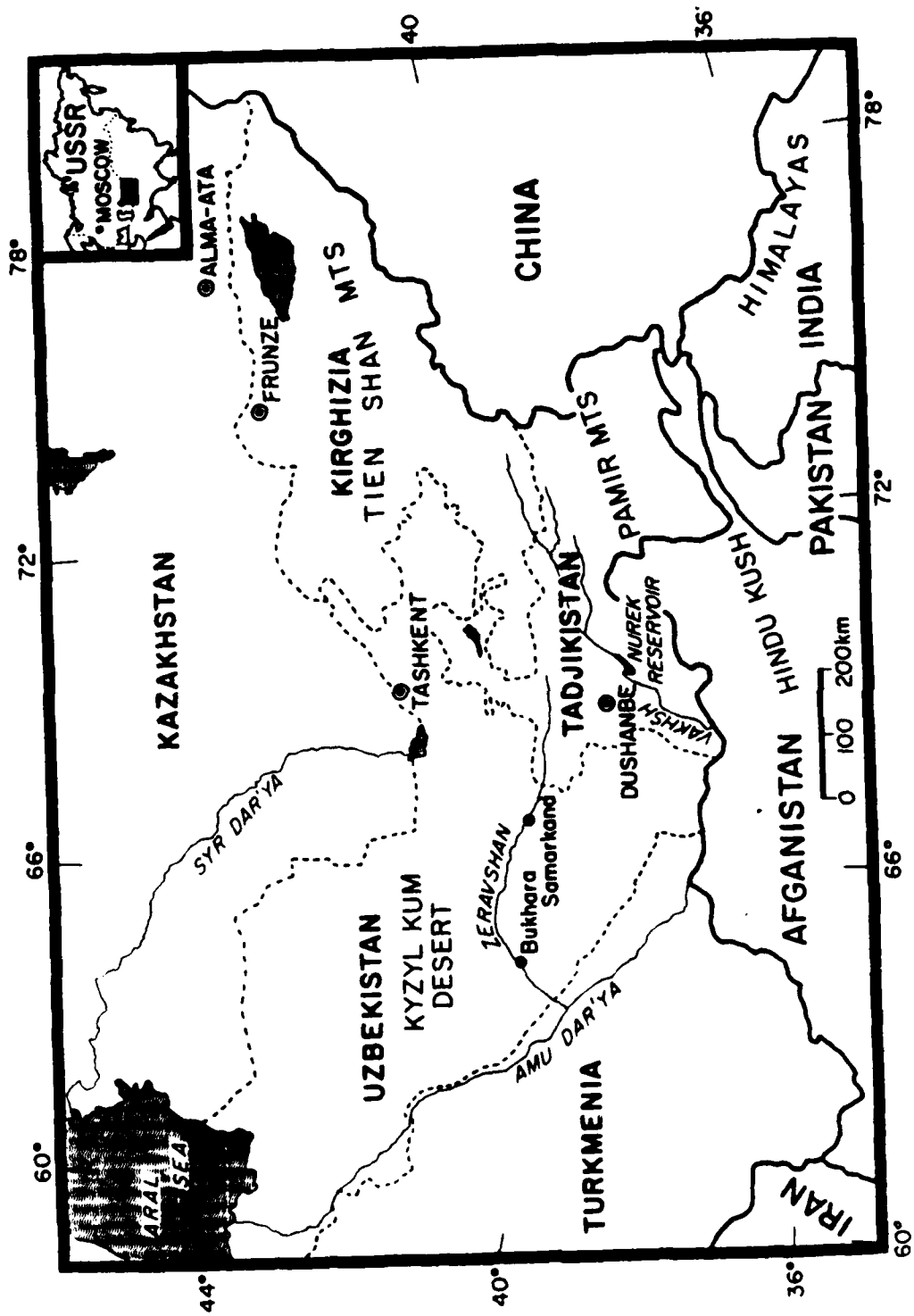


Figure 1 Soviet Central Asia and surrounding areas.

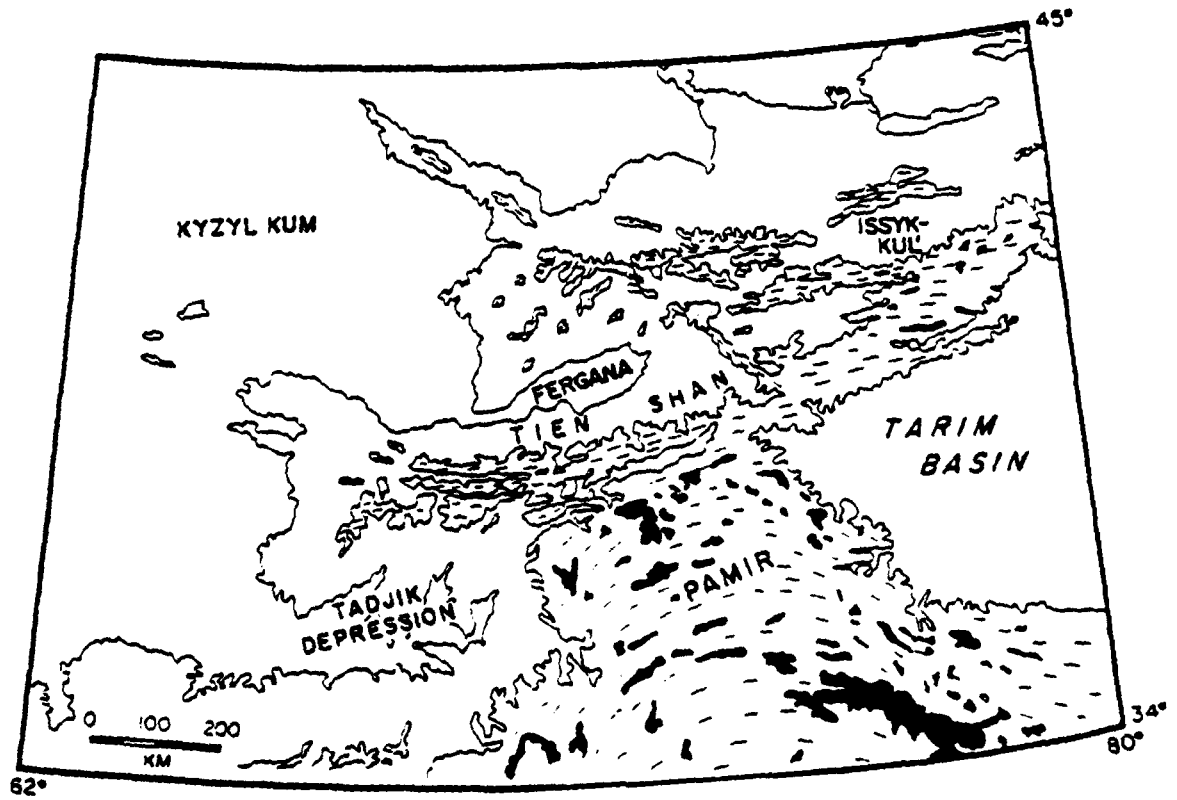
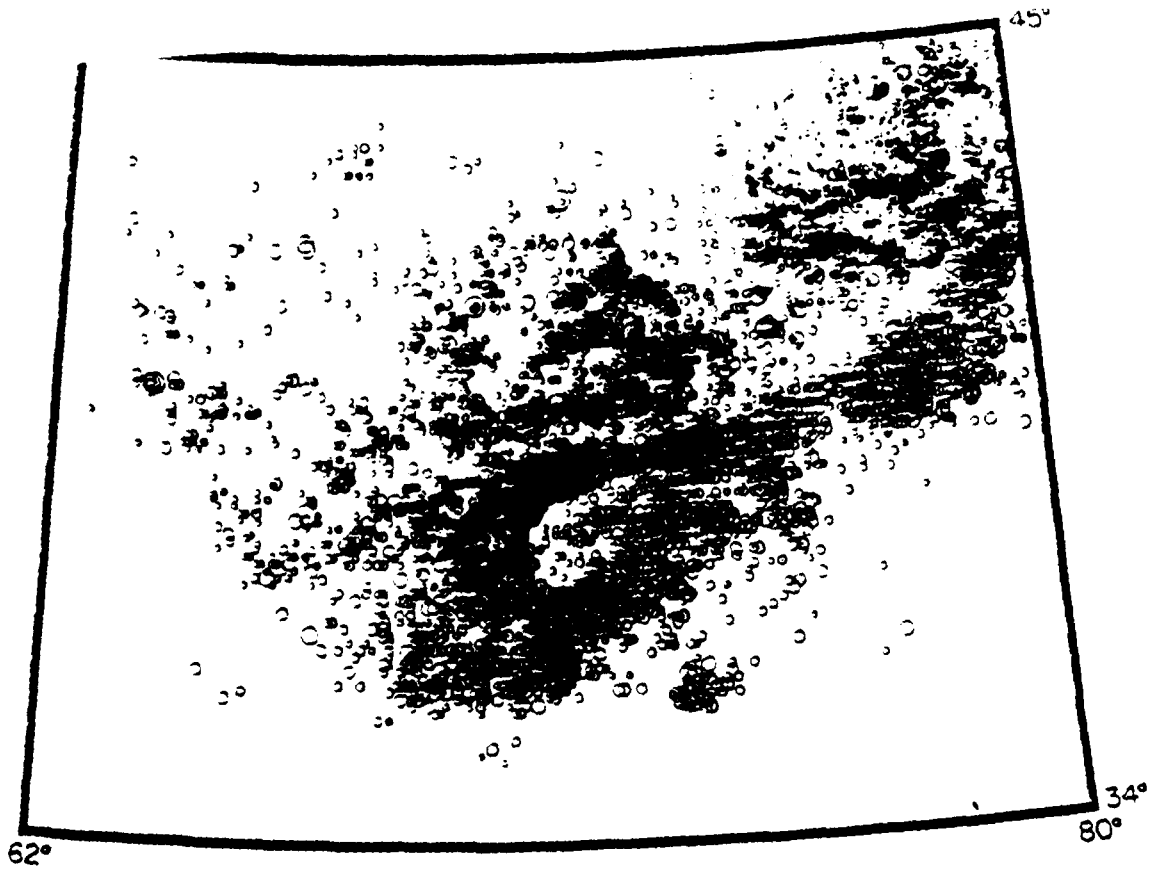


Figure 2 Epicenter map of earthquakes in ZSSR 1964-1977. A comparison with the simplified topographic map (bottom, same area) shows that many of the active seismic zones occur along the edges of the major mountain ranges, with relatively low activity within the the ranges themselves and within major basins.

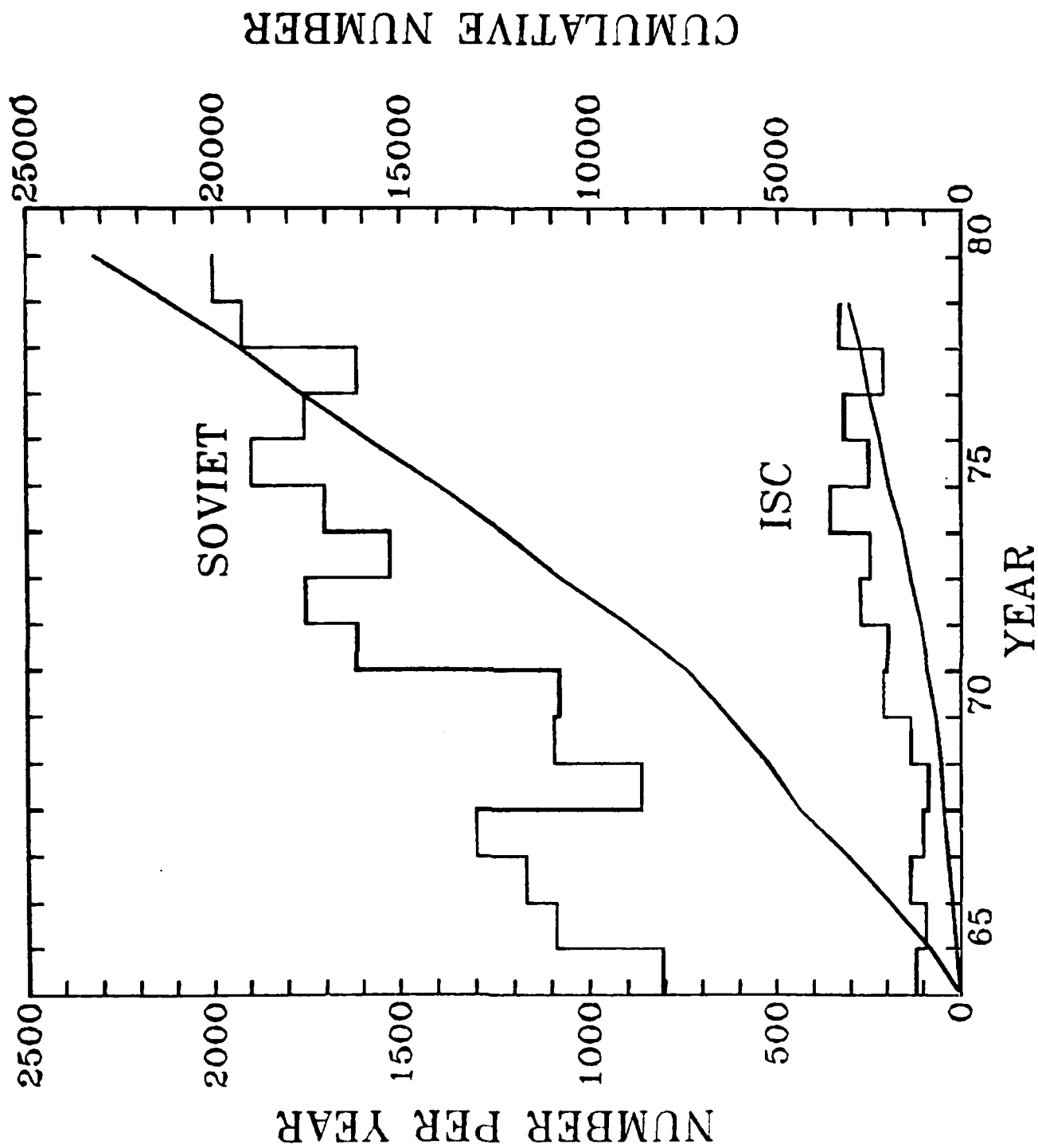
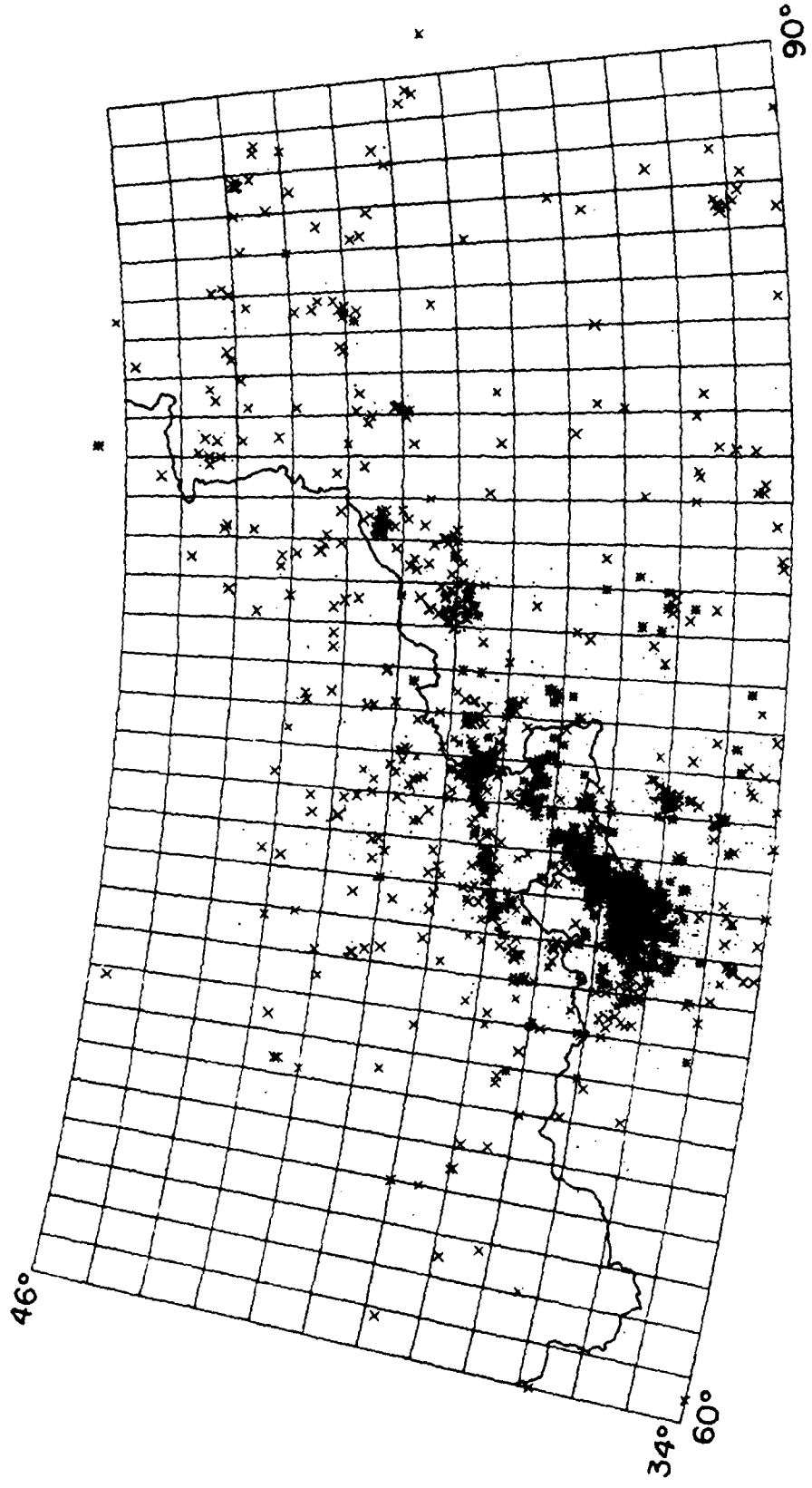


Figure 3 Cumulative and annual numbers of earthquakes in the ZSSSR and ISC catalogs.

IS 62 741 LAMB ELL. CORR. ST. (LAT. 38.42) ST. 3-65



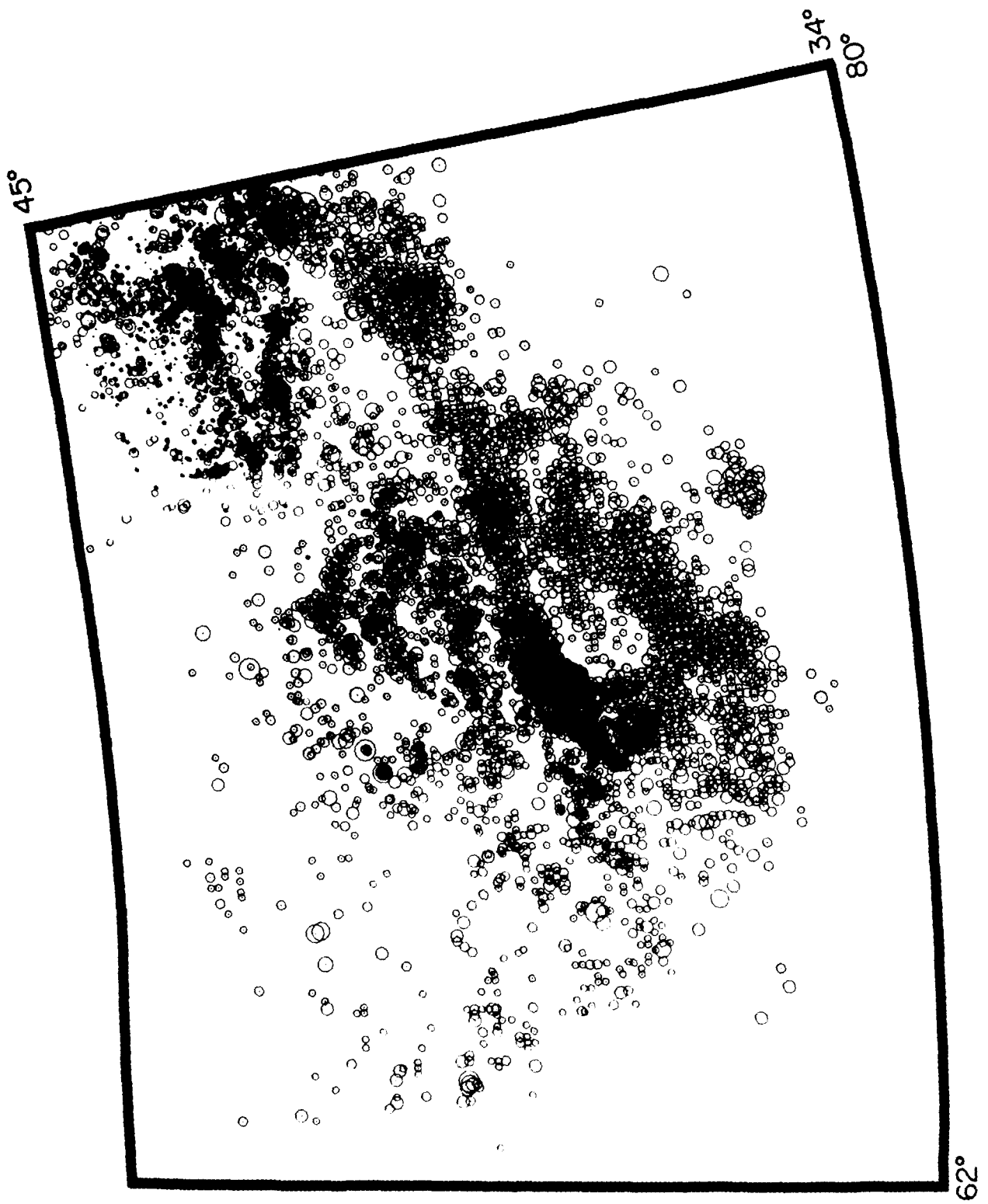
ISC 1962-1974

X - depth < 70 km

\* - depth > 70 km

Figure 4 Epicenter map of earthquakes in ISC catalog 1962- 1974.

Figure 5 Epicenter map of earthquakes in ZSSSR catalog 1964-1977.



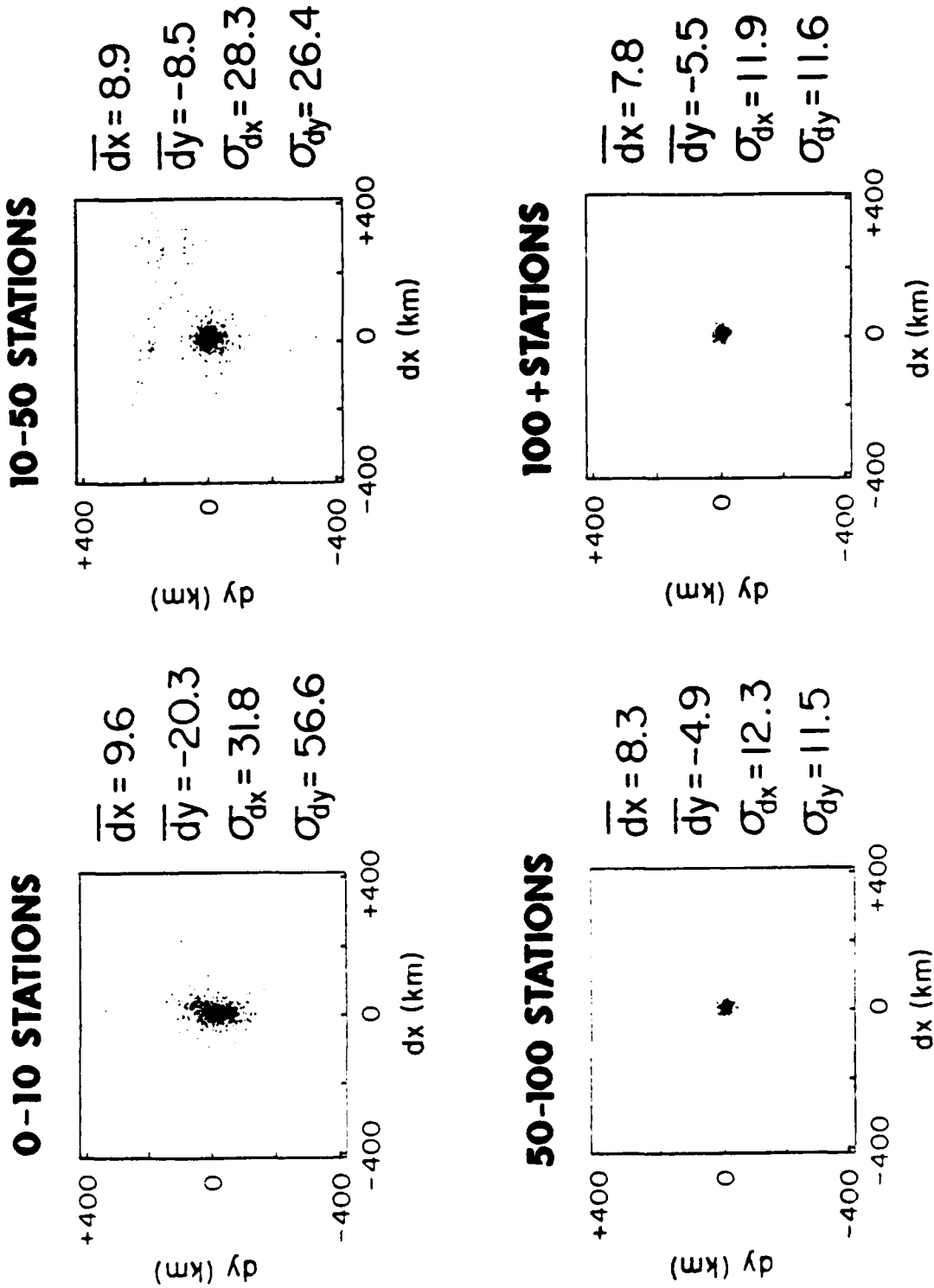


Figure 6 Difference in latitude and longitude (dy and dx) between ZSSSR location (origin in each graph) and ISC location for all earthquakes common to both catalogs, as a function of the number of stations used for location by ISC.

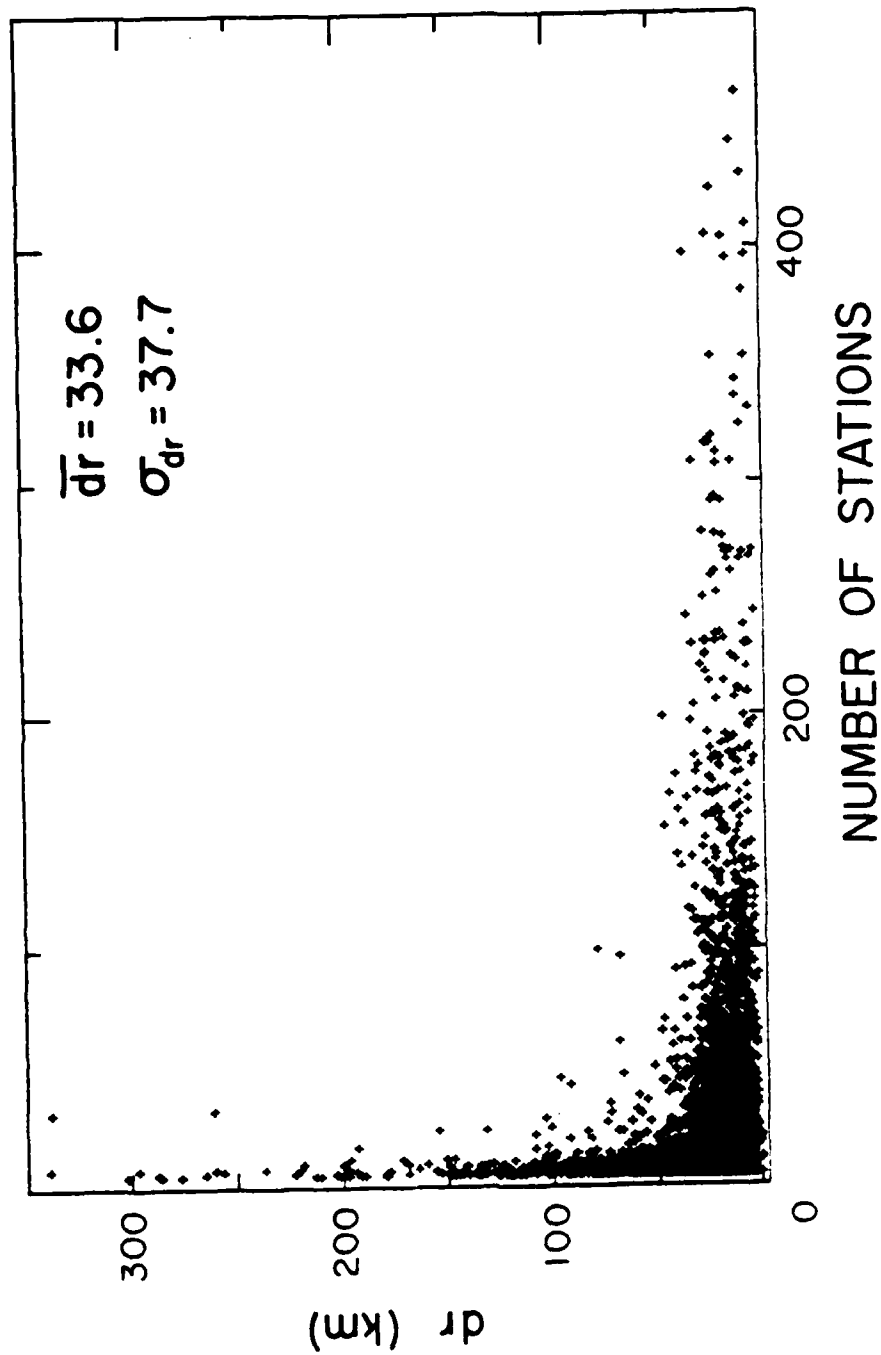


Figure 7 Difference in epicentral location (dr) between ISC and ZSSSR catalogs as a function of the number of stations used for location by ISC.

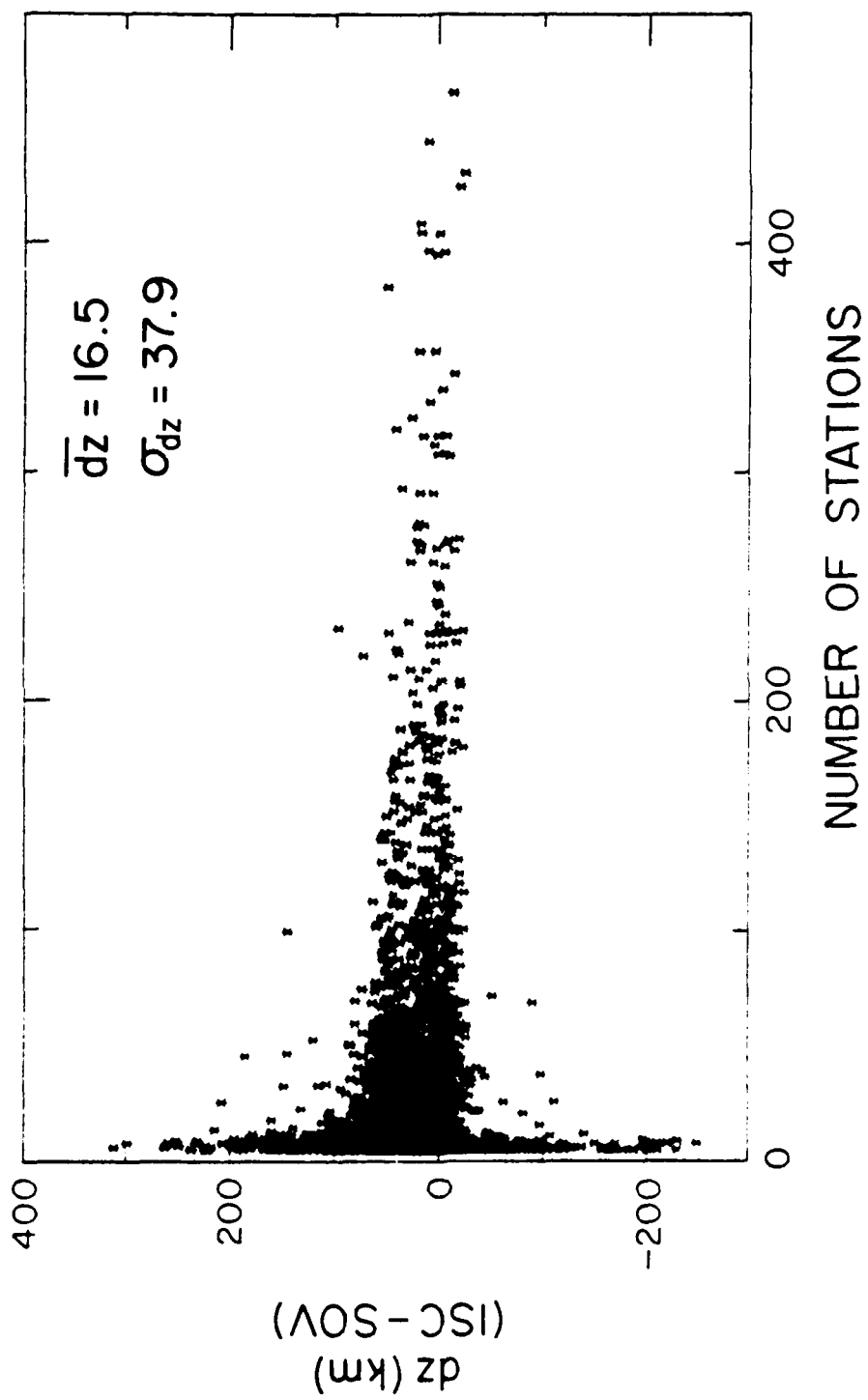


Figure 8 Difference in depth (dz) between ISC and ZSSSR catalogs as a function of the number of stations used for location by ISC.

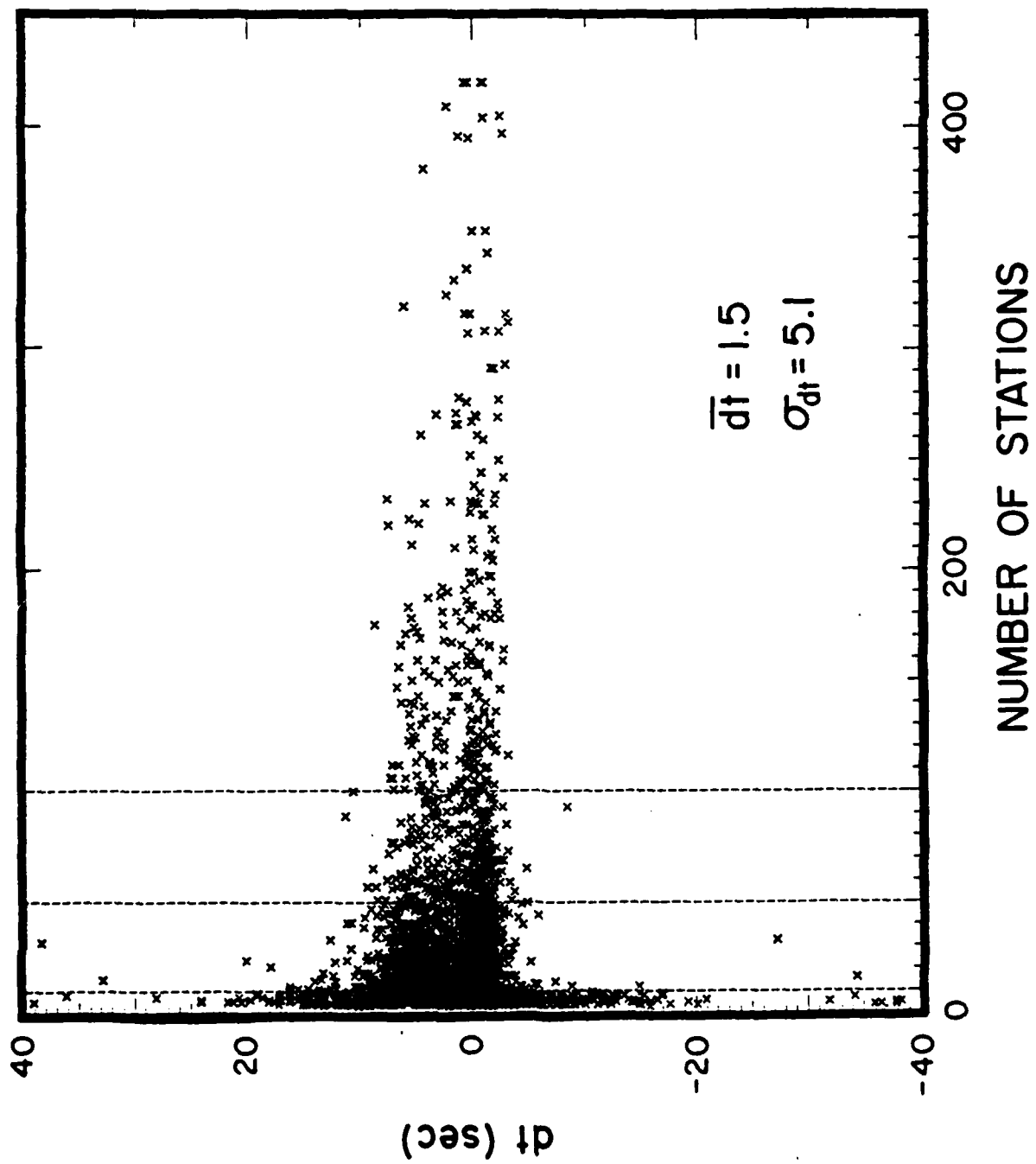


Figure 9 Difference in origin time (dt) between ISC and ZSSSR catalogs as a function of the number of stations used for location by ISC.

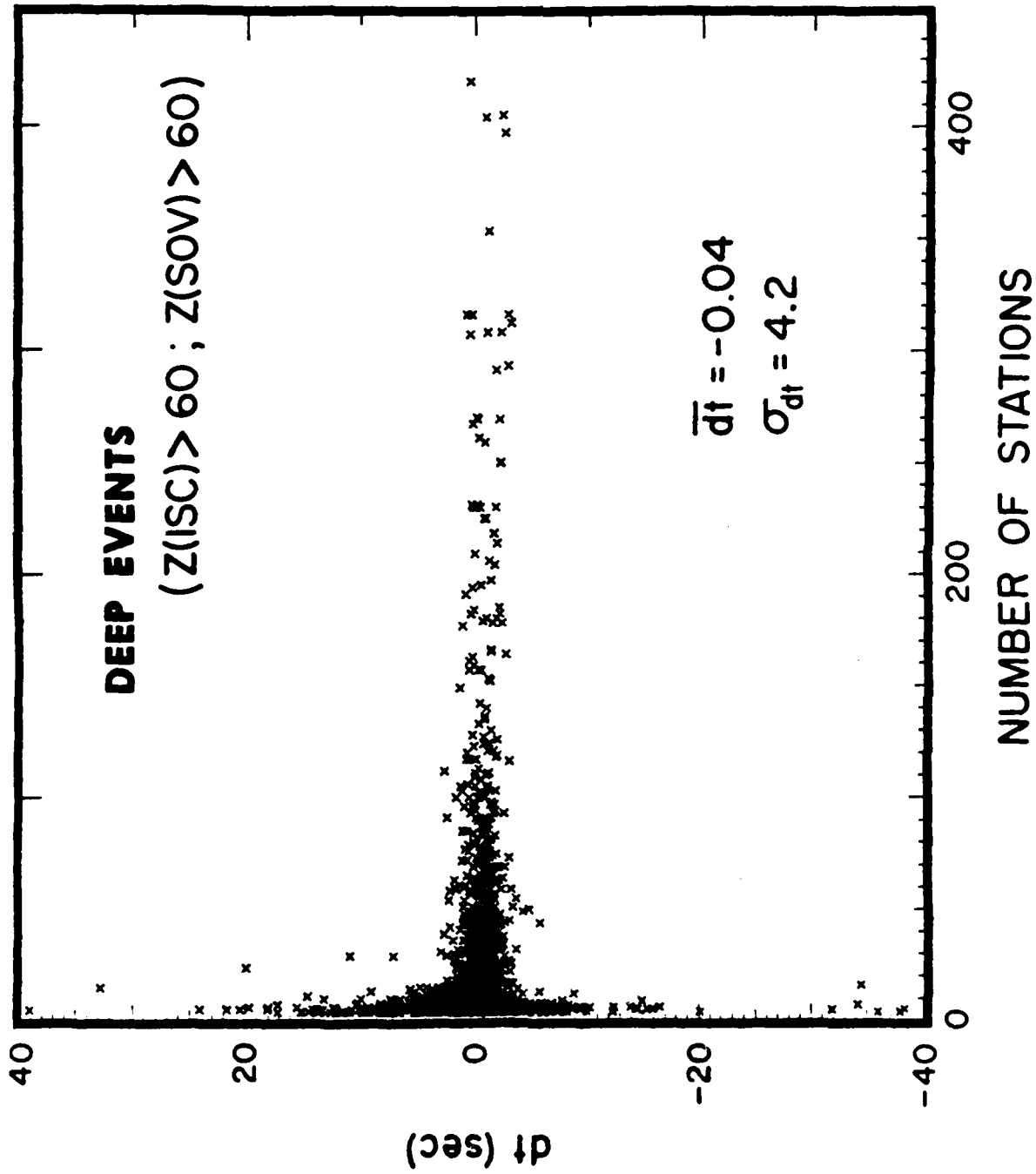


Figure 10 Difference in origin time (dt) between ISC and ZSSSR catalogs, as a function of the number of stations used for location by ISC, for deep events (those for which both the ZSSSR and ISC depths are greater than 60 km). (Note - positive dt is for ISC origin times later than ZSSSR).

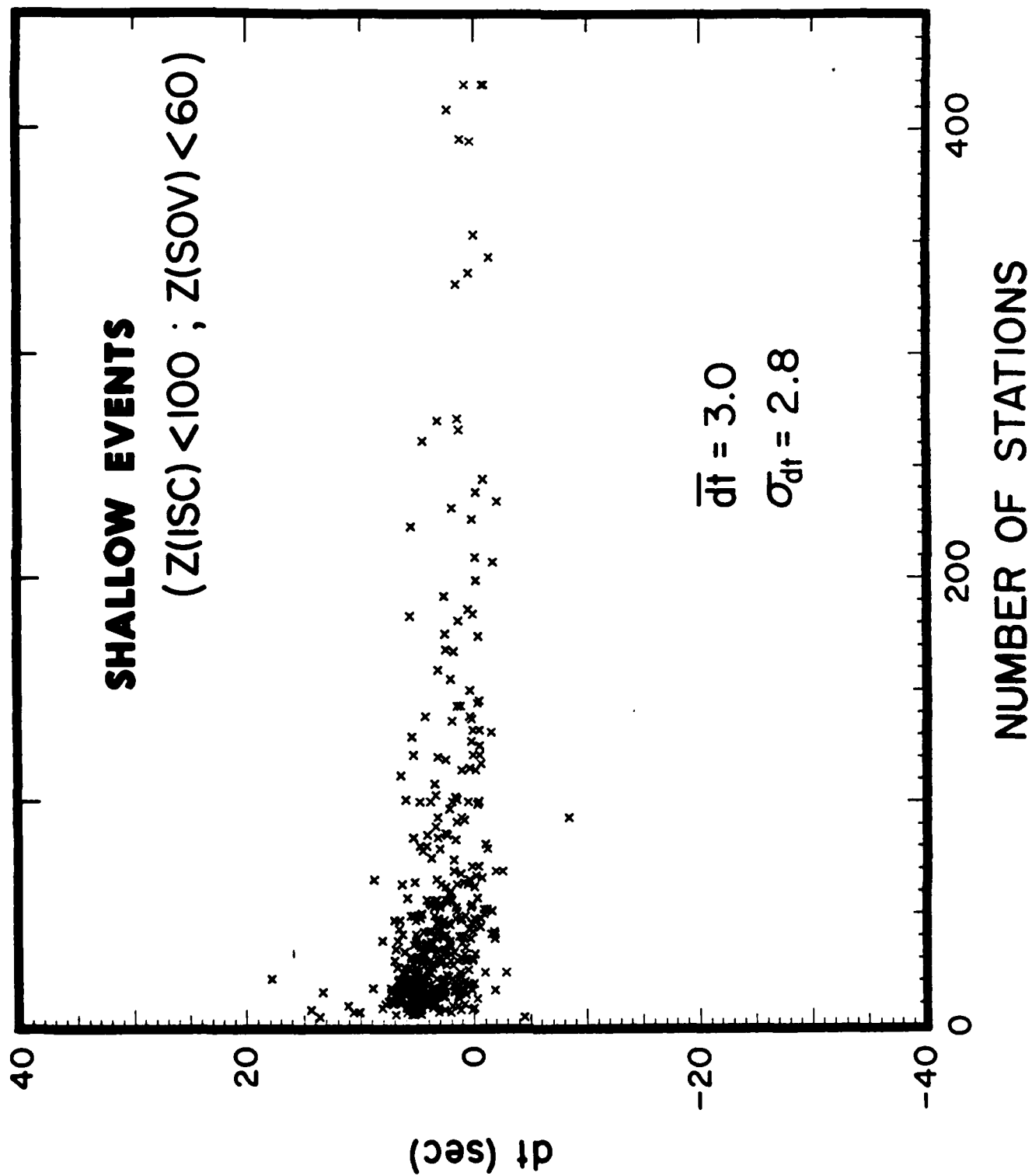


Figure 11 Same as Figure 10, but for shallow events (those for which the ZSSSR depth is less than 100 km and the ISC depth is less than 60 km, but neither are the default depths of 0 or 33 km).

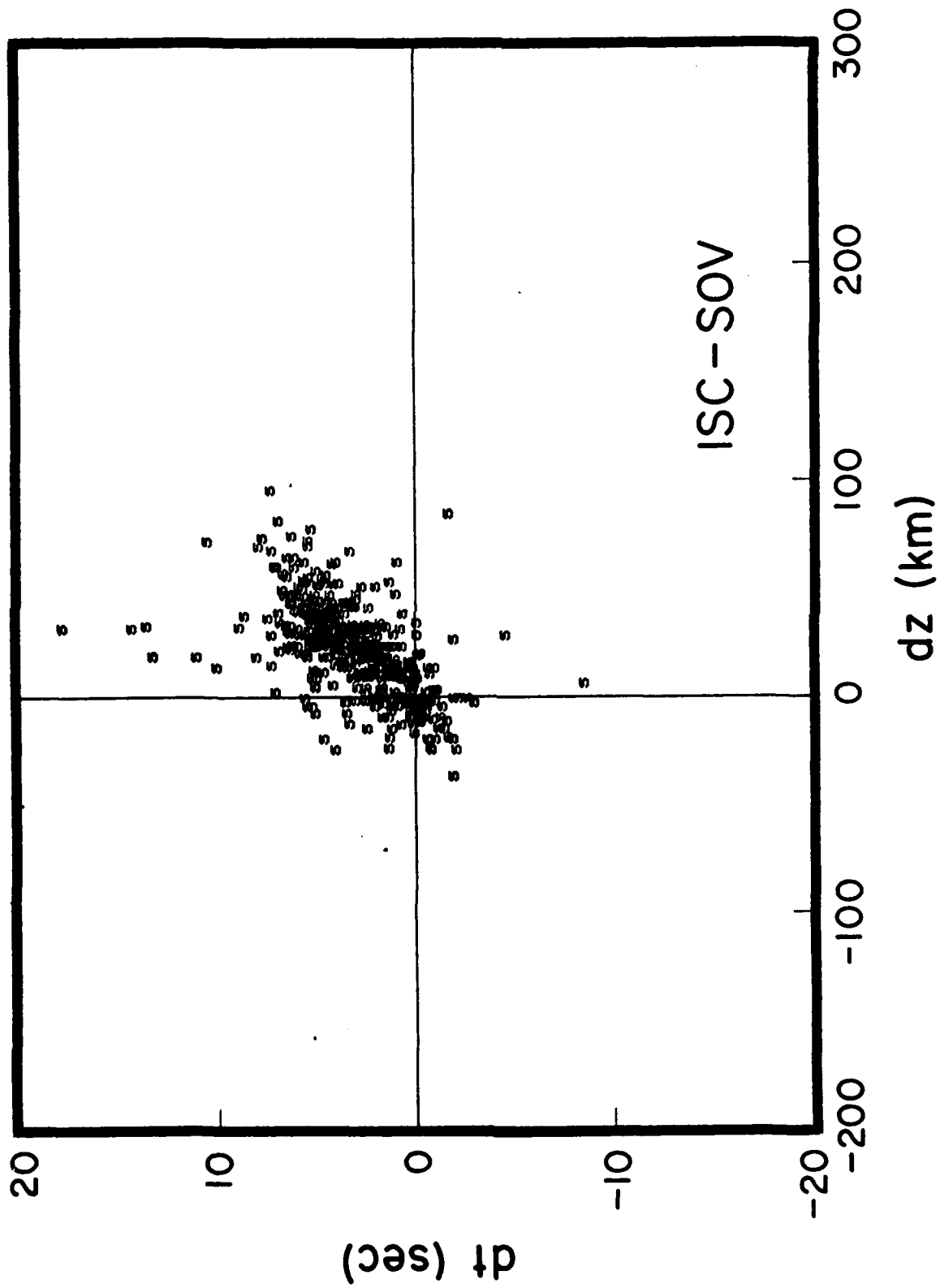


Figure 12 Difference in origin time ( $dt$ ) vs difference in depth ( $dz$ ) for shallow events (as defined in Figure 11).

$$k_{\text{less}} = 1.93 * \text{mag} + 3.29$$

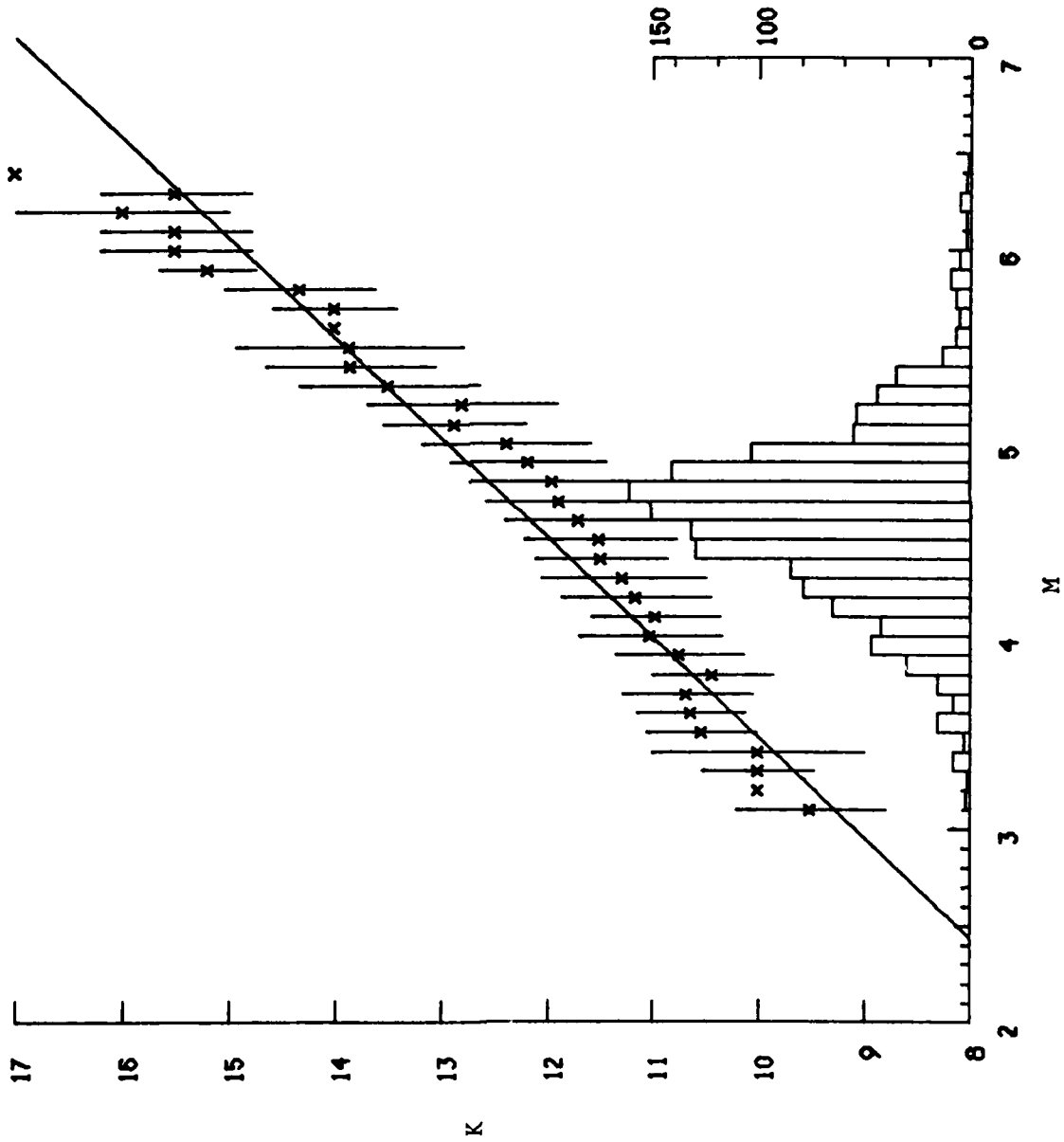


Figure 13 ZSSSR energy class (k) vs ISC magnitude ( $m_p$ ) and number of earthquakes in ISC for each 0.1 magnitude increment. Least squares regression (with weight inversely proportional to square of the standard deviation of the average magnitude for each magnitude interval) is shown and compared to the standard formula of Rautian.

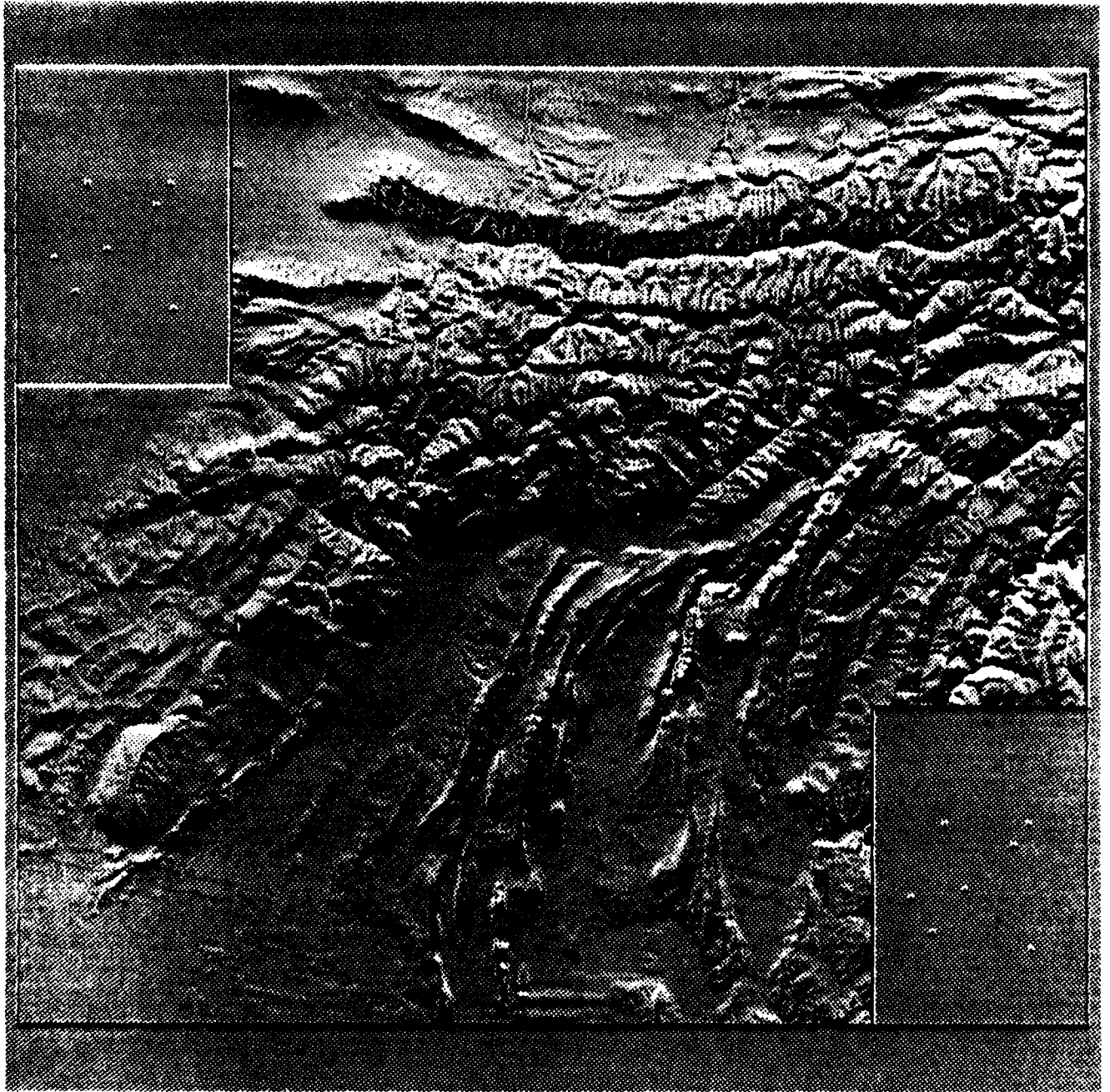


Figure 14 Topographic map of the Tadjik Depression and Southern Tien Shan created from DMA digital terrain data. Blanks in upper left and lower right are missing data. Geographic locations are indicated for comparison with other maps. Shading is for illumination from the north.

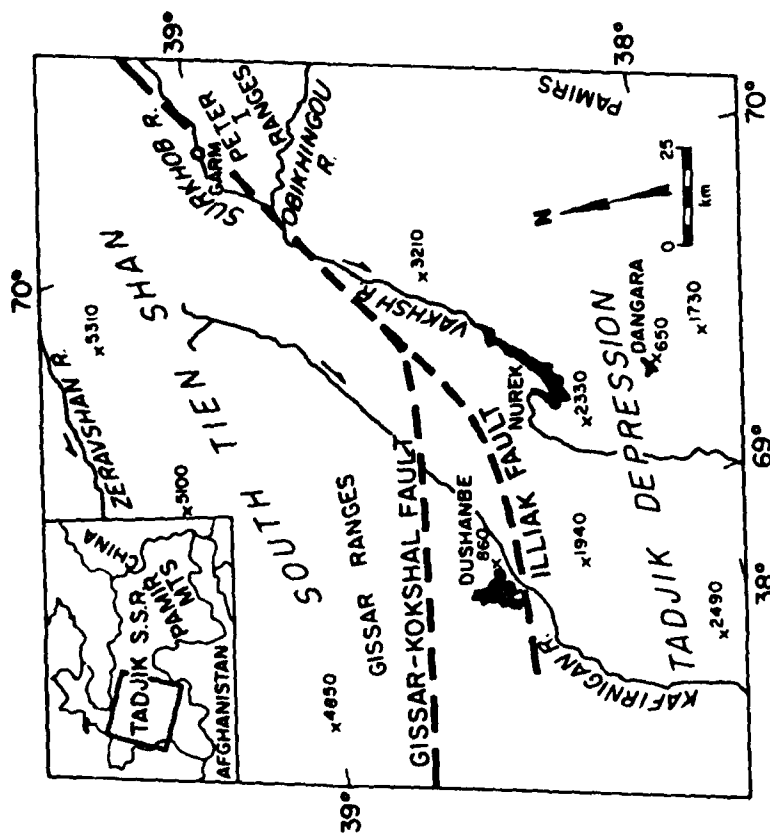
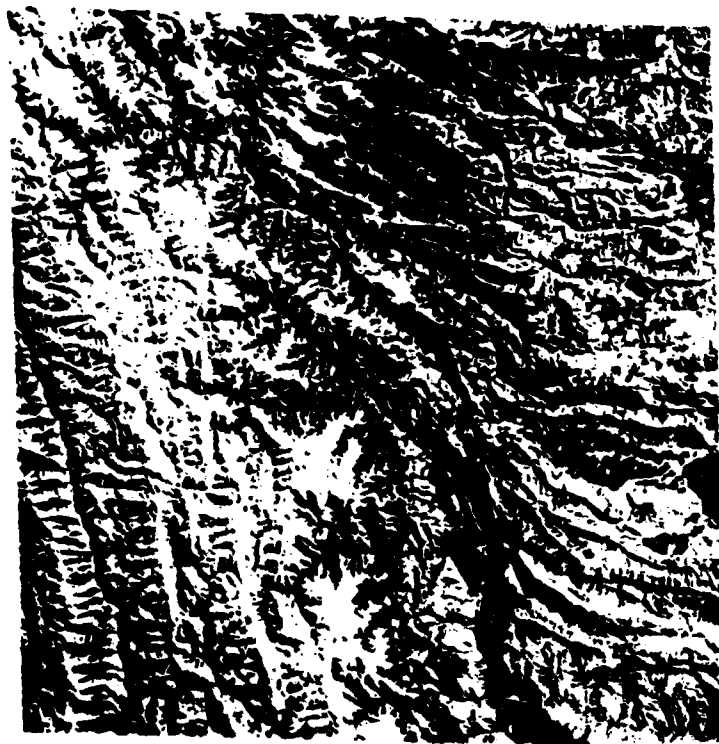


Figure 15 Landsat image (right) and location map (left) for a portion of the region shown in Figure 14 (from Simpson and Negmatullaev, 1981).



Figure 16 Raw digital terrain data with intensity proportional to elevation.

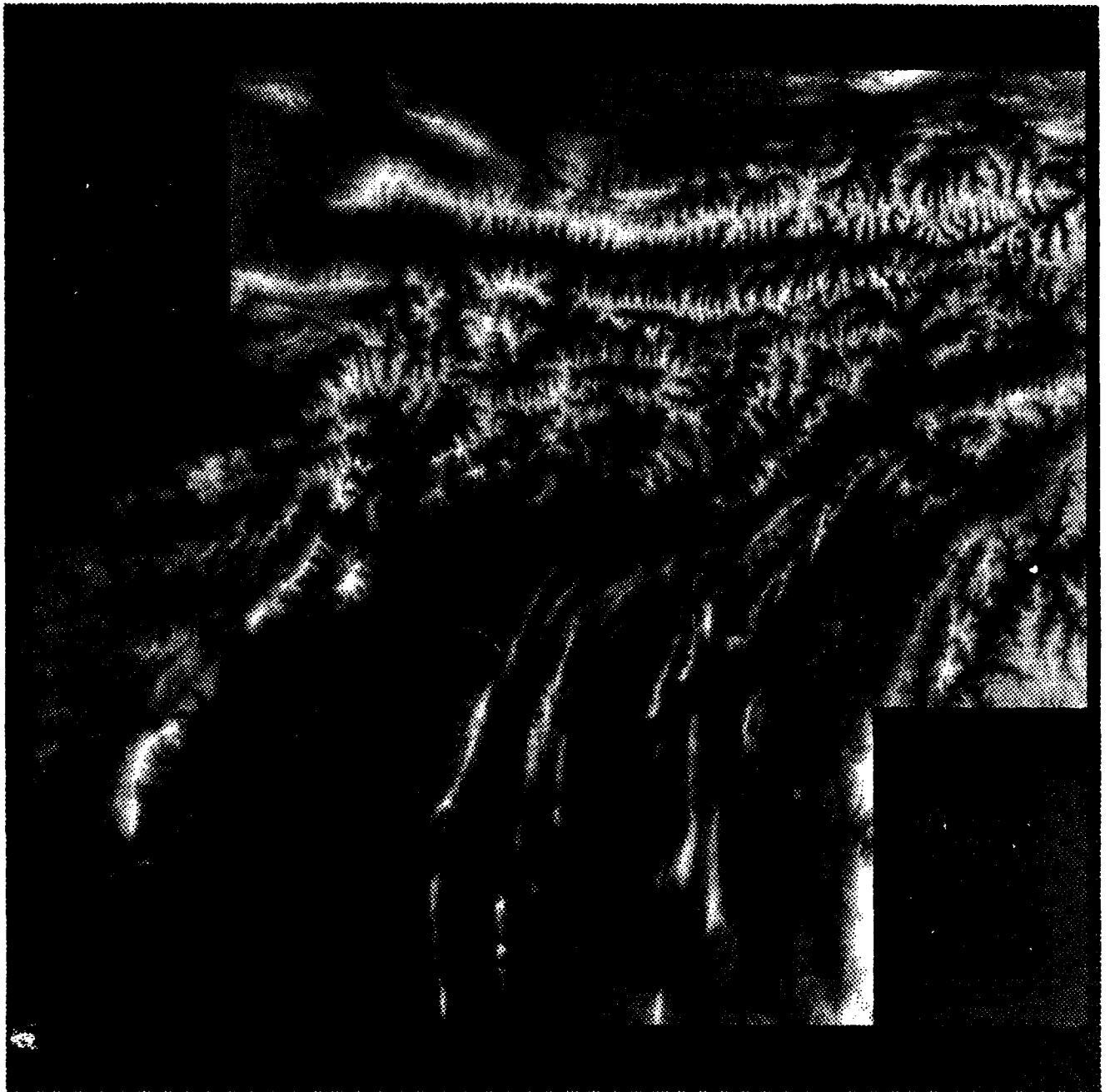


Figure 17 Terrain data with enhancement to locally adjust contrast for higher resolution of small scale features.

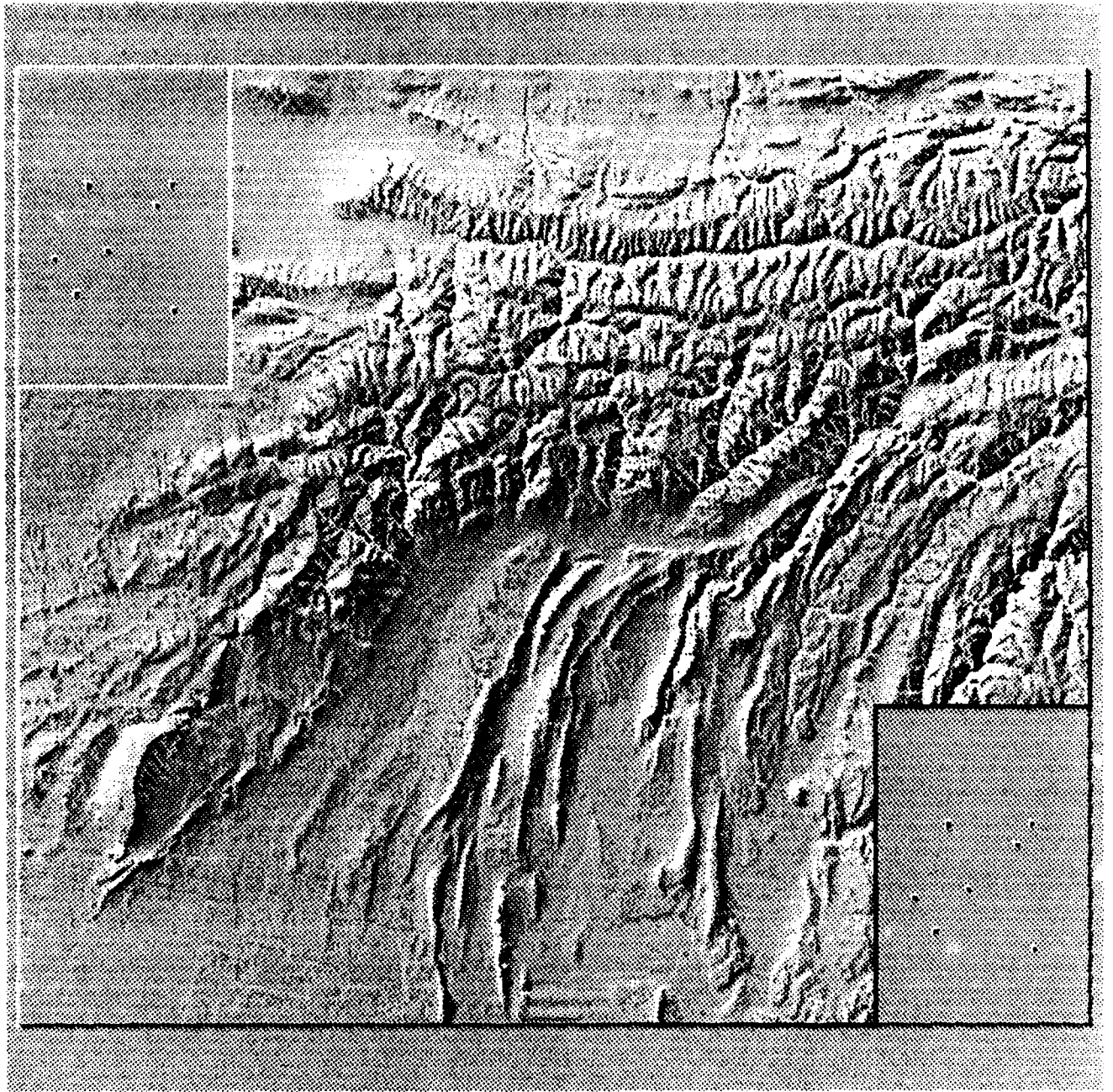


Figure 18 Shaded relief map with illumination from the northwest.

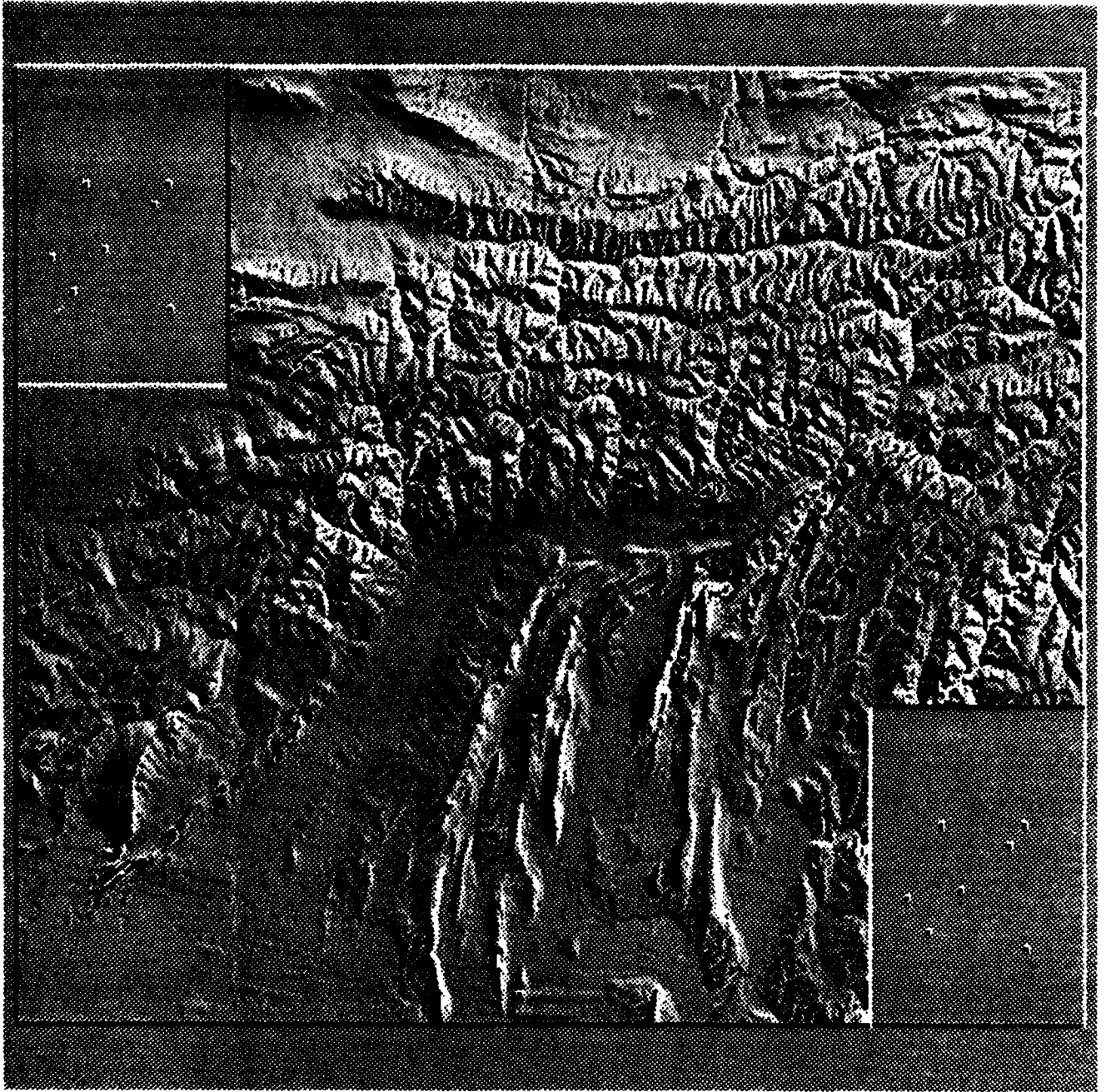


Figure 19 Shaded relief map with illumination from the northeast. Comparison with Figures 14 and 18, especially of river valleys in the northeast segment, shows how different gradient determinations (illumination directions) enhance features at different azimuths.

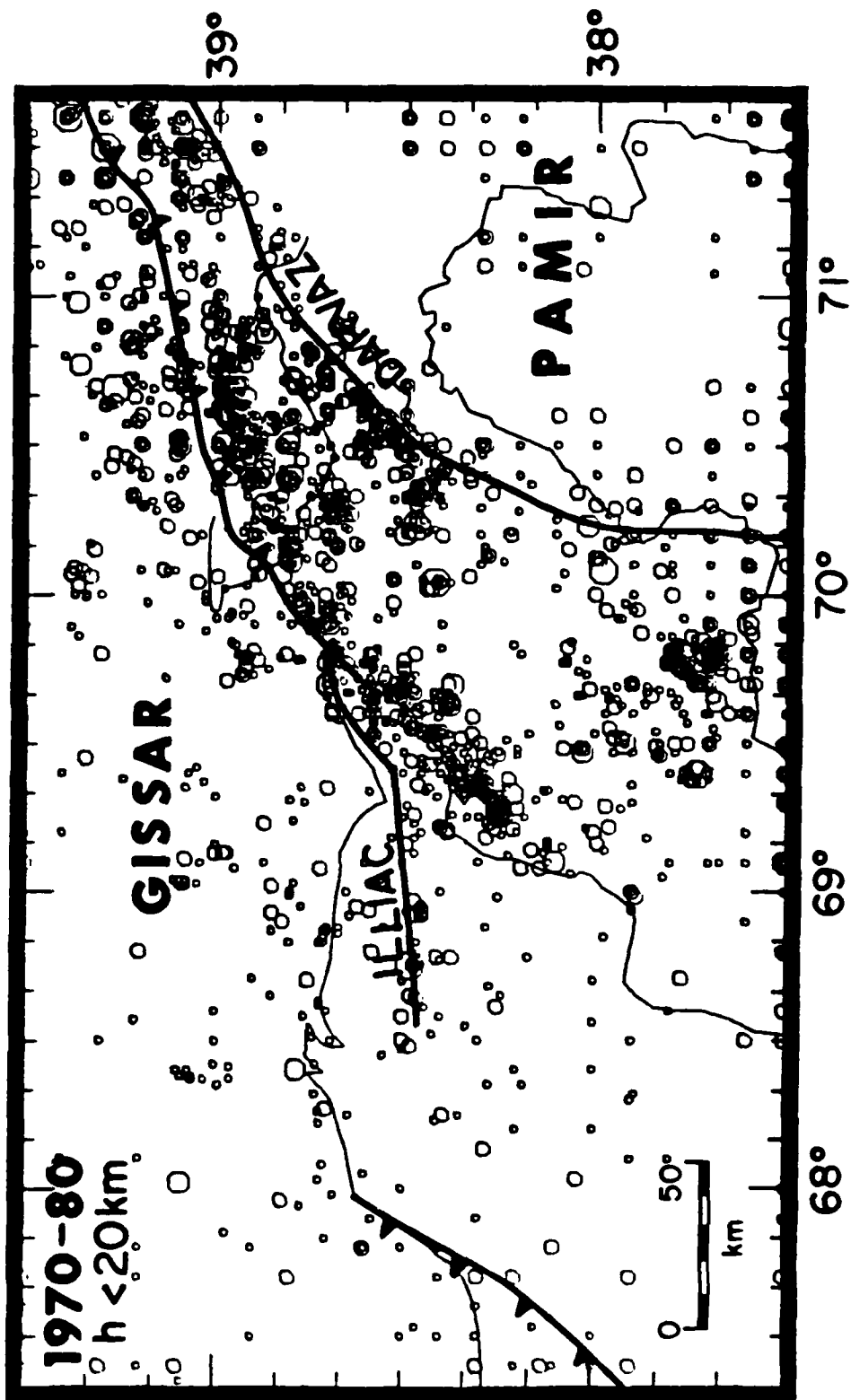
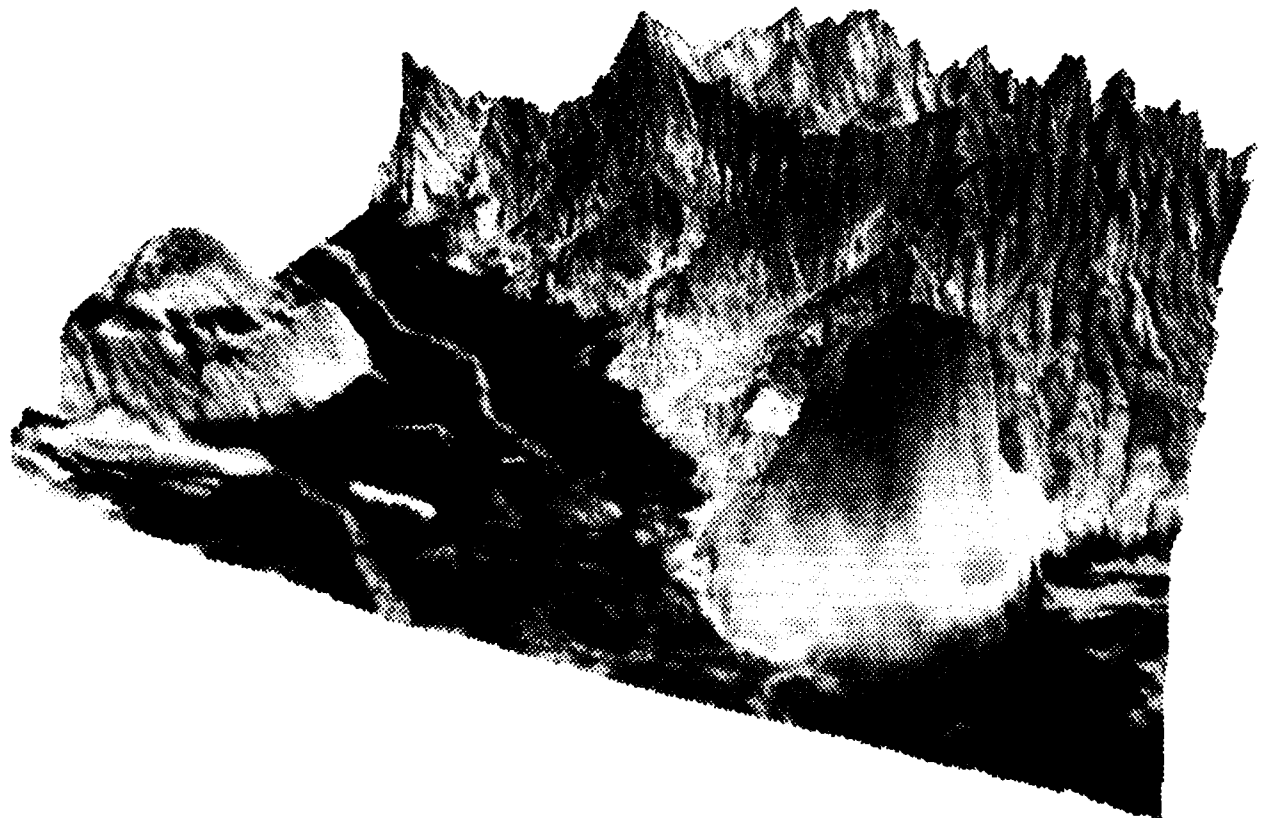


Figure 20 Seismicity of the Tadjik Depression and Gissar Kokshal seismic zones from the ZSSSR earthquake catalog for 1970-80. Kulyab seismicity is the cluster in the southern part of the map near 69°45' E.



Figure 22 Perspective view of the area show in Figure 21. Digital terrain data have been used to create a perspective image (viewed from the southwest) and the Landsat image has been registered with it to create surface texturing. The salt dome in the lower right stands more than 800 m above the surrounding valley.



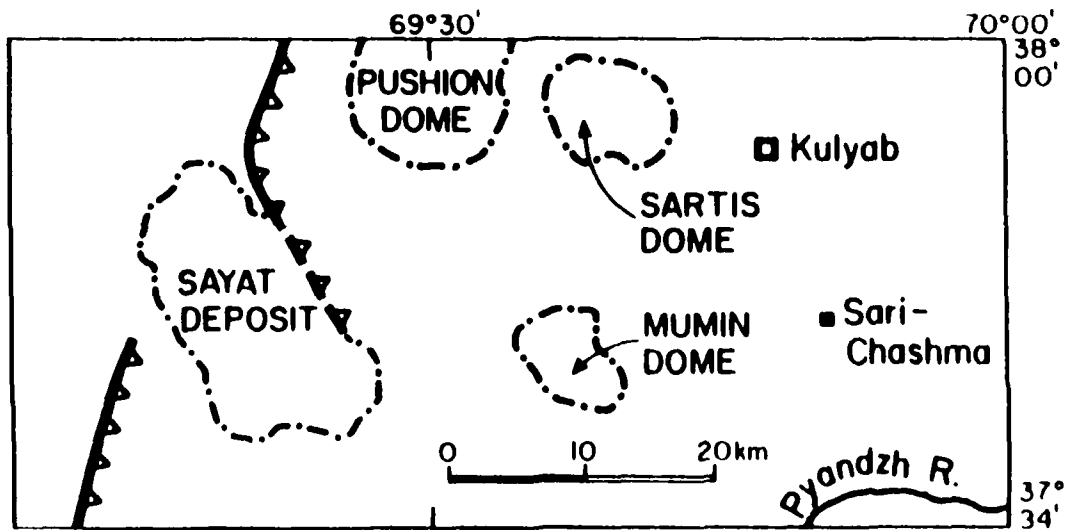
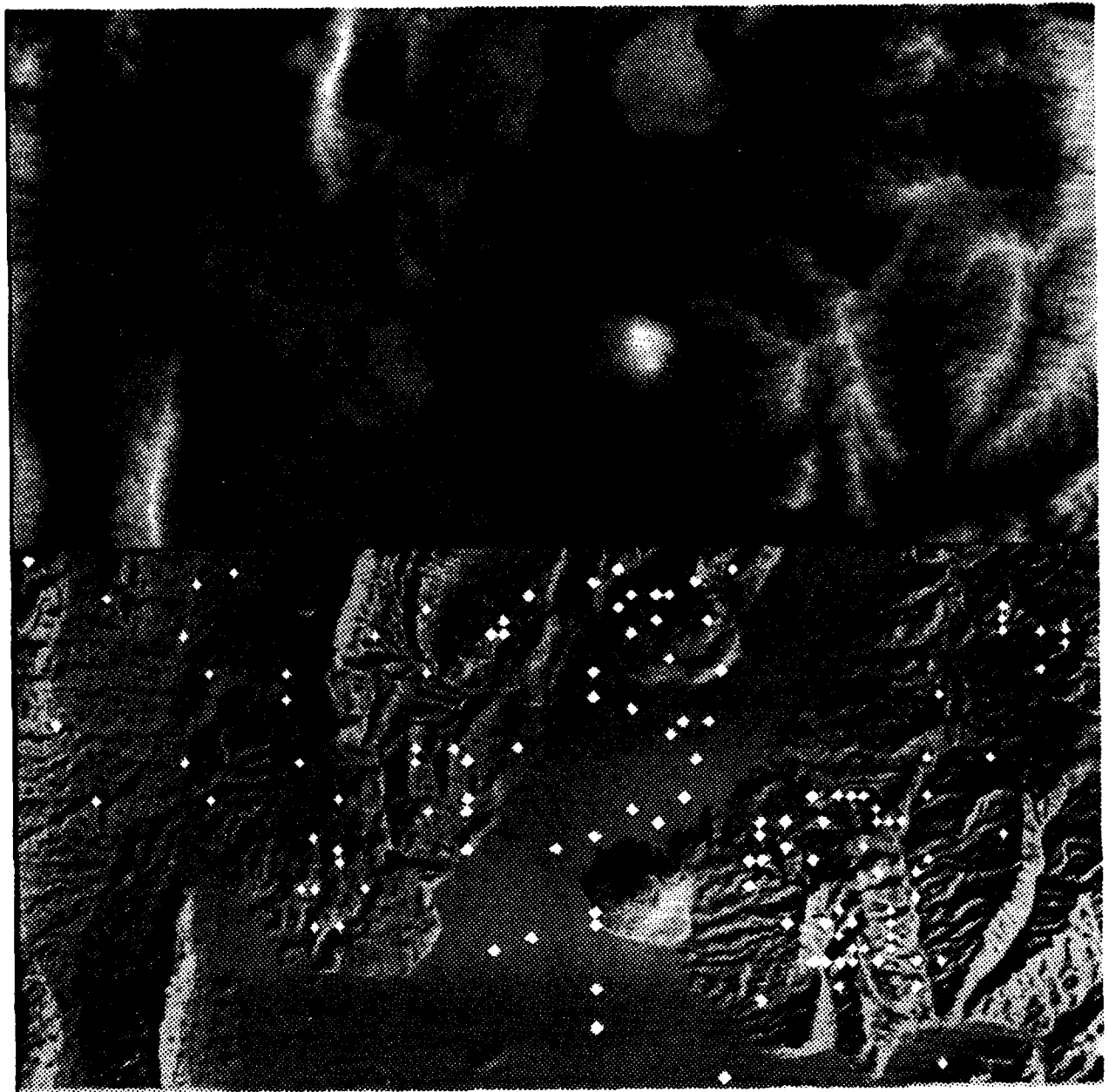


Figure 23 (top) Raw digital terrain data for the Kulyab area. (middle) Shaded relief map with seismicity superimposed. (bottom) Location map (from Leith and Simpson, 1986).

## **REFERENCES**

- Keith, C., D. W. Simpson, and O. Soboleva, Induced seismicity and deformation style at Nurek reservoir, Tadjik, SSR, J. Geophys. Res., **87**, 4609-4624, 1982.
- Kristy, M., and D. W. Simpson, Seismicity changes preceding two recent Central Asian earthquakes, J. Geophys. Res., **85**, 4829-4837, 1980.
- Leith, W., and W. Alvarez, Structure of the Vakhsh fold-and-thrust belt, Tadjik SSR: Geologic Mapping on a Landsat image base, Geol. Soc. Am. Bull., **96**, 875-885, 1985.
- Leith, W., and D. W. Simpson, Seismic domains within the Gissar Kokshal seismic zone, Soviet Central Asia, J. Geophys. Res., **91**, 689-699, 1986a.
- Leith, W., and D. W. Simpson, Earthquakes related to active salt doming near Kulyab, Tadjikistan, USSR, Geophys. Res. Lett., **13**, 1019-1022, 1986b.
- Leith, W., D. W. Simpson, and W. Alvarez, Structure and permeability: Geologic controls on induced seismicity at Nurek reservoir, Tadjikistan, USSR, Geology, **9**, 440-444, 1981.
- Rautian, T. G., Earthquake energy (in Russian), in Methods of Detailed Investigations of Seismicity, U. V. Riznisenko, ed., Academy of Sciences USSR, Moscow, pp. 75-113, 1960.
- Simpson, D. W., and S. K. Negmatullaev, Induced seismicity at Nurek reservoir, Tadjikistan, USSR, Bull. Seismol. Soc. Am., **71**, 1561-1586, 1981.

## EARTHQUAKES RELATED TO ACTIVE SALT DOMING NEAR KULYAB, TADJIKISTAN, USSR

William Leith and David W. Simpson

The Lamont-Doherty Geological Observatory of Columbia University

*Abstract.* In the region near Kulyab, Tadjikistan, hundreds of shallow earthquakes with magnitudes greater than 2½ have been reported in Soviet yearly catalogs since 1964. This area appears as a well-defined cluster of activity, distant from the line of epicenters that defines the Gissar-Kokshal seismic zone, to the north of the Pamir ranges. The geology of this region is dominated by the presence of numerous salt domes, surrounded by Neogene and Quaternary continental deposits. The spatial relationship between these earthquakes and the salt domes suggests that the two phenomena may be related. Moderate earthquakes ( $M > 5$ ) occurred in 1972 and 1973, and intensities of surface shaking greater than  $MM=6$  were reported from earthquakes in 1937, 1952, 1969, 1972, 1973 and 1978. The earthquake on 2 April 1973 and its aftershocks were located in a region where no salt domes have been mapped at the surface. However, a buried salt diapir has been mapped at depth by geophysical means. These earthquakes may result from active salt diapirism at depth. The mechanism for producing this seismicity could be either the active fracturing of the cap rock by the rising diapir, or the concentration of tectonic stresses in the thinned section above and adjacent to the diapir. The salt-related earthquakes may produce lower frequency radiation than other events of the same size.

### Introduction

Salt deposits, and specifically salt domes, are currently of special interest as possible sites for decoupling of underground nuclear explosions [Hannon, 1985], or for the underground storage of radioactive nuclear waste, petroleum or gas condensate [Cohen, 1977; Borg, 1983]. The relatively structureless, homogeneous nature of salt formations, combined with the high solubility of rock salt, lend these formations to the mining of the large stable cavities that would be required to decouple a small underground nuclear explosion. In contrast with bedded salt deposits, salt domes are considered ideal cavity sites because of their large vertical dimensions and relatively pure salt content. In terms of explosion decoupling and the detection of clandestine nuclear weapons tests, earthquakes that are spatially associated with salt domes pose the obvious problem of discrimination. In terms of engineering activities, either on the surface or within the salt dome, earthquakes represent a hazard to the stability of any cav-

ity constructed. Also, as potential sites for hazardous waste or other liquid storage, they may affect the short-term permeability of the cavity walls.

There is an extensive literature on salt diapirism [e.g., Lerche, 1986]. Salt domes are produced by the post-depositional flow of bedded salt upward through the overlying rock formations, because of the gravity (density) instability inherent in buried salt. It is generally considered necessary for salt dome regions to have undergone some degree of tectonism (associated with sedimentary loading) in order for diapirs to develop. Therefore, the process of salt dome formation is unstable and episodic and the rates of salt dome uplift are highly variable, depending on both the tectonics of the region and the state of maturity of the diapir [Jackson and Talbot, 1986].

Salt is an extremely weak rock, and deforms ductilely at geological strain rates [Carter and Hansen, 1983]. Salt areas are generally not associated with earthquakes, and to date there is no literature associating earthquakes with active salt doming. Where studies have been made of the seismicity of salt dome areas in East Texas and the Gulf Coast [Dorman and others, 1977; Racine and Klouda, 1979], no definitive correlations between salt structures and earthquakes have been made. Nevertheless, sounds of salt movement have been detected in salt dome regions in Iran [Kent, 1979], and rock bursts have occurred in underground salt mines [see Baar, 1977]. Those salt dome areas where detailed seismicity studies have been made (east Texas, Louisiana, Oklahoma) are also areas where the domes are mature [Jackson and Talbot, 1986] and tectonic strain rates are low. Our study, from an area that is currently deforming at a relatively high rate, therefore contrasts with studies of the seismicity of salt dome areas in the U.S.

This letter describes the geological and seismological attributes of the Kulyab salt dome area, in the southwestern Tadjik SSR. The seismicity that marks this area stands out as a cluster of epicenters distinct from the main trend of the Gissar-Kokshal seismic zone (Figure 1), 50-100 km north of Kulyab [Leith and Simpson, 1986].

### Geology

The Soviet republic of Tadjikistan is marked by an active tectonics and a high rate of natural seismicity. As part of the India-Asia collision, the Jurassic and younger sediments that fill the sedimentary basin of the Tadjik Depression, a relatively low region that forms most of southwest Tadjikistan (Figure 2), have been deformed by folding and thrusting in the zone between the Pamir and Tien Shan ranges.

Copyright 1986 by the American Geophysical Union.

Paper number 6L7011.  
0094-8276/86/006L-7011\$03.00

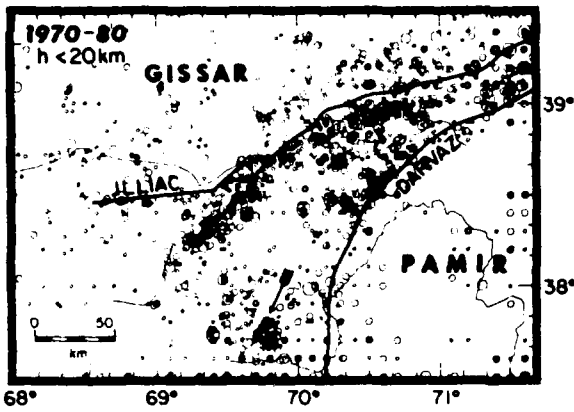


Fig. 1. Shallow earthquakes for the area of southwestern Tadjikistan from 1970-1980. Seismicity is most intense within the frontal (northern) portions of the Vakhsh fold/thrust belt and along a portion of the Darvaz fault. The cluster of seismicity in the lower portion of the figure (arrow) occurs near the salt domes mapped in Fig. 2, and well away from the belt of epicenters that marks the fold/thrust belt. A detail of this area is shown in Fig. 3.

Throughout the Depression, Jurassic evaporites form the base of the sections exposed along thrust faults at the surface, and the overall structure of the Depression suggests that these basal evaporites form the decollement across which the thrusts are displaced [Leith and Alvarez, 1986]. Basin formation in mid-Jurassic time was followed by the deposition of large thicknesses of evaporites. Since the end of the Jurassic, shallow-water marine sedimentation in the Depression proceeded at a relatively slow rate, as the basin subsided following the rifting event [Leith,

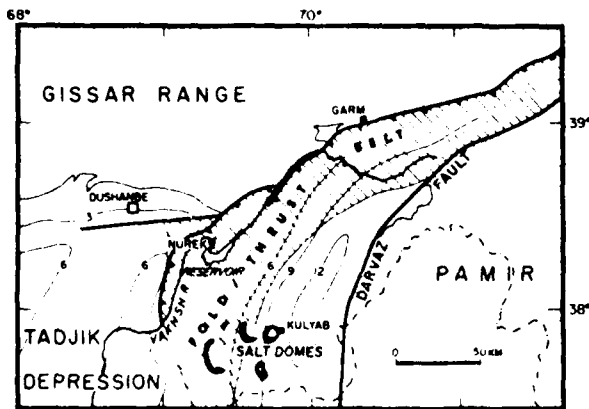


Fig. 2. Generalized crustal structure and geology of the northern Tadjik Depression. Salt domes are located near Kulyab in the southeastern Tadjik Depression, 10-50 km from the Soviet-Afghan border, which follows the Pyandzh river (dash-dot line). Depth to basement beneath the Mesozoic and Cenozoic sediments of the Tadjik Depression is contoured in 3 km intervals (thin lines).

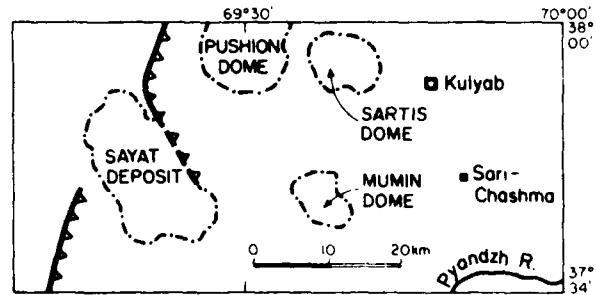


Fig. 3. (a) Earthquake epicenters from the Soviet Catalogs for the Kulyab region, mapped on shaded digital terrain data. (b) Sketch shows salt deposits, major faults and geography. There is a close spatial correlation between some groups of earthquakes and mapped salt domes. The cluster of earthquakes in the lower right is associated with the buried Sari Chashma salt diapir (detail in Fig. 4). Location accuracy for most events is listed as  $\pm 10$  km.

1985]. Adjacent to the Pamir range in the region of Kulyab, this was followed in about middle Oligocene time by the deposition of more than 8 km of Neogene molasse in a north-south trending trough of thick and, now, gently-folded rocks (the Kulyab synclinorium). This rapid loading of the Jurassic-Paleogene section has provided the drive for the salt migration.

The Kulyab area, along the western limb of the Kulyab synclinorium, is marked by the outcrop of several large bodies of Jurassic-Lower Cretaceous salt [Luchnikov, 1982]. Some are obvious domes (Figure 3), while others mark the traces of mapped thrust faults. Several of the domes have prominent topographic relief. For example, at the Mumin dome, south of Kulyab (see Figures 3, 4), the central salt stock rises more than 870 m above the surrounding plain. This feeds an oblate glacial salt flow above folded and faulted upper Tertiary strata [Sadikov, 1982].

Geophysical studies and exploratory drilling that have accompanied the search for oil and gas in the Kulyab area have helped to delineate the distribution of salt at depth [Luchnikov, 1982; Azimov and others, 1982], and have enabled the mapping of a zone of overpressured formations to the west of Kulyab [Kalomazov and Vakhtikov, 1975]. A well drilled in the northern dome in Figure 3 ("Sartis") encountered



Fig. 4. Epicenters from the April 2nd, 1973 earthquake and its aftershocks, mapped on a Landsat image of the Kulyab area. The location of a mapped subsurface diapir (dashed line) is from Kon'kov [1974]. This earthquake sequence apparently occurred at shallow depth along the northern margin of the diapir.

pressures of 1.6 and 1.8 times hydrostatic in Turonian age strata at depths of 2642 and 2695 m, respectively. In general, the westernmost (up-structure) fields are overpressured (up to twice hydrostatic) while those to the east are not.

#### Seismicity

Epicenters of earthquakes in the Kulyab area from 1964-1980, from the yearly catalogs, *Zemletracenniye v SSSR* (hereafter, 'ZSSSR catalogs'), are shown in Figure 3, along with shaded digital topography. There are 352 earthquakes listed in the catalogs (many duplicate locations do not appear in the figure), all with magnitudes greater than about 2.5. All earthquakes in this area are shallow (< 20 km), and there is a clear association of some events with the mapped salt domes. The large cluster of activity in the lower right corner of the figure occurred following the  $M=5.2$  earthquake on 02 April 1973 (hereafter, "1973 earthquake"). This sequence is associated with a diapir at depth, discussed below.

(A Soviet regional catalog lists some smaller events for the Kulyab area (to  $M < 2$ ) but is incomplete. A map showing some smaller events was published in the 1979 ZSSSR catalog (p. 30 overleaf), but we cannot specify location accuracy and salt structures are not located on the map).

For the region of Figure 3, the  $b$ -value is approximately 1.1-1.2 for earthquakes from 1964-1980. This is relatively high in comparison with the western por-

tion of the Vakhsh fold/thrust belt, and is, in fact, comparable to that of the reservoir-induced seismicity at Nurek [Simpson and Negmatullaev, 1981]. Induced earthquakes are triggered by effective stress changes resulting from changes in the subsurface pore pressure regime [Simpson, 1986], and relatively high  $b$ -values are typical of induced seismic activity [Gupta and Rastogi, 1976]. We suggest that the high  $b$ -value that we have determined for the Kulyab region may be "normal" for that area, because of the existence of the naturally high formation pressures noted above. The high  $b$ -values may thus be a fluid pressure effect that distinguishes this region from other areas in western Tadjikistan.

The Kulyab area has produced several earthquakes with magnitudes of about 5 in this century [Gubin, 1960], including those in 1937, 1952, 1959, 1972, 1973 and 1978. From these, the April 2nd, 1973 earthquake ( $M=5.2$ ) is the best studied to date. Kon'kov [1974] combined data from the Kulyab seismic station with macroseismic data to relocate the epicenter of the main shock, which lies 15 km NNW of the epicenter reported in ZSSSR, at a depth of 12 km. It lies near the northern edge of the buried Sari-Chashma diapir, 10 km SE of Kulyab. The sequence is plotted with geologic and geographic data in Figure 4. The earthquakes apparently occurred along the northern margin of the Sari-Chashma diapir, at depths from 0 to 10 km. The main event (April 2, 00h02m43s) was included in a spectral study of Central Asian earthquakes by Zapol'skiy and Loginova [1984; figure 2], which suggests that this event produced lower frequency seismic waves than other earthquakes of comparable size. Low frequency microearthquakes near Nurek reservoir may also be associated with salt deposits, but more work needs to be done to determine the cause of the spectral anomaly.

#### Discussion

Salt diapirism in active tectonic regions can be associated with very high rates of deformation. It is therefore more appropriate to compare the dynamics of the Kulyab salt domes with those of the active salt dome area of southern Iran [Ala, 1974], rather than the more stable region of extensive salt domes along the U.S. coast of the Gulf of Mexico. For example, a detailed study of salt dynamics has been made for the Kuh-e-Namak intrusion in Iran [Talbot and Jarvis, 1984]. This salt stock maintains the highest known natural rate of salt extrusion, estimated by Talbot and Jarvis [1984] to average 170 mm/yr (or about 1 km/6000 yr). This represents an extremely high strain rate in the salt stock, and a significant additional shear stress in the adjacent country rock [D. Davis, pers. comm., 1986].

Because of the very active nature of the tectonics of Tadjikistan, we suspect that the diapirs near Kulyab reflect the same high degree of activity as the Iranian intrusions. For comparison, the Mumin dome (which is more than 7 km wide and rises more than 870 m above the adjacent alluvial plain; see Fig. 4) is

approximately the same size as the Kuh-e-Namak intrusion, and the domes are both in similar arid environments. The Mumin dome must, therefore, maintain a rate of salt extrusion of the order of the Kuh-e-Namak, in order to maintain comparable topography. Unfortunately, data on the deep structure of the Sari Chashma diapir or surface strains in the local area of the diapir are unavailable. Thus, we are currently not able to determine the amount or character of the deformation that is associated with the growth of this salt body.

Elsewhere in the Tadjik Depression, shallow seismicity is largely confined to the sedimentary section above the salt-layer decollement [Leith and Simpson, 1986], and salt is generally thought too weak to hold the large elastic strains that would be necessary to produce a moderate-size earthquake. Thus, we suspect that the 1974 earthquake sequence reflects fracturing of the country rock above or adjacent to the Sari Chashma diapir, and not the seismic release of stored elastic strains within the salt itself. However, depths and focal mechanisms of earthquakes in the Kulyab area are poorly constrained, and we must await further data before speculating on the mechanics of the deformation.

*Acknowledgements.* We thank L. Sykes, D. Davis and J. Rachlin for reviewing the manuscript, and J. Lewkowiec and DARPA for providing the digital terrain data for this region. This work was supported by DARPA/AFGL under contract F19628-85-K-0022 and by USGS contract G14080001-1168. Lamont-Doherty Geological Observatory contribution 4041.

#### References

- Ala, M. H., Salt diapirism in southern Iran, *Am. Assoc. Petrol. Geol. Bull.* 58, 1758-1770, 1978.
- Azimov, P. K., Ye. V. Lebzi and Yu. M. Ovchinnikov, 1982, Deep structure and problems of completion of the sub-salt sediments of southwest Tadjikistan, *Neftegazovaya Geol. i Geofiz.* 3, 23-27.
- Baar, C. A., *Applied Salt Rock Mechanics 1. The in situ Behavior of Salt Rocks*, 294 pp., Elsevier, Amsterdam, 1977.
- Borg, I., Peaceful nuclear explosions in Soviet gas condensate fields, in *Energy and Technol. Rev.*, pp. 30-37, Lawrence Livermore Nat. Lab., 1983.
- Carter, N. L. and F. D. Hansen, Creep of rocksalt, *Tectonophysics* 92, 275-333, 1983.
- Cohen, B. L., The disposal of radioactive wastes from fission reactors, *Sci. Am.* 236, 21-31, 1977.
- Dorman, J., G. V. Latham, J. L. Worzel and D. Dumas, Geophysical investigations of salt at the University of Texas geophysics laboratory, in *Proc. Conf. Salt Dome Utilization and Environmental Considerations*, Inst. Environ. Sci. Louis. St. Univ., p. 333-351, 1977.
- Gubin, I. Ye., *Patterns of Seismic Activity in Tadjikistan*, 450 pp., Acad. Sci. Tadjikistan, Dushanbe, 1960.
- Gupta, H. K. and B. K. Rastogi, *Dams and Earthquakes*, 229 pp., Elsevier, Amsterdam, 1976.
- Hannon, W. J., Seismic verification of a comprehensive test ban, *Science* 227, 251-257, 1985.
- Jackson, M. P. A. and C. J. Talbot, External shapes, strain rates and dynamics of salt structures, *Bull. Geol. Soc. Am.* 97, 305-323, 1986.
- Kalomazov, R. U. and M. A. Vakhtikov, Appearance and Nature of anomalously high formation pressures in the Kulyab megasycline of the Tadjik Depression, *Neftegazovaya Geologiya i Geofizika* 10, 3-6, 1975.
- Kent, P. E., The emergent salt plugs of southern Iran, *J. Petrol. Geol.* 2, 117-144, 1979.
- Kon'kov, A. A., The Kulyab earthquake of 2 April, 1973, in *Zemletryacennii v SSSR v 1973 Godu*, edited by I.V. Gorbunova and others, p. 86-93, Nauka, Moscow, 1976.
- Leith, W., A Mid-Mesozoic extension across Central Asia?, *Nature* 313, 567-570, 1985.
- Leith, W. and W. Alvarez, Structure of the Vakhsh fold-and-thrust belt, Tadjik SSR (Reply), *Bull. Geol. Soc. Am.* 97, 906-908, 1986.
- Leith, W. and D. W. Simpson, Seismic domains within the Gissar Kokshal seismic zone, Soviet central Asia, *J. Geophys. Res.* 91, 680-690, 1986.
- Lerche, I., ed., *Review of Salt Domes and Salt Tectonics*, Academic, in press, 1986.
- Luchinkov, V. S., Upper Jurassic halogen deposits of southeast Central Asia, *Trudy Inst. Geol. i Geofiz.* 535, 19-33, 1982.
- Racine, D. and P. Klouda, Seismicity of the salt areas of Texas, Louisiana, Oklahoma and Kansas, *Tech. Report AL-79-3*, 27 pp., Teledyne Geotech, Alexandria, 1979.
- Sadikov, T. S., Halogenic formations of southwest Tadjikistan, in *Structure and Condition of Formation of Salt Formations*, edited by A. L. Yanshin, pp. 137-143, Nauka, Novosibirsk, 1981.
- Simpson, D. W. and S. K. Negmatullaev, Induced seismicity at Nurek reservoir, Tadjikistan, USSR, *Bull. Seis. Soc. Am.* 71, 1561-1586, 1981.
- Simpson, D. W., Triggered earthquakes, *Ann. Rev. Earth Planet. Sci.* 14, 21-42, 1986.
- Talbot, C. J. and R. J. Jarvis, Age, budget and dynamics of an active salt extrusion in Iran, *J. Struct. Geol.* 6, 521-533, 1984.
- Zapol'skiy, K. K., and G. M. Loginova, Features of strong, shallow-focused earthquakes in Tadjikistan, *Physics of the Solid Earth* 20 (4), p.305-310, 1984.
- Zemletryacenniy v SSSR, 1964-1980*, Nauka, Moscow.

William Leith and David W. Simpson, Lamont-Doherty Geol. Obs., Palisades, N.Y. 10964.

(Received July 3, 1986  
revised August 22, 1986  
accepted August 25, 1986)

# Potential Uses of the New York State Seismic Array for Teleseismic and Regional Studies

Arthur L. Lerner-Lam

Lamont-Doherty Geological Observatory, Columbia University

## 1. Introduction

Apart from their utility to the study of regional seismicity, the use of regional seismic networks for the study of the properties of teleseismic travel times and waveforms is well established. Studies of the crust and upper mantle subjacent to array installations have been done at LASA and NORSAR [e.g. Aki, 1973; Aki et al., 1977] and SCARLET [e.g. Humphreys et al., 1984]. Arrays have also been useful for the study of distal structure. Bungum and Capon [1974] used LASA recordings to measure apparent back azimuths of Rayleigh waves. Engdahl [1968] used LASA records to identify and study *PKiKP* and *PmKP* arrivals. Husebye et al. [1976] used NORSAR to measure the properties of *PKiKP* precursors, and Chang and Cleary [1978, 1981] and Doornbos [1980] used arrays to measure the properties of *PKKP*. NORSAR has also been used to study the nature of *P*-diffracted and its decay into the core shadow [Doornbos and Mondt, 1979]. The recently operational NARS network [Dost et al., 1984] is being used to assemble a broad range of observations of fundamental and higher-mode surface waveform characteristics and to study the properties of phases converted at upper-mantle discontinuities [Paulssen, 1985; Dost, 1986]. In this report, we explore the utility of the New York State Seismic Array (NYSSA), operated by Lamont-Doherty, for studies of regional variability of structure and the properties of the core-mantle boundary and *D''*.

Waveform studies using arrays offer the advantage of signal enhancement by assuming (with some justification) that the background noise is uncorrelated at frequencies of interest. Various stacking and beaming procedures have been designed to optimize the response of the array to the particular signal being evaluated [e.g. Capon et al., 1967; Nolet and Panza, 1976; Husebye et al., 1976; Ingate et al., 1985]. Such procedures depend critically upon the physical design of the array, that is, the disposition of the instruments. While these procedures elevate the accuracy of various sorts of signal measurements, of somewhat more importance for global studies is the position of the array relative to seismogenic regions [Gee et al., 1985]. NYSSA is situated ideally with respect to the seismogenic zones of the southwestern Pacific for the study of the core phases belonging to the *PKP* group. In addition to their intrinsic interest, *PKP* phases arrive at the array with nearly vertical incidence, and provide a reasonable input signal with which near-receiver transfer function can be evaluated, and small-scale regional structure can be estimated. Of importance to the accurate interpretation of these arrivals is a measure of the coherence of the signal, and the response of the array to incoming signals of near vertical incidence. In this report, we assess the utility of using NYSSA for the analysis of these phases. Initial estimates of spatial coherence over a restricted

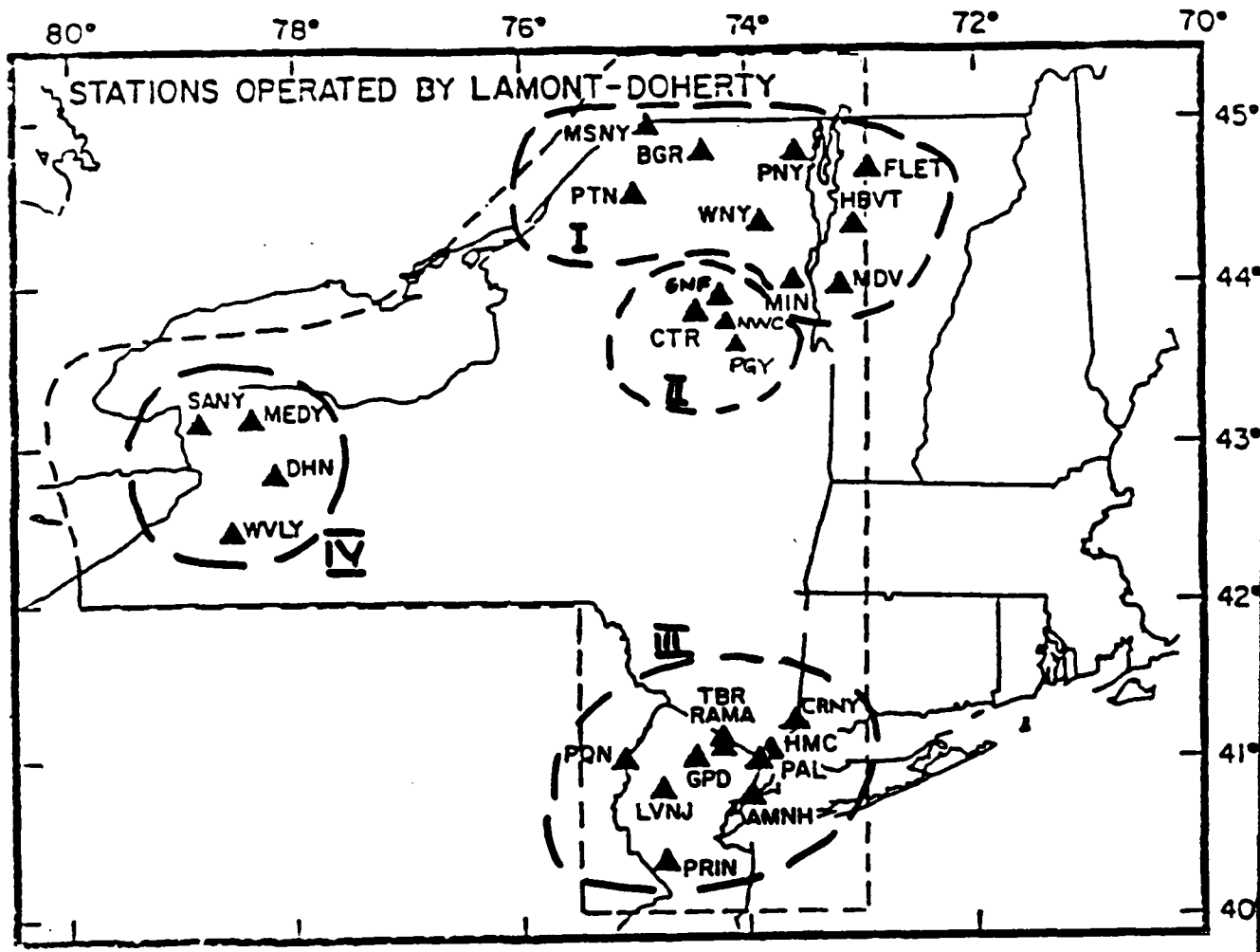


**Figure 1:** Configuration of New York State Seismic Array as of December 10, 1986. LDGO is located near station PAL in southeastern New York State. Roman numerals refer to subnetworks; each will have a central data recording / transmission site tied to LDGO.

portion of the array will be presented. These measurements are important to a thorough understanding of higher-frequency regional wave propagation, a program of interest to DARPA. Future DARPA-funded research at LDGO will be concerned with the robust estimation of spatial coherence using NYSSA and specially installed sub-arrays, and the implications for crustal and mantle heterogeneity beneath the array.

## 2. Network configuration

The New York State Seismic Array (NYSSA) was developed and installed by Lamont-Doherty Geological Observatory (LDGO) to monitor seismicity in the northeastern United States. The current configuration, shown in Figure 1, comprises 27 stations partitioned into four sub-regional networks in northern New York State, the Adirondacks, southeastern New York and northern New Jersey, and western New York. Station sites were chosen to provide optimal array characteristics for local and regional seismic monitoring experiments. The dotted line surrounds the region in which there is nearly complete detection of events above magnitude 2.0. Sensors have fundamental periods of one or two seconds; together with associated electronics, the total system response is flat to acceleration between .1 and 1 Hz and flat to velocity between 1 and 10 Hz (Figure 2). System output is digitized using a 12-bit A/D with 100 Hz sampling, giving a usable response to 30 Hz. The pre-event memory is variable, and can be adjusted to a maximum of 68 seconds.

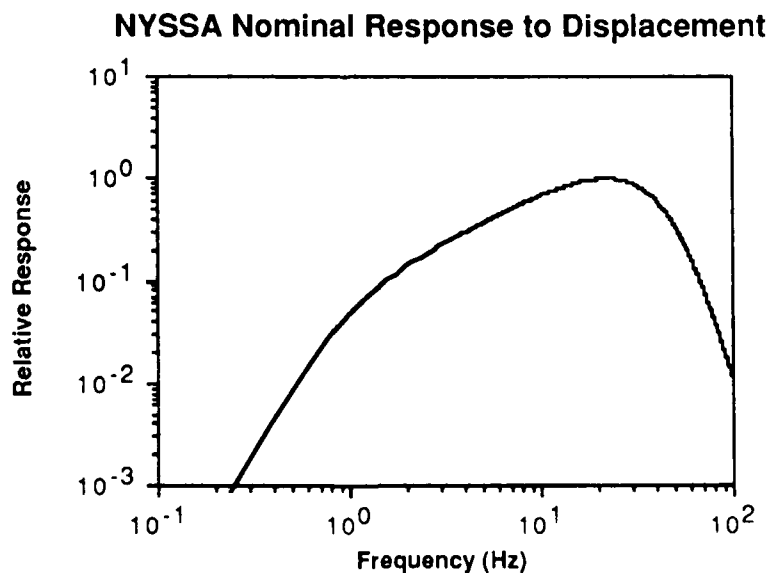


**Figure 2:** Nominal NYSSA instrument displacement response, after *Lee and Stewart* [1981].

The network operates in triggered mode using a short-term average – long-term average algorithm tuned to seismicity levels in the Northeast. Detected events are transmitted over leased

telephone lines to LDGO using analog telemetry. Although the triggering algorithm is designed to detect local and regional events reliably, teleseismic arrivals, particularly those having higher frequency content, will trigger the network and be recorded. Since the network trigger must be tuned to avoid saturation on small local events, the effective magnitude threshold for teleseisms at core-study distances is greater than about  $m_b = 6.0$ . Selected analog recordings have been made of events with body-wave magnitudes as low as 5.2 – 5.5, however, with sufficient "eyeball" signal-to-noise levels to be useful for core-phase analysis. To trigger on these events, and to avoid saturation by small local events, the triggering algorithm must be modified to make near real-time estimates of incoming signal azimuth and incidence angle.

### 3. Comparison of NYSSA and NORSAR for PKP analysis

The New York State Seismic Array (NYSSA) was established principally to monitor regional seismicity in the northeastern United States. Teleseismic triggers typically have been used to provide external checks on instrument polarities. NORSAR, on the other hand, was established principally as a network with a well-defined array response to incoming teleseismic arrivals in order to resolve questions associated with nuclear event detection and discrimination, though it has proven very successful in addressing basic earth structure problems [*e.g.* Husebye *et al.*, 1976; Aki *et al.*, 1977; Doornbos and Mondt, 1979].

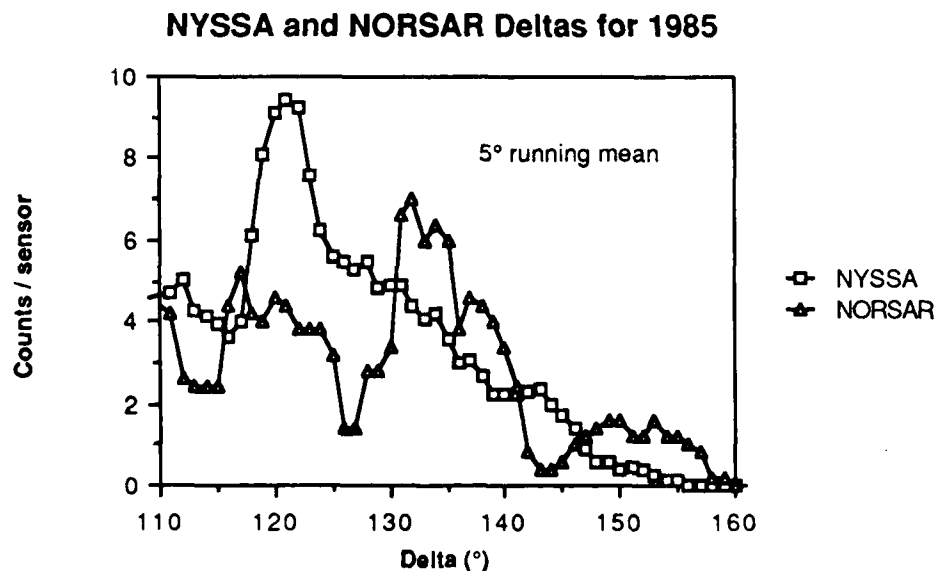


**Figure 3:** Histogram of expected arrivals per sensor at NYSSA (squares) and NORSAR (triangles) for Pacific Rim earthquakes with  $m_b > 5.5$ . A  $5^\circ$  running mean has been applied to simulate wider aperture. Seismicity is taken from 1985 PDE catalogs.

Figure 3 shows a comparison of expected annual arrivals (per sensor) at NYSSA and NORSAR as a function of epicentral distance from Pacific rim events with  $m_b$  greater than 5.5, using events in the 1985 PDE catalog. The number of arrivals integrated over the distance range  $110^\circ - 160^\circ$  is about the same for both arrays, but the distributions are different. The NYSSA array has a peak in the arrival histogram between  $117^\circ$  and about  $130^\circ$ , with roughly double the number

of expected arrivals at NORSAR, while NORSAR should see about 50% more arrivals between  $130^\circ$  and  $140^\circ$  than NYSSA. (Indeed, the study of *DF*-precursors by *Husebye et al.* [1976] used events concentrated around  $131^\circ$  and  $136^\circ$ , corresponding roughly to the peaks in the NORSAR histogram in Figure 3.) Overall the NYSSA histogram is smoother, reflecting a more favorable distribution of event geometry and a wider aperture. NORSAR, however, should have greater detection capabilities due to its more controlled array response [*Dahle et al.*, 1975], a factor which we will investigate for NYSSA. The total azimuthal sampling is comparable between the two arrays, though of course, the patches of the core sampled by each array are different. Our point here is not to focus on dissimilar aspects of NYSSA and NORSAR, but merely to demonstrate that both NORSAR and NYSSA are potentially capable of illuminating equivalent portions of  $P'$  branches. Examples of *DF*-precursor waveforms from NORSAR are published in *Husebye et al.* [1976]. Examples of waveforms from NYSSA are shown in the next section.

#### 4. Initial observations of *PKP*

We have examined 22 teleseismic triggers from events in the southwest Pacific and Indonesia covering an epicentral range from  $111^\circ$  to  $148^\circ$ . The network triggers on  $P'_{DF}$  or  $P'_{BC}$  for these events, and there is enough pre-event memory in the standard configuration to obtain good recordings of *DF*-precursors or the *AB - BC - DF* crossovers. At these azimuths, the network aperture is about  $5^\circ$ . Examples of three record sections exhibiting *DF*-precursors are shown in Figures 4, 5, and 6. Figure 7 shows a record section illuminating the *BC - DF* crossover.

Event 860115.2017, shown in Figure 4, is one of the closest events for which we have observed unambiguous precursors ( $119^\circ - 124^\circ$ ). (To our knowledge, these are among the closest observations of *DF*-precursors yet collected.) *DF*-precursors are well-observed on stations beyond  $122^\circ$  (these are Adirondack sites) with impulsive onset and a ringing behavior of nearly constant amplitude up to the *DF* arrival. Total length of the precursive wavetrain is 11 - 12 seconds. Noise levels at the stations vary, and the precursor is not detected easily at BING, WND, or SANY, although there is some indication of anomalous energy preceding *DF* by about 6 - 7 seconds at DHN ( $119.8^\circ$ ). Figures 5 and 6 display events 840806.1201 and 850111.1441, respectively, each illuminating the same portion of the  $P'$  travel-time curve ( $132^\circ - 137^\circ$ ). Precursive arrivals to *DF* are clear in Figure 5, but the wavetrain is longer (13 - 16 seconds) and more emergent than in Figure 4, with amplitudes increasing toward the *DF* arrival (compare, for example, WPNY in Figures 4 and 5). These events are at two different azimuths, however, and it is not yet certain whether we are observing source effects, source site effects, or differences in the characteristics of  $D''$  or the CMB between the two paths. Observations of short-period  $P$  at closer distances can assist in the interpretation of this difference. We note, however, that the onset times are qualitatively consistent with the theoretical least times given in *Haddon and Cleary* [1974, Figure 6]. We contrast 840806.1201 in Figure 5 with 850111.1441 in Figure 6, where precursive arrivals, if present at all, are of much smaller amplitude relative to *DF*. Again, we cannot tell

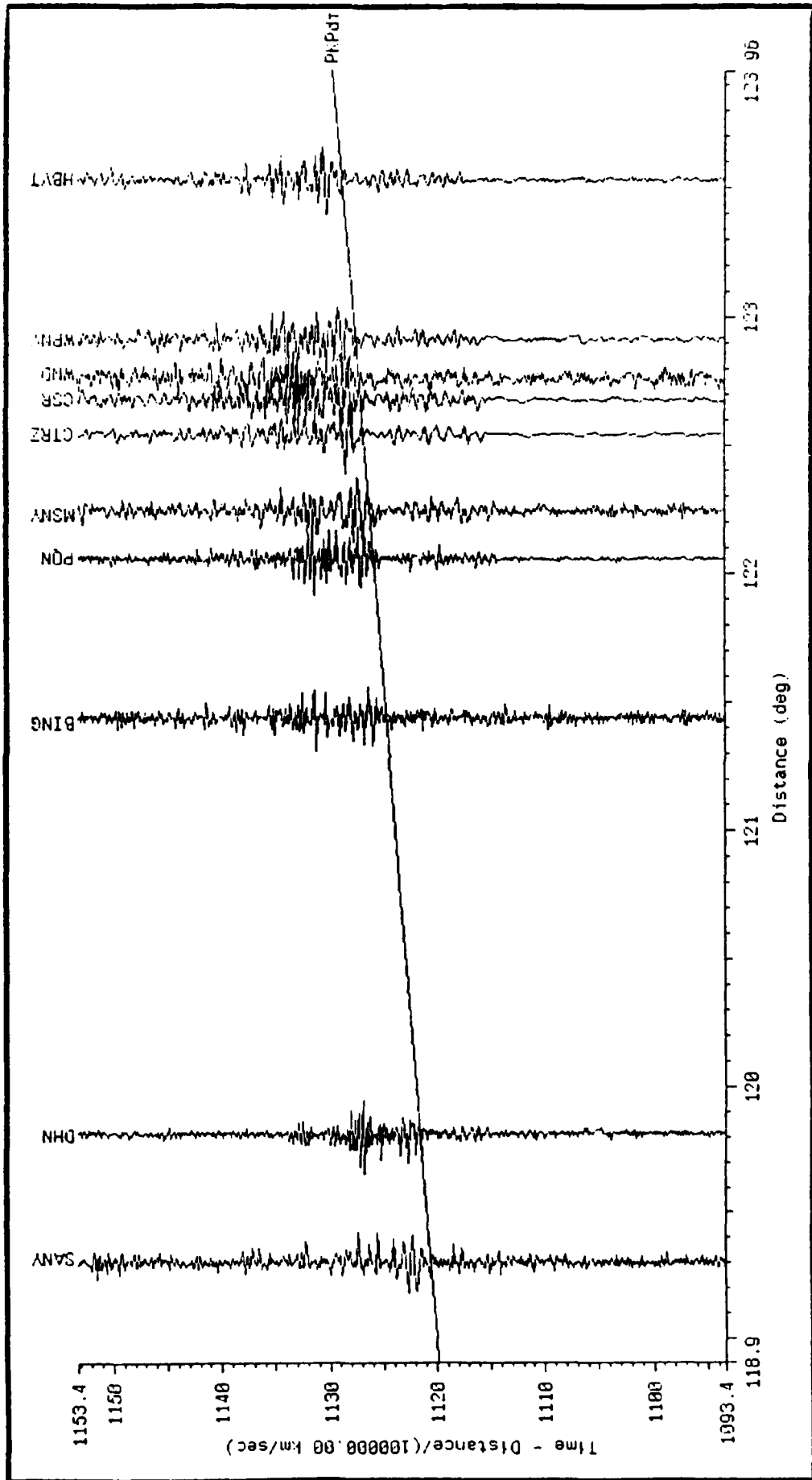
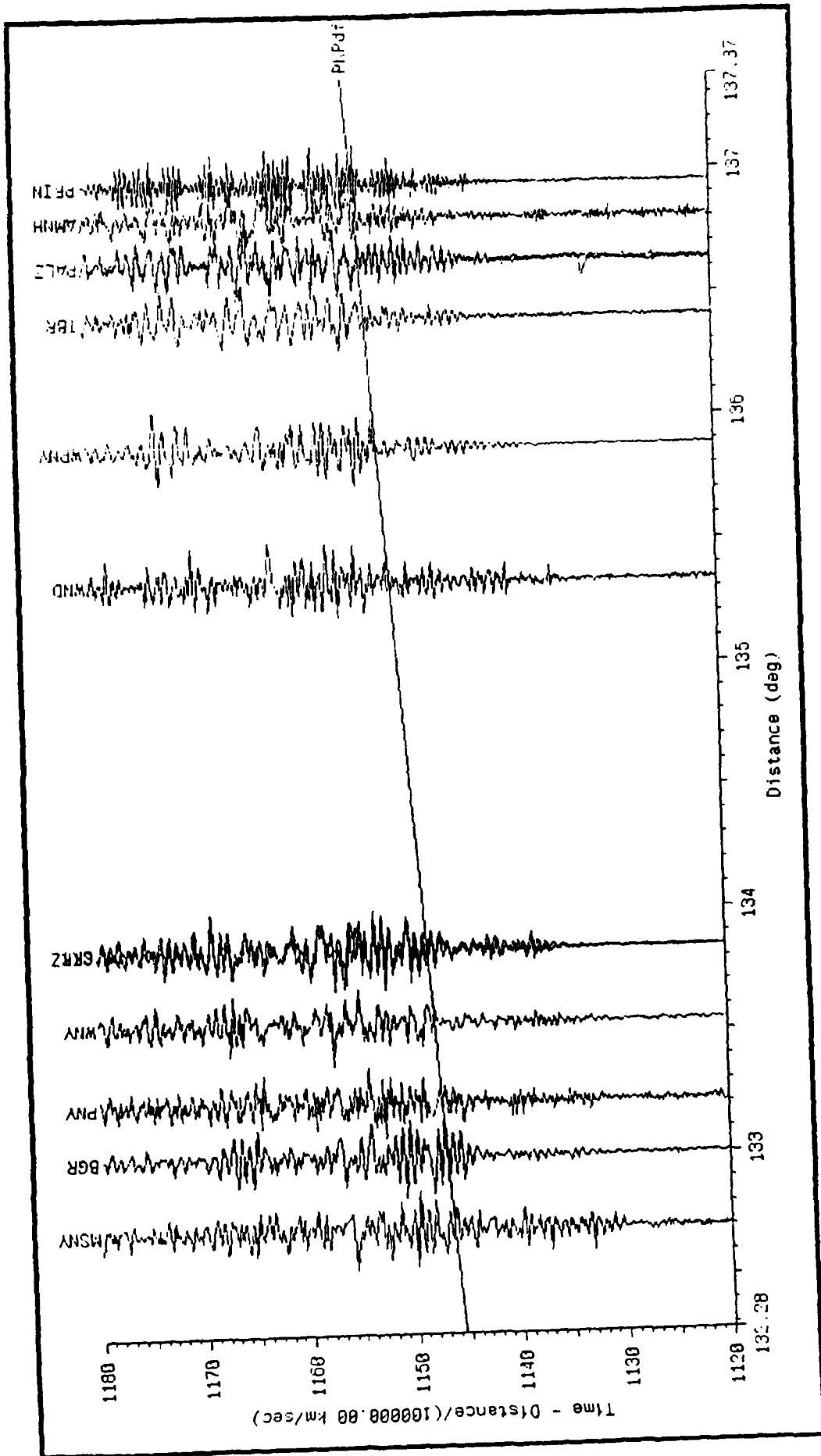


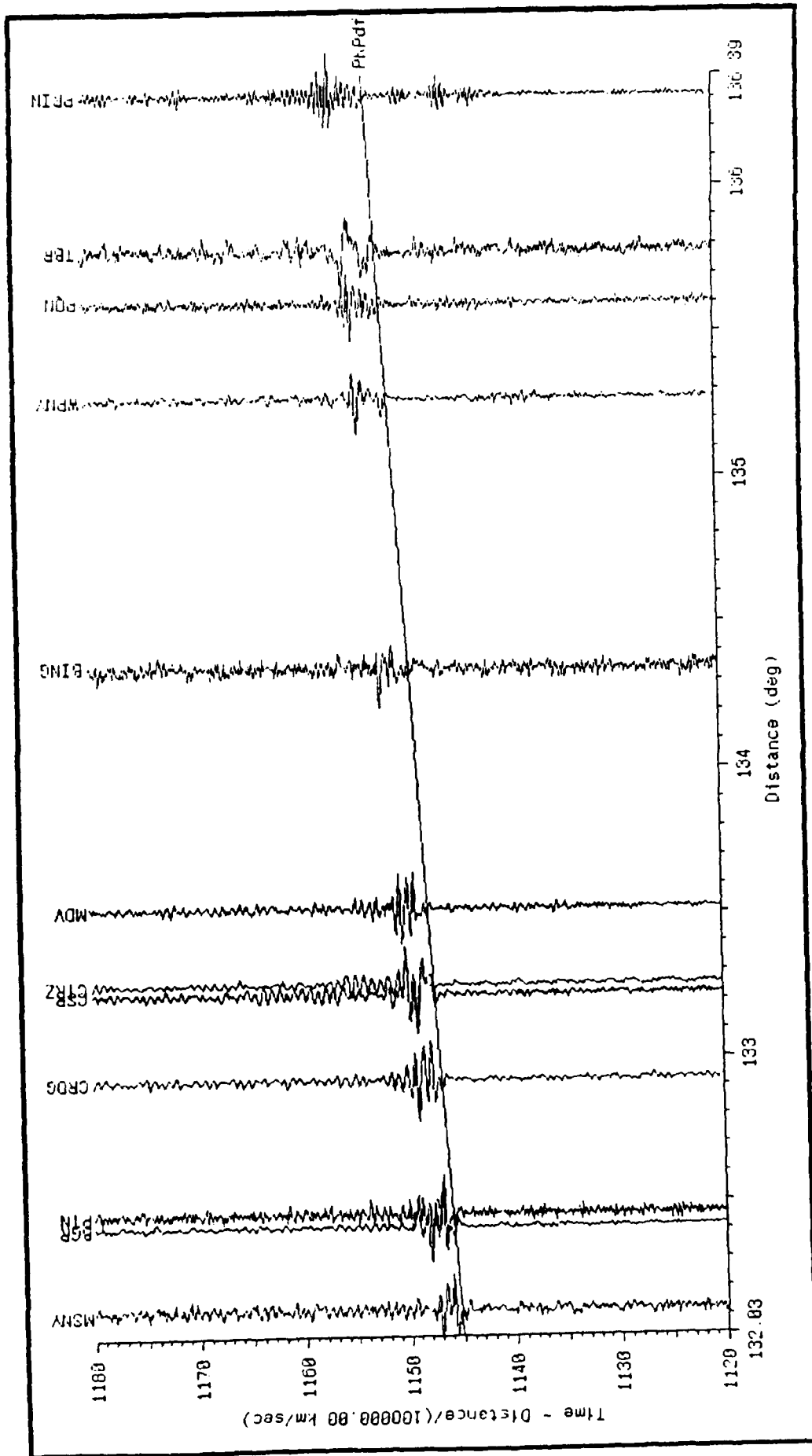
Figure 4: Record section comprising selected recordings on NYSSA of event 860115.2017,  $h=145$  km. *DF*-precursor arrivals are evident as distributed waveforms with impulsive onsets at distances beyond 122°. Travel-time curve is JB with constant offset added to match observed *DF* moveout. One minute of record is shown.

screen dump in progress ...



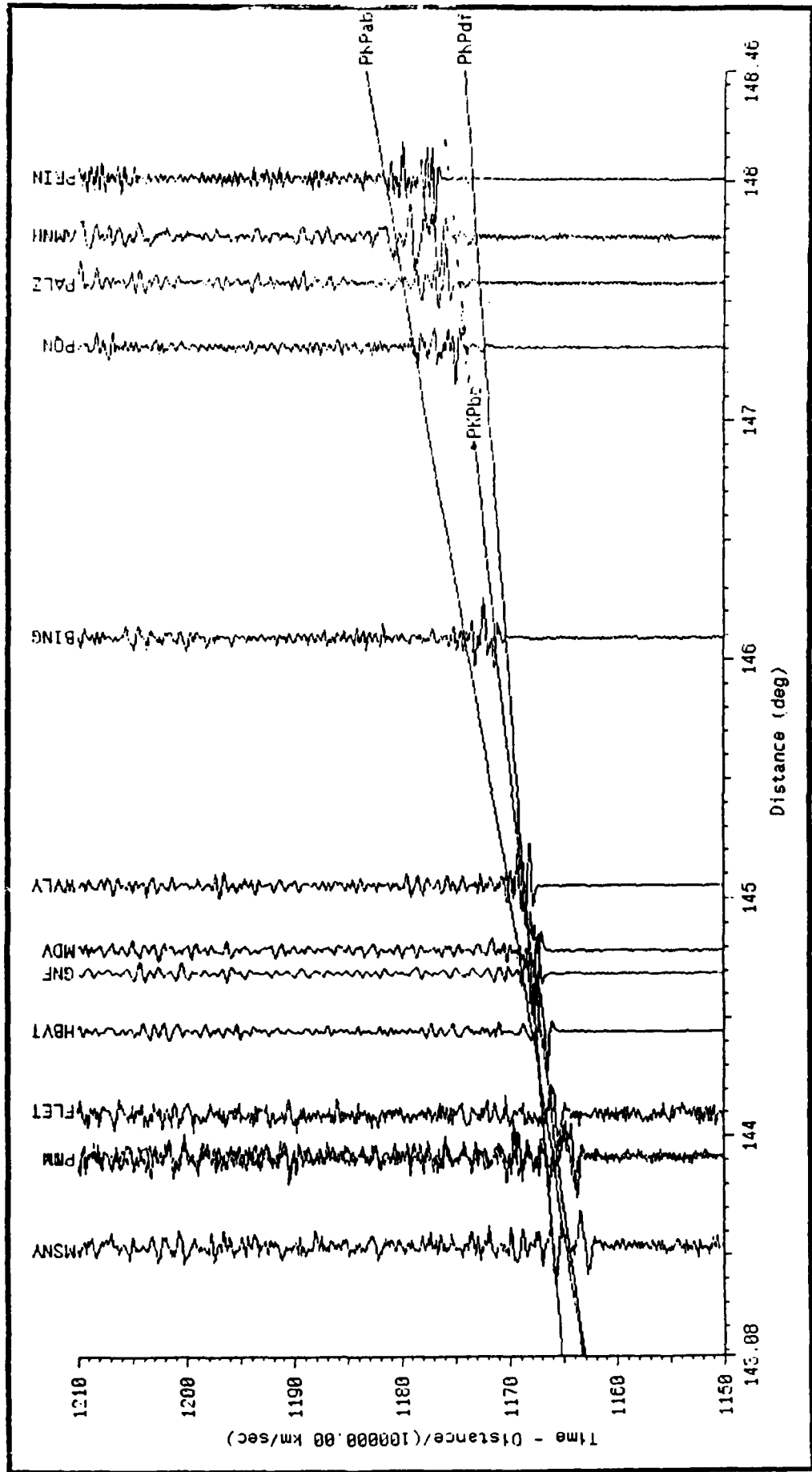
Screen dump in progress

Figure 5: Record section comprising selected recordings on NYSSA of event 840806.1201, h=242 km. Clear precursive arrivals are evident at all distances, although the onset of the precursor is more emergent than observed in Figure 4.



**Figure 6:** Record section comprising selected recordings on NYSSA of event 850111.1441,  $h=189$  km. Though having nearly the same range and back azimuth as the record section shown in Figure 5, the *DF*-precursors shown here are much less evident. Note also that the *P'* arrival is much simpler.

screen dump in progress



**Figure 7:** Record section comprising selected recordings on NYSSA of event 850413.0:106,  $h=99$  km. The large amplitude arrival is  $P_{BC}$ ;  $DF$  appears as the much smaller arrival beyond  $147^\circ$ . Travel-time curves are  $JB$ , with a constant offset added to match the  $DF$  branch.

Screen dump in progress

without further study whether we are observing the effects of source complexity or CMB heterogeneity (the  $DF$  waveforms in Figure 6 are much simpler than those in Figure 5).

Figure 7 displays a record section collected just beyond the  $B$ -cusp at about  $143^\circ$ . The dominant arrival is  $P'_{BC}$ , with  $P'_{DF}$  appearing only as a small, low-amplitude arrival beyond  $145^\circ$ . The travel-time curves shown are calculated for the JB model, with a constant time offset of 2.1 s added in order to line up  $P'_{DF}$  with the data. The  $P'_{DF}$  and  $P'_{BC}$  travel times appear to be well fit by the offset model at distances greater than  $146^\circ$ , but for distances closer than the  $BC - DF$  crossover, the  $P'_{BC}$  arrivals are much earlier (about 2 seconds) than predicted.

Figures 4 – 7 are given as examples of the data quality and the detail available when station sites are densely distributed at appropriate epicentral distances. A more comprehensive analysis of these data is underway at LDGO, and will be the subject of another publication.

In the discussion that follows, we use the  $PKP_{DF}$  waveform from event 840806.1201 to estimate signal coherences.

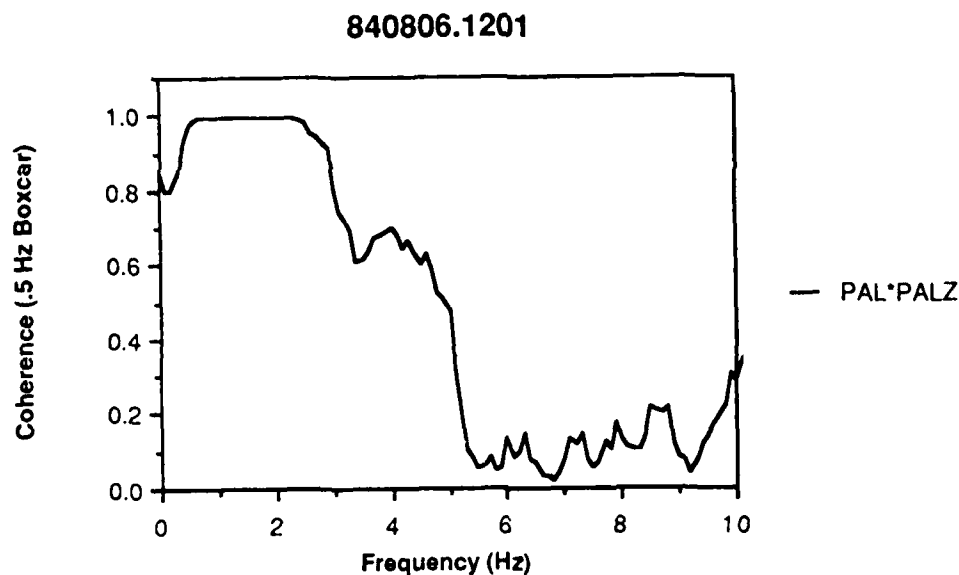


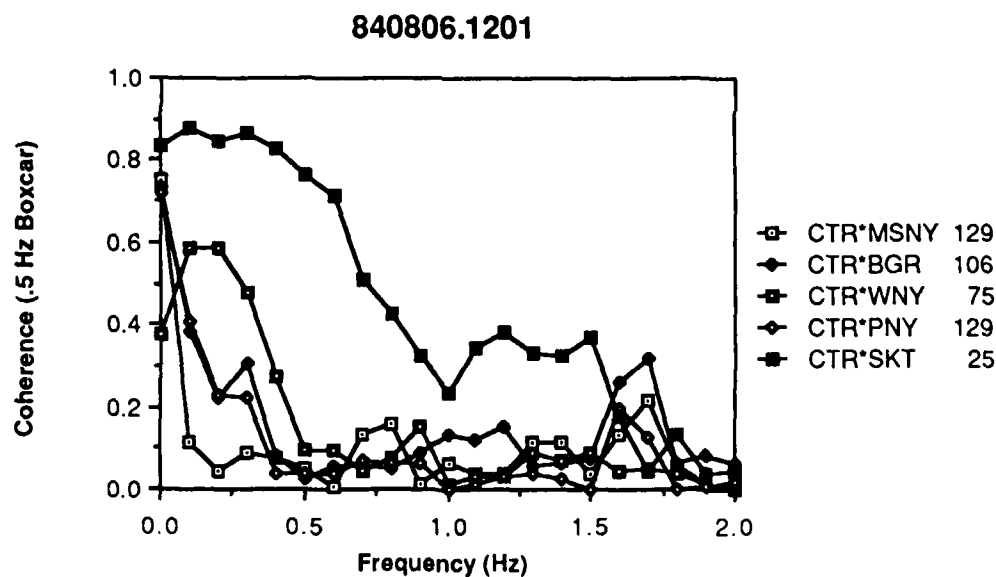
**Figure 8:** Amplitude coherence between two different sensors situated on the same pier, for one-minute signal duration, using the  $PKP-DF$  trigger for event 840806.1201. Cross-spectrum and auto-spectra estimates are smoothed with a .5 Hz frequency boxcar. Coherence is high out to 3 Hz, and acceptable to 5 Hz. Lower values of coherence at low frequencies are due to instrumental drift.

## 5. Coherence estimates

For a period of time, LDGO operated two sensors (Geospace HS-10 and a Ranger, both with natural periods of 1 s) on the same pier at PAL, using amplifiers and filters having characteristics identical to the rest of the network. Figure 8 shows their normalized coherence

(smoothed over .5 Hz spectral window) from DC to 10 Hz for the  $PKP_{DF}$  signal produced by 840806.1201. The coherence is near unity between .5 and 2.5 Hz, and maintains a level of about .6 to 5 Hz. There is some incoherency below .5 Hz which is noticeable in the time series as long-period drift. This is easy to spot upon examination, however, and is not a factor in our interpretation of the waveforms. Evidently, there are no pathologic instabilities in the electronics which might impact signal coherence below 2 Hz. In what follows, we use 2 Hz as the upper frequency limit for our analysis.

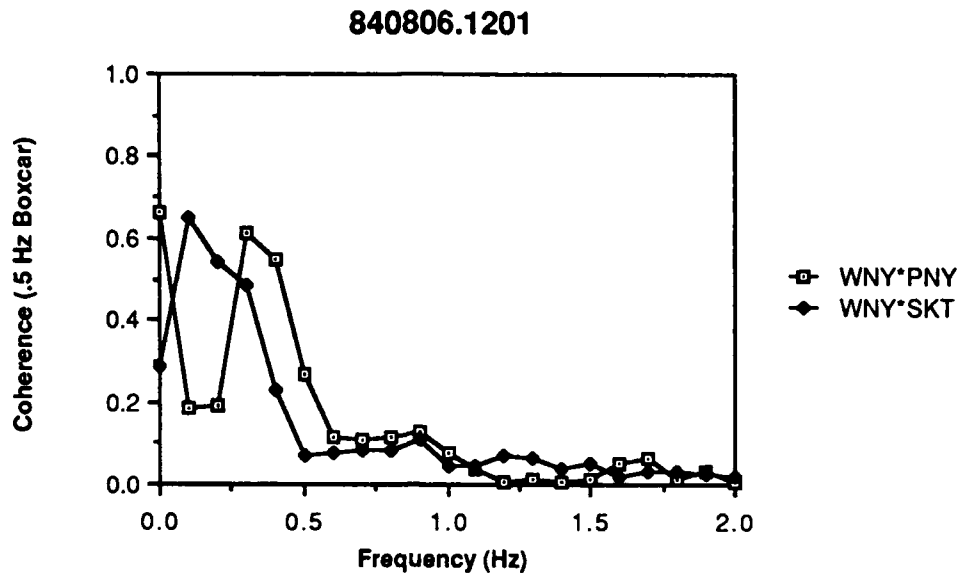
We concentrate in this report on coherence measurements at the Adirondack and northern New York sites (sub-nets I and II in Figure 1), using six vertical-component stations at CTR, MSNY, BGR, WNY, PNY, and SKT (near GNF). For the most part, the stations are situated on hard-rock with some glacial till cover with low cultural and microseismic noise characteristics [LDGO field reports]. Inter-station spacing ranges from 24.7 km to 128.8 km, and the median spacing is 97.7 km. For these preliminary studies, we extracted one minute of  $PKP$  signal beginning with the  $DF$ -precursor and tapered the time series with a 10% cosine. We assume that the instrument responses are characterized by the nominal poles and zeros given in *Lee and Stewart* [1981].



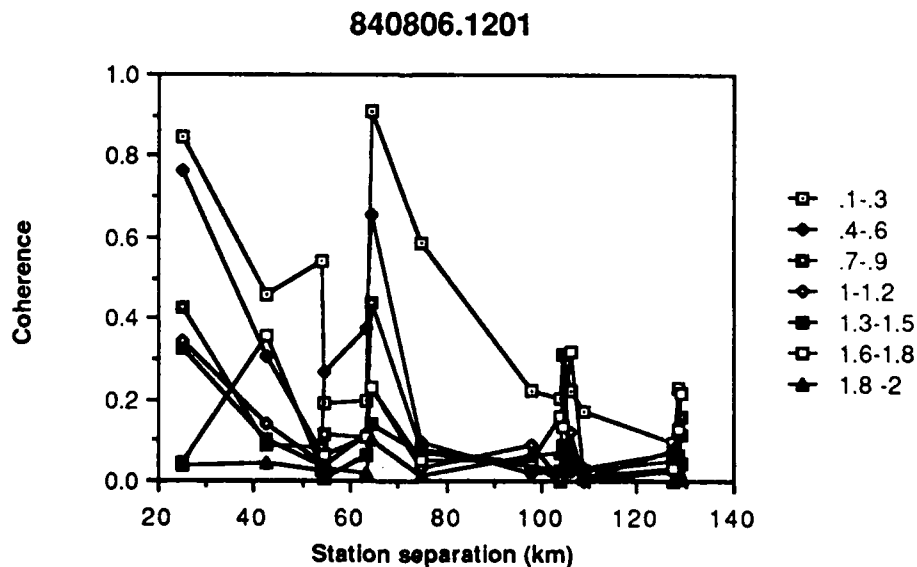
**Figure 9:** Inter-station coherence as a function of frequency between CTR and other stations of the Adirondack and northern New York subnets, for one-minute signal duration. Numbers to the right of the legend give inter-station spacing in kilometers. Coherence levels are lower for increased station separation as expected.

Figure 9 shows coherence estimates (.5 Hz spectral window smoothing) between CTR and the other five stations as a function of frequency. The best coherence is exhibited for CTR\*SKT, which also have the closest inter-station spacing (between 2 and 3 signal wavelengths). Even so, the coherence drops below .5 above .75 Hz. Not surprisingly, sub-array heterogeneity affects the

coherence estimate. Figure 10 displays coherence for two station pairs having nearly identical inter-station spacing (WNY\*PNY and WNY\*SKT). Differences in the coherence curves are indicators of differences in station response or station site effects (noise, transmission losses, differences in structure, and so on). The curves have similar fall-offs above about .7 Hz, though the WNY\*SKT coherence is lower.



**Figure 10:** Coherence between WNY, PNY, and SKT. WNY is 54 km from both PNY and SKT. PNY is 109 km from SKT. Differences in coherence indicate that the distribution of heterogeneities is not isotropic.



**Figure 11:** Coherence as a function of inter-station spacing for each of several narrow bands. The "hole" between 50 and 60 km is probably due to improper instrument response.

Figure 11 displays coherence as a function of inter-station spacing for several narrow bands

in frequency. The coherence "hole" between 50 and 60 km is presumably due to problems with the station at WNY (1-second vs. 2-second seismometer, site characteristics), though nothing in the field installation notes indicates any special siting problems or instrumental defects. Relatively high coherence is seen at low-frequencies (<5 Hz) out to distances of about 60 to 80 km (3-5 crustal wavelengths), somewhat greater than observed at LASA [Aki, 1973] or NORSAR [Bungum *et al.*, 1971].

While these results are very preliminary (and point to the necessity of obtaining appropriate instrument response functions), they nevertheless show the potential usefulness of a well-situated array for teleseismic structural studies and subjacent site structure.

## 6. Plans for further analysis

Future work will include the reconstruction of individual station calibration responses (particularly phase responses) from field installation and maintenance notes. We will also develop more robust coherence estimation techniques, and include more events in our coherence estimates. The one-minute time windows used in our estimation include not only primary signal but some clearly reverberatory waveforms; future analyses will examine shorter time windows and will use polarization analysis to detect mode conversions. In addition, LDGO is installing new permanent instrumentation and acquiring new portable instruments. These will be deployed in various configurations for both intra-network coherence and *PKP* studies.

## 7. References

- Aki, K., Scattering of *P* waves under the Montana LASA, *J. Geophys. Res.*, **78**, 1334-1346, 1973.
- Aki, K., A. Christoffersson, and E.S. Husebye, Determination of the three-dimensional structure of the lithosphere, *J. Geophys. Res.*, **82**, 277-296, 1977.
- Bungum, H., and J. Capon, Coda pattern and multipath propagation of Rayleigh waves at NORSAR, *Phys. Earth Planet. Int.*, **9**, 111-127, 1974.
- Bungum, H., E.S. Husebye, and F. Ringdal, The NORSAR array and preliminary results of data analysis, *Geophys. J. R. Astr. Soc.*, **25**, 115-126, 1971.
- Capon, J., R.J. Greenfield, and R.J. Kolker, Multidimensional maximum likelihood processing of a large aperture array, *Proc. IEEE*, **55**, 192-211, 1967.

- Chang, A.C., and J.R. Cleary, Precursors to *PKKP*, *Bull. Seism. Soc. Am.*, **68**, 1059-1079, 1978.
- Chang, A.C., and J.R. Cleary, Scattered *PKKP*: further evidence for scattering at a rough core-mantle boundary, *Phys. Earth Planet. Int.*, **24**, 15-29, 1981.
- Dahle, A., E.S. Husebye, K.A. Berteussen, and A. Christoffersson, Wave scattering effects and seismic velocity measurements, in *Exploitation of Seismograph Networks*, 559-576, Noordhoff, Leoden, Netherlands, 1975.
- Doornbos, D.J., The effect of a rough core-mantle boundary on *PKKP*, *Phys. Earth Planet. Int.*, **21**, 351-358, 1980.
- Doornbos, D.J., and J.C. Mondt, *P* and *S* waves diffracted around the core and the velocity structure at the base of the mantle, *Geophys. J. R. Astr. Soc.*, **57**, 381-395, 1979.
- Dost, B., Preliminary results from higher-mode surface wave measurements in western Europe using the NARS array, *Tectonophysics*, **128**, 289-301, 1986.
- Dost, B., A. van Wettum, and G. Nolet, The NARS Array, *Geol. Mijnbouw*, **63**, 381-386, 1984.
- Engdahl, E.R., Core phases and the earth's core, Ph.D. thesis, St. Louis University, St. Louis, Mo., 1968.
- Gee, L.S., A.L. Lerner-Lam, and T.H. Jordan, Resolving power of higher-mode waveform inversion for Eurasian upper-mantle structure, Semiannual report, Defense Advanced Research Projects Agency, 1985.
- Haddon, R.A.W., and J.R. Cleary, Evidence for scattering of seismic *PKP* waves near the mantle-core boundary, *Phys. Earth Planet. Int.*, **8**, 211-234, 1974.
- Humphreys, E., R.W. Clayton, and B.H. Hager, A tomographic image of mantle structure beneath southern California, *Geophys. Res. Lett.*, **11**, 625-627, 1984.
- Husebye, E.S., D.W. King, and R.A.W. Haddon, Precursors to *PKIKP* and seismic wave scattering near the core-mantle boundary, *J. Geophys. Res.*, **81**, 1870-1882, 1976.
- Ingate, S.F., E.S. Husebye, and A. Christoffersson, Regional arrays and optimum data processing schemes, *Bull. Seism. Soc. Am.*, **75**, 1155-1177, 1985.

Lee, W.H.K., and S.W. Stewart, Principles and applications of micrearthquake networks, in, *Advances in Geophysics*, ed. B. Saltzman, Academic Press, 1981.

Paulssen, H., Upper mantle converted waves beneath the NARS array, *Geophys. Res. Lett.*, **12**, 709-712, 1985.

Nolet, G., and J. Panza, Array analysis of seismic surface waves: limits and possibilities, *Pageoph.*, **114**, 775-790, 1976.

DISTRIBUTION LIST

Dr. Monem Abdel-Gawad  
Rockwell International Science Center  
1049 Camino Dos Rios  
Thousand Oaks, CA 91360

Professor Keiti Aki  
Center for Earth Sciences  
University of Southern California  
University Park  
Los Angeles, CA 90089-0741

Professor Shelton S. Alexander  
Geosciences Department  
403 Deike Building  
The Pennsylvania State University  
University Park, PA 16802

Professor Charles B. Archambeau  
Cooperative Institute for Research in  
Environmental Sciences  
University of Colorado  
Boulder, CO 80309

Dr. Thomas C. Bache Jr.  
Science Applications Int'l Corp.  
10210 Campus Point Drive  
San Diego, CA 92121

Dr. James Bulau  
Rockwell International Science Center  
1049 Camino Dos Rios  
P.O. Box 1085  
Thousand Oaks, CA 91360

Dr. Douglas R. Baumgardt  
Signal Analysis and Systems Division  
ENSCO, Inc.  
5400 Port Royal Road  
Springfield, VA 22151-2388

Dr. S. Bratt  
Science Applications Int'l Corp.  
10210 Campus Point Drive  
San Diego, CA 92121

Professor John Ebel  
Department of Geology & Geophysics  
Boston College  
Chestnut Hill, MA 02167

Woodward-Clyde Consultants  
Attn: Dr. Lawrence J. Burdick  
Dr. Jeff Barker  
P.O. Box 93245  
Pasadena, CA 91109-3245 (2 copies)

Dr. Roy Burger  
1221 Serry Rd.  
Schenectady, NY 12309

Professor Robert W. Clayton  
Seismological Laboratory  
Division of Geological and Planetary  
Sciences  
California Institute of Technology  
Pasadena, CA 91125

Dr. Vernon F. Cormier  
Earth Resources Laboratory  
Department of Earth, Atmospheric and  
Planetary Sciences  
Massachusetts Institute of Technology  
42 Carleton Street  
Cambridge, MA 02142

Professor Anton M. Dainty  
Earth Resources Laboratory  
Department of Earth, Atmospheric and  
Planetary Sciences  
Massachusetts Institute of Technology  
42 Carleton Street  
Cambridge, MA 02142

Dr. Zoltan A. Der  
Teledyne Geotech  
314 Montgomery Street  
Alexandria, VA 22314

Prof. Adam Dziewonski  
Hoffman Laboratory  
Harvard University  
20 Oxford St.  
Cambridge, MA 02138

Professor John Ferguson  
Center for Lithospheric Studies  
The University of Texas at Dallas  
P.O. Box 830688  
Richardson, TX 75083-0688

Dr. Jeffrey W. Given  
Sierra Geophysics  
11255 Kirkland Way  
Kirkland, WA 98033

Prof. Roy Greenfield  
Geosciences Department  
403 Deike Building  
The Pennsylvania State University  
University Park, PA 16802

Professor David G. Harkrider  
Seismological Laboratory  
Division of Geological and Planetary  
Sciences  
California Institute of Technology  
Pasadena, CA 91125

Professor Donald V. Helmberger  
Seismological Laboratory  
Division of Geological and Planetary  
Sciences  
California Institute of Technology  
Pasadena, CA 91125

Professor Eugene Herrin  
Institute for the Study of Earth & Man  
Geophysical Laboratory  
Southern Methodist University  
Dallas, TX 75275

Professor Robert B. Herrmann  
Department of Earth and Atmospheric  
Sciences  
Saint Louis University  
Saint Louis, MO 63156

Professor Lane R. Johnson  
Seismographic Station  
University of California  
Berkeley, CA 94720

Professor Thomas H. Jordan  
Department of Earth, Atmospheric and  
Planetary Sciences  
Massachusetts Institute of Technology  
Cambridge, MA 02139

Dr. Alan Kafka  
Department of Geology & Geophysics  
Boston College  
Chestnut Hill, MA 02167

Professor Charles A. Langston  
Geosciences Department  
403 Deike Building  
The Pennsylvania State University  
University Park, PA 16802

Professor Thorne Lay  
Department of Geological Sciences  
1006 C.C. Little Building  
University of Michigan  
Ann Arbor, MI 48109-1063

Dr. George R. Mellman  
Sierra Geophysics  
11255 Kirkland Way  
Kirkland, WA 98033

Professor Brian J. Mitchell  
Department of Earth and Atmospheric  
Sciences  
Saint Louis University  
Saint Louis, MO 63156

Professor Thomas V. McEvelly  
Seismographic Station  
University of California  
Berkeley, CA 94720

Dr. Keith L. McLaughlin  
Teledyne Geotech  
314 Montgomery Street  
Alexandria, VA 22314

Professor Otto W. Nuttli  
Department of Earth and Atmospheric  
Sciences  
Saint Louis University  
Saint Louis, MO 63156

Professor Paul G. Richards  
Lamont-Doherty Geological Observatory  
of Columbia University  
Palisades, NY 10964

Dr. Norton Rimer  
S-Cubed  
A Division of Maxwell Laboratory  
P.O. 1620  
La Jolla, CA 92038-1620

Professor Larry J. Ruff  
Department of Geological Sciences  
1006 C.C. Little Building  
University of Michigan  
Ann Arbor, MI 48109-1063

Professor Charles G. Sammis  
Center for Earth Sciences  
University of Southern California  
University Park  
Los Angeles, CA 90089-0741

Dr. David G. Simpson  
Lamont-Doherty Geological Observatory  
of Columbia University  
Palisades, NY 10964

Dr. Jeffrey L. Stevens  
S-CUBED,  
A Division of Maxwell Laboratory  
P.O. Box 1620  
La Jolla, CA 92038-1620

Professor Brian Stump  
Institute for the Study of Earth  
and Man  
Geophysical Laboratory  
Southern Methodist University  
Dallas, TX 75275

Professor Ta-liang Teng  
Center for Earth Sciences  
University of Southern California  
University Park  
Los Angeles, CA 90089-0741

Dr. R. B. Tittmann  
Rockwell International Science Center  
1049 Camino Dos Rios  
P.O. Box 1085  
Thousand Oaks, CA 91360

Professor M. Nafi Toksoz  
Earth Resources Laboratory  
Department of Earth, Atmospheric and  
Planetary Sciences  
Massachusetts Institute of Technology  
42 Carleton Street  
Cambridge, MA 02142

Professor Terry C. Wallace  
Department of Geosciences  
Building #11  
University of Arizona  
Tucson, AZ 85721

Prof. John H. Woodhouse  
Hoffman Laboratory  
Harvard University  
20 Oxford St.  
Cambridge, MA 02138

Dr. G. Blake  
US Dept. of Energy/DP 331  
Forrestal Building  
1000 Independence Ave.  
Washington, D.C. 20585

Dr. Michel Bouchon  
Universite Scientifique et  
Medicale de Grenoble  
Laboratoire de Geophysique  
Interne et Tectonophysique  
I.R.I.G.M.-B.P. 68  
38402 St. Martin D'Herès  
Cedex FRANCE

Dr. Hilmar Bungum  
NTNF/NORSAR  
P.O. Box 51  
Norwegian Council of Science,  
Industry and Research, NORSAR  
N-2007 Kjeller, NORWAY

Dr. Alan Douglas  
Ministry of Defense  
Blacknest, Brimpton, Reading RG7-4RS  
UNITED KINGDOM

Professor Peter Harjes  
Institute for Geophysik  
Rhur University  
Bochum  
P.O. Box 102148  
4630 Bochum 1  
FEDERAL REPUBLIC OF GERMANY

Dr. James Hannon  
Lawrence Livermore National Laboratory  
P.O. Box 808  
Livermore, CA 94550

Dr. E. Husebye  
NTNF/NORSAR  
P.O. Box 51  
N-2007 Kjeller, NORWAY

Dr. Arthur Lerner-Lam  
Lamont-Doherty Geological Observatory  
of Columbia University  
Palisades, NY 10964

Mr. Peter Marshall  
Procurement Executive  
Ministry of Defense  
Blacknest, Brimpton, Reading RG7-4RS  
UNITED KINGDOM

Dr. B. Massinon  
Societe Radiomana  
27, Rue Claude Bernard  
75005, Paris, FRANCE

Dr. Pierre Mechler  
Societe Radiomana  
27, Rue Claude Bernard  
75005, Paris, FRANCE

Mr. Jack Murphy  
S-CUBED  
Reston Geophysics Office  
11800 Sunrise Valley Drive  
Suite 1212  
Reston, VA 22091

Dr. Svein Mykkeltveit  
NTNF/NORSAR  
P.O. Box 51  
N-2007 Kjeller, NORWAY

Dr. Carl Newton  
Los Alamos National Laboratory  
P.O. Box 1663  
Mail Stop C 335, Group ESS3  
Los Alamos, NM 87545

Dr. Peter Basham  
Earth Physics Branch  
Department of Energy and Mines  
1 Observatory Crescent  
Ottawa, Ontario  
CANADA K1A 0Y3

Professor J. A. Orcutt  
Geological Sciences Division  
Univ. of California at San Diego  
La Jolla, CA 92093

Dr. Frank F. Pilotte  
Director of Geophysics  
Headquarters Air Force Technical  
Applications Center  
Patrick AFB, Florida 32925-6001

Professor Keith Priestley  
University of Nevada  
Mackay School of Mines  
Reno, Nevada 89557

Mr. Jack Raclin  
USGS - Geology, Rm 3C136  
Mail Stop 928 National Center  
Reston, VA 22092

Dr. Frode Ringdal  
NTNF/NORSAR  
P.O. Box 51  
N-2007 Kjeller, NORWAY

Dr. George H. Kothe  
Chief, Research Division  
Geophysics Directorate  
Headquarters Air Force Technical  
Applications Center  
Patrick AFB, Florida 32925-6001

Dr. Alan S. Ryall, Jr.  
Center for Seismic Studies  
1300 North 17th Street  
Suite 1450  
Arlington, VA 22209-2308

Dr. Jeffrey L. Stevens  
S-CUBED,  
A Division of Maxwell Laboratory  
P.O. Box 1620  
La Jolla, CA 92038-1620

Dr. Lawrence Turnbull  
OSWR/NED  
Central Intelligence Agency  
CIA, Room 5G48  
Washington, DC 20505

Professor Steven Grand  
Department of Geology  
245 Natural History Bldg  
1301 West Green Street  
Urbana, IL 61801

DARPA/PM  
1400 Wilson Boulevard  
Arlington, VA 22209

Defense Technical Information Center  
Cameron Station  
Alexandria, VA 22314 (12 copies)

Defense Intelligence Agency  
Directorate for Scientific and  
Technical Intelligence  
Washington, D.C. 20301

Defense Nuclear Agency  
Shock Physics Directorate/SS  
Washington, D.C. 20305

Defense Nuclear Agency/SPSS  
ATTN: Dr. Michael Shore  
6801 Telegraph Road  
Alexandria, VA 22310

AFOSR/NPG  
ATTN: Director  
Bldg 410, Room C222  
Bolling AFB, Washington, D.C. 20332

AFTAC/CA (STINFO)  
Patrick AFB, FL 32925-6001

AFWL/NTEC  
Kirtland AFB, NM 87171

U.S. Arms Control & Disarmament Agency  
ATTN: Mrs. M. Hoinkes  
Div. of Multilateral Affairs, Rm 5499  
Washington, D.C. 20451

U.S. Geological Survey  
ATTN: Dr. T. Hanks  
National Earthquake Research Center  
345 Middlefield Road  
Menlo Park, CA 94025

SRI International  
333 Ravensworth Avenue  
Menlo Park, CA 94025

Center for Seismic Studies  
ATTN: Dr. C. Romney  
1300 North 17th Street  
Suite 1450  
Arlington, VA 22209 (3 copies)

Dr. Robert Blandford  
DARPA/GSD  
1400 Wilson Boulevard  
Arlington, VA 22209-2308

Ms. Ann Kerr  
DARPA/GSD  
1400 Wilson Boulevard  
Arlington, VA 22209-2308

Dr. Ralph Alewine III  
DARPA/GSD  
1400 Wilson Boulevard  
Arlington, VA 22209-2308

Mr. Edward Giller  
Pacific Sierra Research Corp.  
1401 Wilson Boulevard  
Arlington, VA 22209

Science Horizons, Inc.  
Attn: Dr. Bernard Minster  
Dr. Theodore Cherry  
710 Encinitas Blvd., Suite 101  
Encinitas, CA 92024 (2 copies)

Dr. Jack Evernden  
USGS - Earthquake Studies  
345 Middlefield Road  
Menlo Park, CA 94025

Dr. Lawrence Braille  
Department of Geosciences  
Purdue University  
West Lafayette, IN 47907

Dr. G.A. Bollinger  
Department of Geological Sciences  
Virginia Polytechnical Institute  
21044 Derring Hall  
Blacksburg, VA 24061

Dr. L. Sykes  
Lamont Doherty Geological Observatory  
Columbia University  
Palisades, NY 10964

Dr. S.W. Smith  
Geophysics Program  
University of Washington  
Seattle, WA 98195

Dr. L. Timothy Long  
School of Geophysical Sciences  
Georgia Institute of Technology  
Atlanta, GA 30332

Dr. N. Biswas  
Geophysical Institute  
University of Alaska  
Fairbanks, AK 99701

Dr. Freeman Gilbert  
Institute of Geophysics &  
Planetary Physics  
Univ. of California at San Diego  
P.O. Box 109  
La Jolla, CA 92037

Dr. Pradeep Talwani  
Department of Geological Sciences  
University of South Carolina  
Columbia, SC 29208

University of Hawaii  
Institute of Geophysics  
Attn: Dr. Daniel Walker  
Honolulu, HI 96822

Dr. Donald Forsyth  
Department of Geological Sciences  
Brown University  
Providence, RI 02912

Dr. Jack Oliver  
Department of Geology  
Cornell University  
Ithaca, NY 14850

Dr. Muawia Barazangi  
Geological Sciences  
Cornell University  
Ithaca, NY 14853

Rondout Associates  
Attn: Dr. George Sutton  
Dr. Jerry Carter  
Dr. Paul Pomeroy  
P.O. Box 224  
Stone Ridge, NY 12484 (3 copies)

Dr. M. Sorrells  
Geotech/Teledyne  
P.O. Box 28277  
Dallas, TX 75228

Dr. Bob Smith  
Department of Geophysics  
University of Utah  
1400 East 2nd South  
Salt Lake City, UT 84112

Dr. Anthony Gangi  
Texas A&M University  
Department of Geophysics  
College Station, TX 77843

Dr. Gregory B. Young  
ENSCO, Inc.  
5400 Port Royal Road  
Springfield, CA 22151

Dr. Ben Menaheim  
Weizman Institute of Science  
Rehovot, ISRAEL 951729

Weidlinger Associates  
Attn: Dr. Gregory Wojcik  
620 Hansen Way, Suite 100  
Palo Alto, CA 94304

Dr. Leon Knopoff  
University of California  
Institute of Geophysics & Planetary  
Physics  
Los Angeles, CA 90024

Dr. Kenneth H. Olsen  
Los Alamos Scientific Laboratory  
Post Office Box 1663  
Los Alamos, NM 87545

Prof. Jon F. Claerbout  
Prof. Amos Nur  
Dept. of Geophysics  
Stanford University  
Stanford, CA 94305 (2 copies)

Dr. Robert Burrige  
Schlumberger-Doll Research Ctr.  
Old Quarry Road  
Ridgefield, CT 06877

Dr. Eduard Berg  
Institute of Geophysics  
University of Hawaii  
Honolulu, HI 96822

Dr. Robert Phinney  
Dr. F.A. Dahlen  
Dept. of Geological & Geophysical Sci.  
Princeton University  
Princeton, NJ 08540 (2 copies)

Dr. Kin-Yip Chun  
Geophysics Division  
Physics Department  
University of Toronto  
Ontario, CANADA M5S 1A7

New England Research, Inc.  
Attn: Dr. Randolph Martin III  
P.O. Box 857  
Norwich, VT 05055

Sandia National Laboratory  
Attn: Dr. H.B. Durham  
Albuquerque, NM 87185

Dr. Gary McCartor  
Mission Research Corp.  
735 State Street  
P. O. Drawer 719  
Santa Barbara, CA 93102

Dr. W. H. K. Lee  
USGS  
Office of Earthquakes, Volcanoes,  
& Engineering  
Branch of Seismology  
345 Middlefield Rd  
Menlo Park, CA 94025

AFGL/XO  
Hanscom AFB, MA 01731-5000

AFGL/LW  
Hanscom AFB, MA 01731-5000

AFGL/SULL  
Research Library  
Hanscom AFB, MA 01731-5000 (2 copies)

Secretary of the Air Force (SAFRD)  
Washington, DC 20330

Office of the Secretary Defense  
DDR & E  
Washington, DC 20330

HQ DNA  
Attn: Technical Library  
Washington, DC 20305

Director, Technical Information  
DARPA  
1400 Wilson Blvd.  
Arlington, VA 22209

Los Alamos Scientific Laboratory  
Attn: Report Library  
Post Office Box 1663  
Los Alamos, NM 87544

Dr. Thomas Weaver  
Los Alamos Scientific Laboratory  
Los Alamos, NM 87544

Dr. Al Florence  
SRI International  
333 Ravenswood Avenue  
Menlo Park, CA 94025-3493

END

7-87

DTIC